AN EXPERIMENTAL INVESTIGATION OF LAMINAR SLIP IN COPPER CRYSTALS

by

George Harry East, Jr.

S.B., Massachusetts Institute
of Technology (1965)

M.S., Massachusetts Institute
of Technology (1966)

SUBMITTED IN PARTIAL FULFILLMENT
OF THE REQUIREMENTS FOR THE
DEGREE OF DOCTOR OF
PHILOSOPHY

at the

MASSACHUSETTS INSTITUTE OF TECHNOLOGY

June 1971

Signature of Author . . . . . .
Department of Mechanical Engineering
February 23, 1971

Certified by . . . . . .
Thesis Supervisor

Accepted by . . . . . .
Chairman, Departmental Committee
on Graduate Students

AN EXPERIMENTAL INVESTIGATION OF LAMINAR SLIP IN COPPER CRYSTALS

by

George Harry East, Jr.

Submitted to the Department of Mechanical Engineering on February 23, 1971 in partial fulfillment of the requirements for the degree of Doctor of Philosophy.

ABSTRACT

Primary dislocations observed in copper on the cross plane by etch pit techniques form clusters of several types. Two varieties, dipole streamers and kink bands, lie at fixed orientations to the slip direction, while the other clusters have preferred orientations. With increasing stress the clusters become more densely packed but lengthen so slowly that newly formed clusters decrease the average length and maintain the internal dislocation density at about 150 dislocations per cluster. The total density of primary dislocations increases with stress but at a decreasing rate and is not influenced by small orientation changes. Strong kink bands form with a mean spacing related to the flow stress according to

$$\tau = 39 + 1.55 \times 10^{14} (b/\ell)^2 \ g/mm^2.$$

Although the forest dislocations are not randomly distributed, they do not show the strong clustering associated with primary dislocations. The forest hardens in response to the applied stress according to the relation

$$N_f = c \cdot \tau^{2.76} \ cm^{-2}$$

where the constant "c" is 3.25 in a crystal oriented most favorably for easy glide but changes rapidly with small variations in orientation.

Measurements of the temperature dependence of the flow stress indicate that 26% of the stress at absolute zero is supported by thermally penetrable obstacles presumed to be repulsive junctions with forest dislocations. The non-thermal contribution to the flow stress is due to attractive junctions which are impenetrable. Since an analysis shows that the results can be fully explained by obstacles, long range stresses need not exist. Although the force-distance curve for the penetrable obstacles has been computed, the data cannot prove whether the activation is a local process.

Thesis supervisor: Prof. A. S. Argon
Title: Professor of Mechanical Engineering

TABLE OF CONTENTS

LIST OF FIGURES

LIST OF TABLES

I. INTRODUCTION

Although laminar slip was first recognized in H.C.P. metal crystals several decades ago, the interpretation of easy glide as a general phenomenon was first expounded in the pioneering work of Andrade and Henderson (1951). In subsequent investigations of hardening in F.C.C. crystals the greatest emphasis was given to stages II and III, the linear and parabolic hardening regions (Fig. 1-1). However, the relatively uncomplicated condition of laminar slip responsible for easy glide suggests that a good understanding of certain basic phenomena in hardening should evolve more readily than in the more complex processes of stages II and III. Several theoretical explanations of the yield stress, of hardening, and temperature and strain rate sensitivities of the flow stress have been proposed (Taylor (1934), Frank and Read (1950), Cottrell (1953), Mott (1953), Friedel (1956), Seeger (1957), Seeger et al. (1961), Johnston and Gilman (1959), Kocks (1966)) with limited success. Recently a more comprehensive statistical theory for easy glide was developed (Argon and East (1968), Argon (1969)). The experiments described here were designed to test certain assumptions made in the development of this theory and to obtain additional understanding to develop it further in certain areas.

The statistical theory assumed that primary edge dislocations contain short segments out of the primary plane produced by the cross slip and elimination of nearby, opposite type screw dislocations encountered when in motion. The

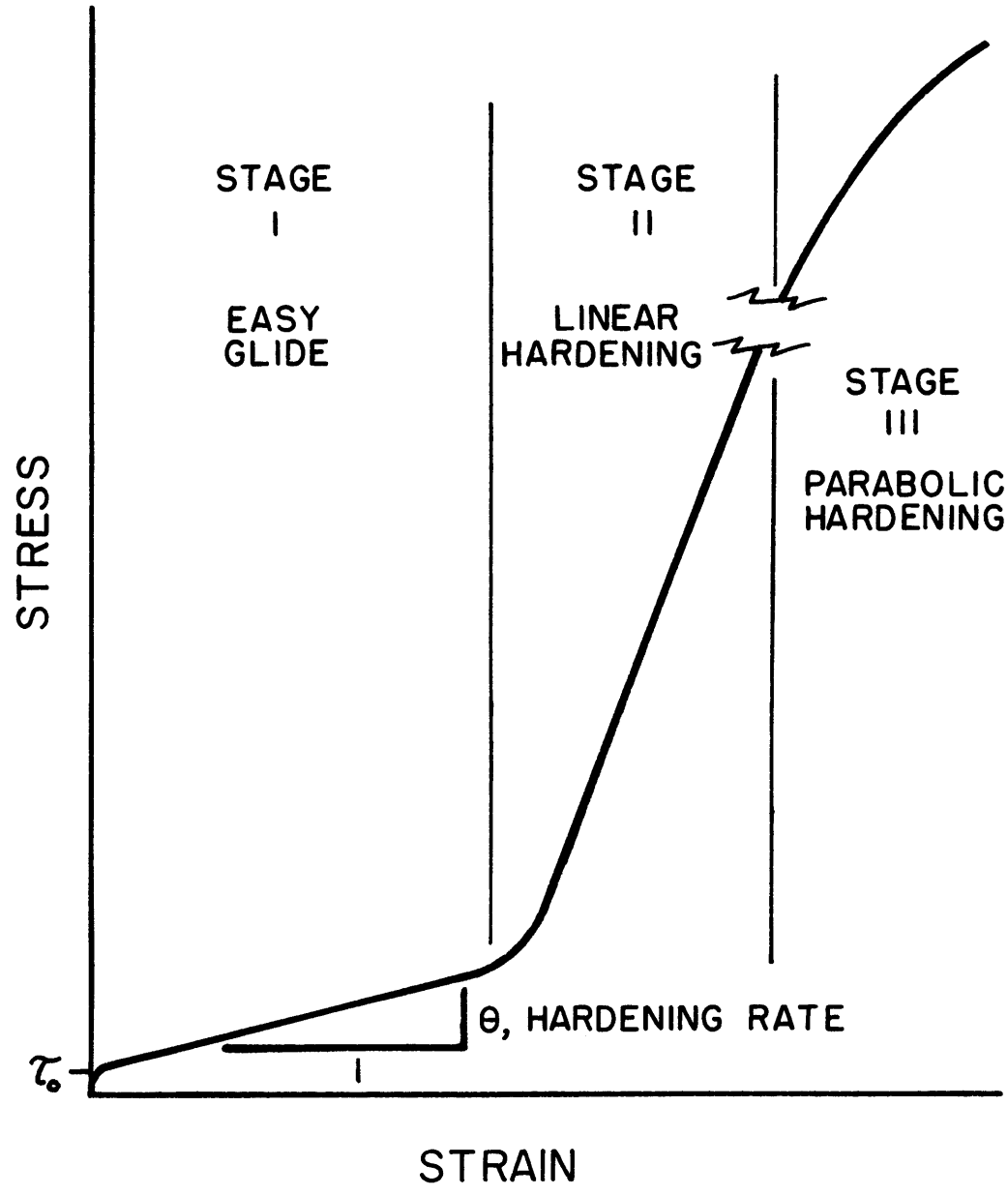

FIGURE 1-1 HARDENING REGIMES OF A COPPER SINGLE CRYSTAL

probable distribution of primary segments was then calculated based on the number of jogs. From this the probability of capturing similar edge dislocations to produce multipoles and of forming and annihilating dislocation sources in such multipoles was derived. The stress and strain dependence of the transmittable dislocation density was also computed. By requiring a constant dislocation flux to maintain a constant strain rate, and by using an expression for dislocation velocity based on forest intersections, a stress-strain curve was obtained. Certain input parameters, such as the average spacing of multipole nuclei, the limiting distance for the cross slip of screw dislocations, and the activation energy were necessary to obtain this stress-strain relation. The first of these was measured by Brydges (1966). The other two parameters were less well known. The cross-slip distance was left as a free parameter which was finally chosen to provide a reasonable yield stress, but a value for the activation energy needed to determine the dislocation velocity could only be found in the literature for stage II. Therefore, one objective of these experiments was to determine the activation energy and its stress dependence in stage I.

To obtain the activation energy, the initial creep rate at several temperatures was correlated with stress using an experimentally derived temperature dependence of the flow stress. The density of penetrable and impenetrable forest obstacles and the force-area curve of these obstacles was also derived. Both the temperature dependence of the flow

stress and the initial creep rate change resulting from applying a step rise in load to prestressed crystals were measured at the beginning and end of the easy glide range. Temperatures covered the interval from 77^0K (which allowed extrapolation to absolute zero) to 460^0K where the temperature dependence of the flow stress, corrected for modulus variation, became nil.

The stress-strain curve produced by the theory has a reasonable shape, showing a slight rounding when yielding but becoming linear at higher stresses. A hardening rate of 2.9 kg/mm^2 was obtained which is well within the limits of experimental data.

Other properties of easy glide could also be predicted from the theory once the nature of the forest dislocations was known. These included the orientation dependence of the flow stress, and the strain rate and temperature sensitivities of both the flow stress and the hardening rate. If the hardening of the secondary slip planes responded only to the resolved shear stress on these planes, excessive strain rate and temperature sensitivities followed. Thus, the theory chose a behavior of the forest dislocations which would give a reasonable result for the orientation sensitivity of the flow stress but which was not fully consistent with the strain rate sensitivity.

Specifically the theory assumed a relationship between the forest dislocation density and the primary density based on the ratio of the Schmid factors on the secondary and

primary slip planes. If this were actually so and the multiplication of secondary dislocations responded only to the resolved shear stress on the secondary slip systems, an orientation-independent proportionality should exist between the stress on the secondary plane and the forest density. To test this assumption, crystals with two orientations were stressed at room temperature and one strain rate to several specified flow stresses throughout the easy glide region and into the transition region to stage II. These crystals were sectioned along the primary plane by damage-free acid machining and the dislocation densities and distributions were observed on this plane and the cross plane using etch pit techniques.

In addition to obtaining data essential to testing these assumptions, the specimens furnished much information on the formation and growth of dislocation multipoles, their various forms, and the effects of the crystal surface. In the course of the study many different dislocation configurations capable of supporting the same flow stress were observed and some information was derived on the stability of clusters.

Copper was selected for several reasons, not the least of which is the wealth of information already available in the literature concerning its behavior in easy glide. Copper is readily refined to ultra purity and grown into single crystals, has an F.C.C. crystal structure and negligible friction stress, and when etched, exhibits pits on certain crystallographic planes indicating the point of emergence of

a dislocation.

Prior to the development of the statistical theory, work on laminar slip in copper had been done in this laboratory by Brydges (1966, 1967a, 1967b, 1968) which provided the qualitative understanding for the creation of the theory. The experiments described here are an extension of this work during which more detailed investigations were conducted. One example is the more careful study of the accumulation of the primary dislocations. Another is the study of the secondary dislocation density which was investigated by Brydges at considerably higher stresses in crystals with forest dislocations produced by torsion. Here the forest was produced by tension for a direct comparison with the other experiments, was studied throughout easy glide beginning at yield, and was observed at two orientations. The creep tests, the thermal analysis, and the resulting force-distance curves have previously not been performed.

II. GENERAL EXPERIMENTAL PROCEDURE

2.1 CRYSTAL GROWTH AND ANNEALING

Crystals of spectrographic purity copper were grown by a modified Bridgman technique and annealed by the method of Kitajima (1968). Tensile prestressing at one strain rate to several specified stresses resulted in many groups of similar crystals which were then studied in further tests. Some were sectioned along the primary slip plane and etched with Livingston's (1960) dislocation etch to observe dislocation densities and distributions both on this plane and on the cross plane. Others were reloaded at several temperatures for creep and flow stress investigations.

The raw material, 99.999% copper, was obtained both from American Smelting and Refining Company and from United Mineral and Chemical Corporation. Analyses of both the starting material and annealed crystals show very few impurities (Table 1). A mold machined from Carbone Corporation grade 5890/PT spectrographic purity graphite was used to grow a cylindrical boule from which a seed crystal was cut using an acid string-saw and an acid miller. Attempts to produce a properly oriented seed by mechanical cutting methods failed due to recrystallization upon heating, indicating that such methods produce excessive damage. Likewise recrystallization will occur if the seed is not made undersize to allow for differential expansion between the copper and graphite. Once a supply of crystals existed, they could be used to replace an accidentally damaged seed or produce a seed with minor orientation changes

SAMPLE / ELEMENT	ASARCO (AS RECEIVED)	UMC CORP. (AS RECEIVED)	SPECIMEN 10-3 9/23/68	SEED 5/21/69
Fe	<0.7 ppm	1 ppm		1 ppm
Mg		<1	≃1 ppm	≃1
Si	<0.1	1	1	1
Ag	<0.3	3		
Sb	<1			
Pb	<1			
Sn	<1			
Ni	<1			
Bi	<0.1			
As	<2			
Cr	<0.5			
Te	<2			
Se	<1			
S	<1			

TABLE 1 ANALYSES OF THE HIGH PURITY COPPER

($<10^0$) by beveling the crystal on the acid miller. The two orientations of Figure 2-1 were chosen so that two opposing faces of the square crystals would be (111) planes as required for dislocation etching. One of these orientations maximized conditions for easy glide while the other was only slightly different to study the effect of small orientation changes on secondary dislocation multiplication. The Schmid factors on the (111)<110> slip systems for these two orientations are listed in Table 2.

The crystal growing furnace was slightly modified from the design described by Brydges (1963). A sectional mold of high purity graphite allows twenty crystals to be grown simultaneously from a single seed at a rate of 0.5 cm per hour. The mold, in a vacuum of 5×10^{-5} torr, is subjected to a vertical temperature gradient and heated until a thermocouple at the base of the mold adjacent to the seed indicates melting. The solidification front moves upward at the desired rate by steadily decreasing the temperature at the thermocouple near the heating element by 5^0C/hr. Improved temperature control resulted from electrostatically shielding the control thermocouple to prevent AC pick-up by the chopper stabilized DC amplifier of the Honeywell Electr-O-Volt controller. Intermittent shorts to ground resulting from the deposit of graphite on the ceramic heating element supports were eliminated by encasing the elements in a refractory cement.

The crystals are separated from the header by sawing-using the mold as support. Each crystal is X-rayed and those

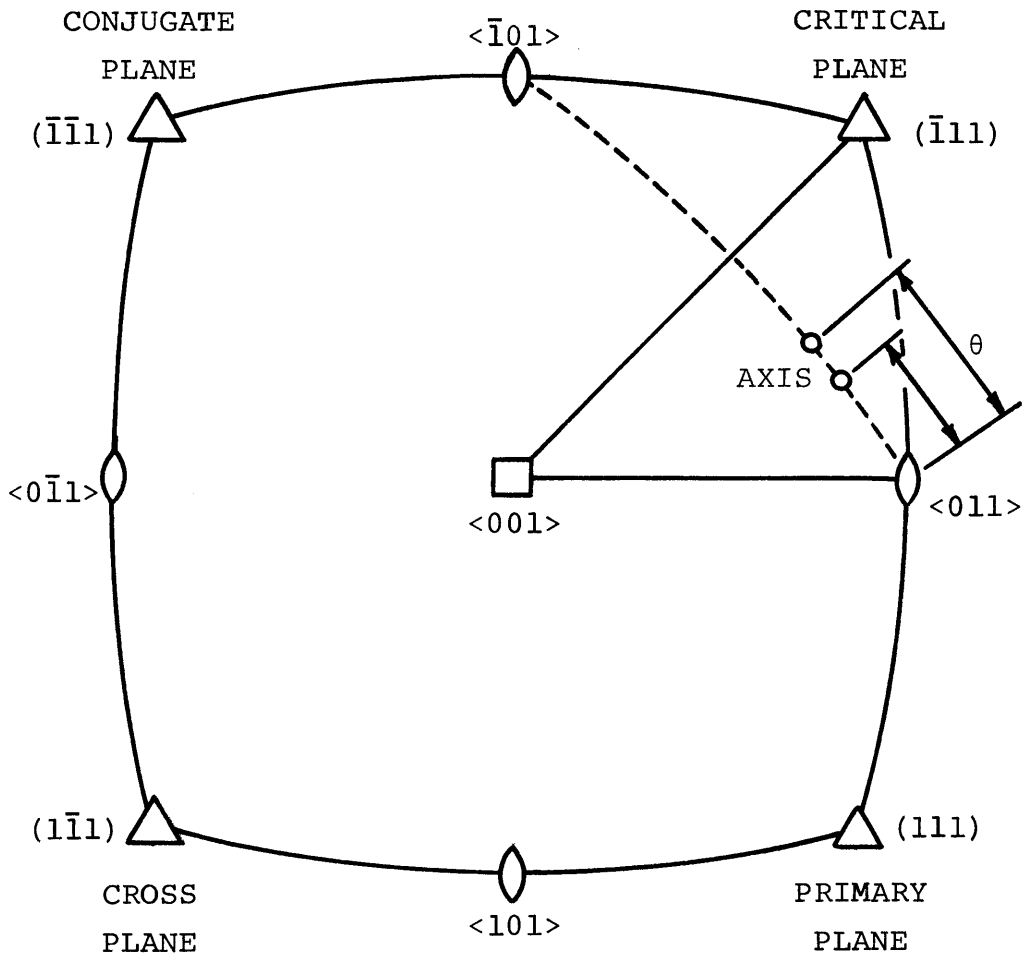

AXIS θ	SCHMID FACTOR	
	PRIMARY SLIP SYSTEM (111) <1̄01>	SECONDARY SLIP SYSTEM (1̄11) <101>
12.5°	0.467	0.384
17.5°	0.467	0.358

FIGURE 2-1 CRYSTAL ORIENTATION AND SLIP SYSTEM NOMENCLATURE

TABLE 2

SCHMID FACTORS FOR ALL (111)<110> SLIP SYSTEMS

SLIP PLANE	SLIP DIRECTION	SCHMID FACTOR	
		FAVORED ORIENTATION	OTHER ORIENTATION
111 (PRIMARY)	$\bar{1}01$	0.467	0.467
	$0\bar{1}1$	0.111	0.084
	$\bar{1}10$	0.358	0.384
$\bar{1}11$ (CRITICAL)	$\bar{1}\bar{1}0$	0.199	0.276
	$0\bar{1}1$	0.160	0.108
	101	0.358	0.384
$\bar{1}\bar{1}1$ (CONJUGATE)	$\bar{1}10$	0.160	0.108
	011	0.271	0.192
	$\bar{1}01$	0.111	0.084
$1\bar{1}1$ (CROSS)	$\bar{1}10$	0.000	0.000
	101	0.000	0.000
	011	0.000	0.000

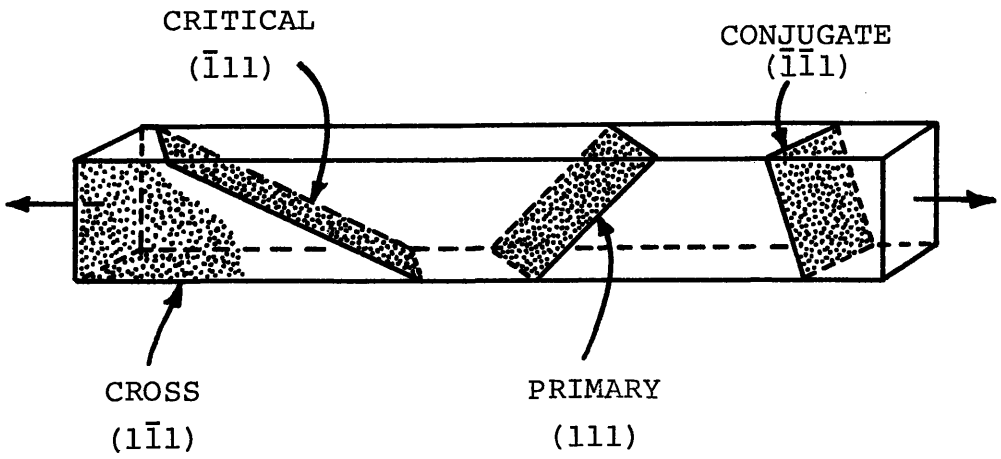

more than $2\frac{1}{2}^0$ from the desired orientation are discarded, leaving about twelve crystals per batch. Before annealing the crystals are cleaned by rinsing in reagent grade methanol and placed on a graphite boat with the (111) faces vertical. A thermocouple is set into a hole in the graphite immediately under the specimens to monitor the varying temperature of the crystals. To prevent devitrification products from the Mullite furnace tube from contaminating the copper, a roof of 99.9% purity copper sheet arches over the boat.

Crystals annealed for one week in a constant temperature environment barely below the melting point have dislocation densities of 0.7-4 x 10^5 cm^{-2} and yield at 30-50 g/mm^2 as determined by Brydges (1966) and confirmed early in this work. Realizing that lower yield points were possible and that lower initial dislocation densities would mean more nearly identical structures and less experimental scatter after prestressing, an alternative annealing method was sought. A trial vacuum furnace with a moving heating unit and a strong temperature gradient was constructed according to the design of Kitajima (1968). Experiments with this furnace showed very little improvement over stationary annealing until the stroke length was set to produce cyclic temperature differentials comparable in magnitude to that used by Kitajima (Appendix A). At this point a rather substantial improvement was noted resulting in yield points as low as 10 g/mm^2. This succes led to the development of a larger furnace capable of annealing five crystals simultaneously which was designed to match as closely

as possible the relevant parameters of Kitajima and which eliminated some mechanical difficulties encountered in the original design. Four days of annealing, followed by one day of controlled cooling to lower the vacancy density, normally produces crystals yielding between 10 and 25 g/mm^2 and having dislocation densities of roughly 2×10^4 cm^{-2}. Some improvement is noted as annealing times are increased.

2.2 TENSION EXPERIMENTS

Annealed crystals were glued into knife-edge supported grips only on the two (111) faces using either epoxy or Duco cement. The axis in the primary slip plane normal to the <110> slip direction and the axis of rotation about the knife edges are not parallel. This, and the boundary conditions imposed by the rigid grips, both introduce end effects in the crystal. In these regions laminar slip will not occur due to activity on other slip systems. This produces some error in the strain measurements. The effect persists roughly to a distance corresponding to the furthest penetration into the gage length of a major slip plane originating at the grips. This distance is 2½ specimen thicknesses for the critical plane and thus effects 1.5 cm at each end of a total gage length of 5 to 8 cm. Observations of dislocation clustering near the grips showed polygonization, indicating bending, and were not used in studies of clustering.

Deformation in tension was monitored by load and strain cells instrumented with semiconductor strain gages arranged in a full bridge configuration and recorded using a Sanborn

model 150 recorder with carrier preamplifiers. The constant strain rate testing machine is of conventional design with a variable speed motor driving a lead screw through a gear train. The machine was modified by inserting a magnetically actuated reversible gear unit to allow unloading at 100 times the rate of loading after a dead time of less than 10 msec. It is hoped that this minimizes dislocation rearrangements which would affect the creep experiments, although as finally executed, the design of the creep test eliminated this requirement. Using a strain rate of 1×10^{-4} sec^{-1}, most crystals were prestressed on this machine at room temperature. Later some were restressed at the same rate while submerged in a constant temperature bath.

The testing temperature was controlled by immersion in fluids over the range from 77^0K to 460^0K. The temperatures 77^0K, 195^0K, and 373^0K were accurately fixed, being the boiling point of liquid nitrogen, the sublimation point of dry ice in methanol, and the boiling point of water, respectively. A Dewar flask of 2-methylbutane was maintained at 123^0K by controlling the flow of liquid nitrogen through a coil of copper tubing immersed in the fluid. The highest temperature, 460^0K, was produced by heating silicone oil with an electric hot plate while monitoring the temperature with a thermometer. Finally, there was room temperature- 298 ± 4^0K. The three temperatures not fixed by a physical transformation varied by no more than four degrees Kelvin from their stated values which is inconsequential when compared to the measured

temperature sensitivity. The specimens were held at temperature for at least fifteen minutes prior to testing with the exception of two minutes at 460^0K where some annealing effect might be possible. Heat transfer calculations showed that in two minutes the center of the specimen would be within 5^0K of the oil bath temperature.

2.3 CREEP EXPERIMENTS

The creep machine consists of a balanced beam with one end weighted and the other supporting a crystal and instrumentation similar to that on the tensile testing machine. The weights were of three varieties: dead weights, a variable weight activated by lowering the water level around a bouyant mass, and a solenoid activated weight with a pointed tip dropped onto a shock absorbing Plasticene wad on the beam. A cam allowed the dead weights to be applied gently, then the load was gradually raised until a perceptible creep rate was obtained. After momentarily monitoring the creep rate at constant stress, the stress was increased in a step function while recording the elongation. Several problems were encountered with the design of this equipment, especially with regards to rapid response and critical damping of the moving parts and to the influence of building vibrations. In its final form the system rise time for a stress increment of 0.85 g/mm^2 is 0.02 seconds. As in the other testing machine provision was made for immersing the specimen in a constant temperature bath for the duration of the test.

2.4 SECTIONING, POLISHING, AND ETCHING

Sectioning of the crystals to observe the primary plane was accomplished by reasonably damage-free acid machining as described by Young and Wilson (1961) but with some revisions. In the acid saw, a cone initially containing 5 km of acid-resistant Dacron thread was found most suitable since it held enough thread in one continuous knot-free multifilament to make several cuts. Held taught between a tensioning device and a motor drive pulling the string at 4 cm/sec., the acid-laden thread passes over two guides surrounding the specimen. The upper guide is designed to wet the string as it passes vertically from a nitric acid bath on top, through the bushing, emerging from a droplet suspended beneath the guide. A slightly irregular surface results from the cutting process which takes about 3 hours for a 6 mm square specimen.

The acid miller consists of a Lucite wheel rotating about a horizontal axis at 60 rpm so that a taught Dacron sheet stretched over its face transfers the cutting solution of hydrochloric acid saturated with cupric chloride to the specimen. The sample rotates about a parallel axis at 100 rpm and is fed intermittently towards the wheel. A dilemma exists since a flat surface will be produced only if the gap between the wheel and the specimen is very small but accidentally touching the wheel will definitely introduce damage. Experiments with an annealed crystal indicate that best results are obtained if the crystal is advanced once a minute until the barely audible sound of rubbing is heard. The damage

introduced in this manner is slight and is eliminated in the subsequent operation of electropolishing (Appendix B).

The specimens are prepared for observation by electropolishing and etching. Using an aqueous solution of 50 volume percent orthophosphoric acid doped with cupric ions, electropolishing proceeds at either 1.9 volts on the normal polishing plateau or at 5 volts where pronounced bubble evolution occurs. A cylindrical copper cathode surrounds the specimen while the polishing solution within is propelled by a magnetic stirrer. After polishing, the specimen is rinsed in water and immediately etched in the bath devised by Livingston (1960) (by volume, 1 part bromine, 15 parts glacial acetic acid, 25 parts 38% hydrochloric acid, and 90 parts water). A fresh solution usually stains the surface so it is advisable to first age a fresh bath by placing some rejected specimens in it. After etching, the crystal is rinsed in water, then reagent grade methanol and air dried.

Observations of dislocation densities and distributions are made visually and photographically using a Zeiss Ultraphot II microscope. Most photographs are taken at the lowest power available (80x) or at 200x and the etch pit counts are made from these photographs. The large deviation in the counted densities actually indicates a property of the crystals on the scale used for the individual counts (125μ square areas). The local etch pit density of a sufficiently large sample of randomly selected areas was measured. Assuming a normal distribution, the variation in the counts determined the standard

deviation indicated by the error bars on the graphs.

The etch pit technique apparently does not reveal all dislocations intersecting the surface. Ruff (1962) did not find a one to one correspondence between etch pits and dislocations revealed by electron microscopy although this may result from the motion of dislocations during specimen preparation by thinning. Likewise Brydges (1966) found a discrepancy when comparing the actual strain in a specimen with the value calculated from

$$\gamma = b\rho\ell$$

where ρ is the mobile density and ℓ the slip line length, both of which were measured by etch pit techniques. However, by bending a crystal Livingston (1960) found good agreement with the excess pits of one type, indicating dislocations of one sign, and the theoretically calculated density excess. Young (1966) also found good agreement between etch pits and dislocations revealed by X-ray methods. Therefore, in this paper etch pits will be considered mostly as ratios at different stresses and generally not as an indication of the absolute dislocation density.

III. EXPERIMENTAL RESULTS

3.1 DISLOCATION CLUSTERING: OBSERVATIONS OF PRIMARY DISLOCATIONS

Several forms of dislocation clusters are present on the cross plane of deformed crystals (Fig. 3.1-1). To categorize these exactly is difficult due to the complexity and irregularity of the groupings, but a systematic classification is necessary to bring meaning and order. After long visual examination, it was decided that the most meaningful parameters were cluster shape, size, angle with the slip plane, internal structure and density in the cluster, separation between clusters, and percentage of the surface occupied by clusters. To varying degrees all of these have been investigated.

Since the character of the clustering often varies markedly between different regions preloaded to the same stress, the area of the surface which should be included in a survey must be large. The mean free path of dislocations, given by the slip line length, is several millimeters (Mader (1957), Argon and Brydges (1968)). Since the width of the crystals in the slip direction is 8 mm, observations should extend across the entire specimen to obtain a meaningful description of the clustering (Figs. 3.1-2a to 3.1-2g).

According to shape it is possible to divide clusters into three categories, including an elementary one which may occur alone or as substructure in more complex clusters. Chains of closely spaced dislocation dipoles, as discussed by Brydges (1966), frequently extend along the slip plane.

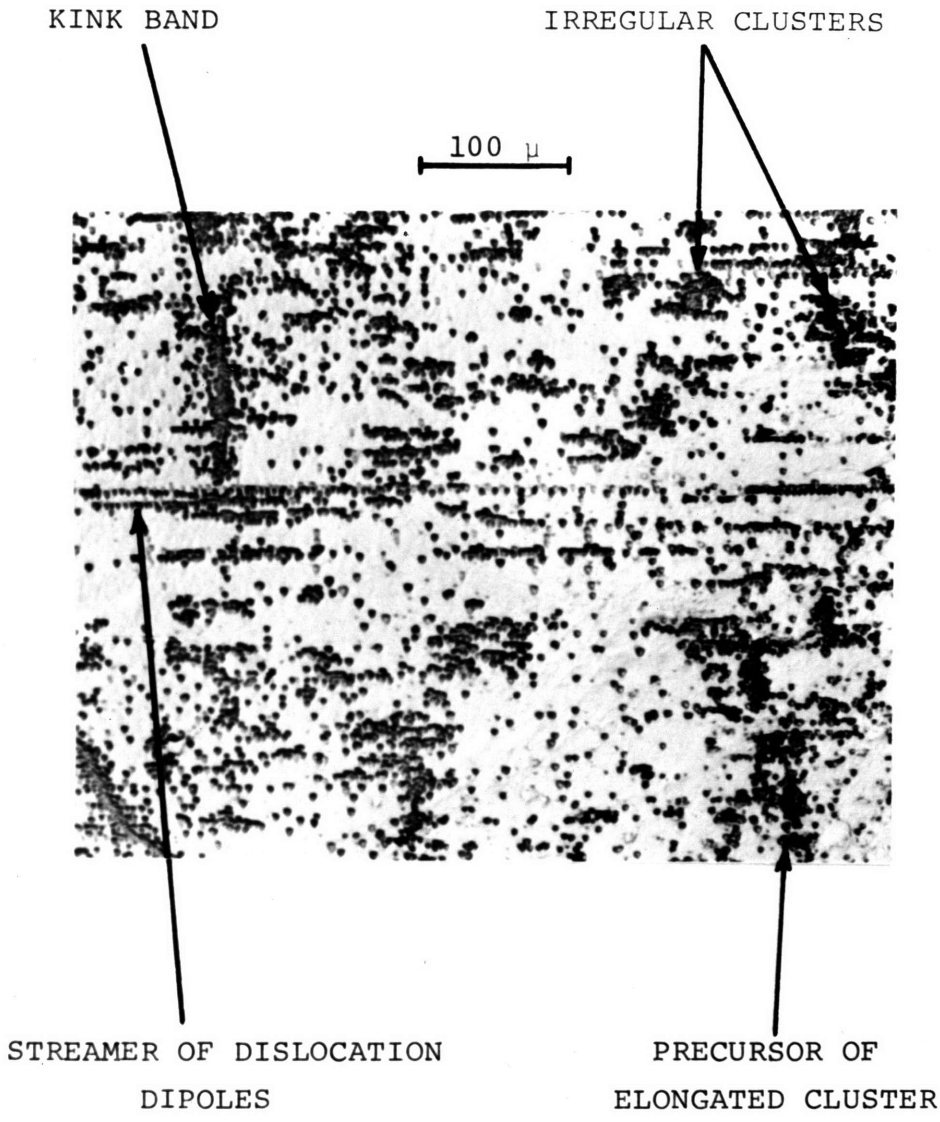

FIGURE 3.1-1 CLASSIFICATION OF DISLOCATION CLUSTERS (200X)

These streamers vary in length and form clusters of the simplest type. There are also elongated clusters lying at angles to the slip plane, occasionally appearing to consist of dipole streamers. One special case of elongated cluster is long, straight, and a right angles to the slip plane. At low stresses where the etch pit density is low enough to discern the light and dark pits which differentiate dislocations of opposite, these clusters show a strong separation of the two and are thus kink bands. Sometimes short kink bands are connected to others by irregular branches resulting in very long, narrow, randomly oriented clusters. Finally there are irregular, roughly circular patches of etch pits, unresolved towards the center, but frequently appearing at the edges to be composed of streamers of dislocation dipoles lying on closely spaced slip planes.

Many enlightening results can be derived using this scheme of classification but its limitations should first be recognized. Not all clusters can be counted. There must be some cut-off below which a dislocation association must be ignored since small groupings are ill-defined and much too numerous to be cataloged. Plots of only two parameters are misleading since they do not simultaneously display all important factors. For example, a plot of orientation versus distance from the edge provides no indication of the importance of each cluster, that is its length and dislocation density, and could be meaningless for clusters of circular shape. However, by treating each important observation

separately and trying occasionally to tie these together, a good overall understanding may be obtained.

The orientation of clusters to the slip plane has been cataloged according to distance from the edge of the crystal at two stresses, 20 and 60 g/mm^2 (strains up to 6%). The results for 20 g/mm^2 are shown in Figure 3.1-3 and totals independent of cluster location are presented for both stresses in Figure 3.1-4. It is clear that at low stresses most clusters are either dipole streamers or short kink bands, both of which are well defined. The few clusters lying at other angles are strongly limited to position angles between 60^0 and 90^0 with a very notable absence from 90^0 to 180^0. Although the tensile axis lies at 47^0 to the intersection of the primary and cross planes, it appears that this behavior is not governed by crystal surfaces parallel to the tensile axis since no correlation exists between orientation an surface proximity.

At higher stresses the appearance is greatly changed. Again the dipole streamers and kink bands persist but now a larger array of elongated clusters appears and is less influenced by position angle. It is readily seen from the histogram (Fig. 3.1-4) that the streamers are ill-defined, frequently making small angles to the slip plane. Direct observation of the photographs indicates that this results from a dipole chain ending on one slip plane but continuing on an adjacent plane. Most streamers are quite short and, while as numerous as at lower stresses, appear unimportant at 60 g/mm^2 compared to the kink bands which have intensified and will continue to do so

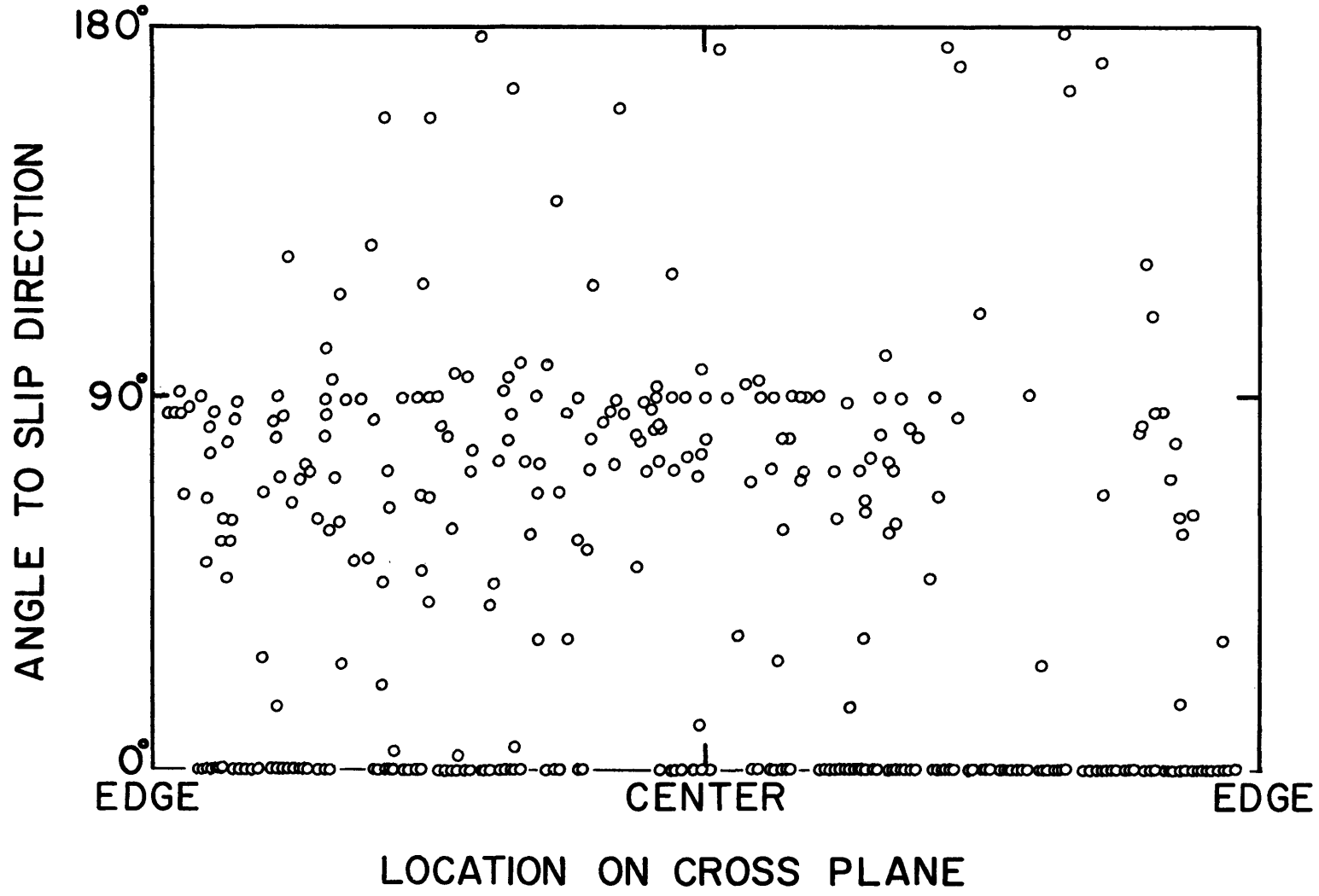

FIGURE 3.1-3 THE LOCATION AND ORIENTATION OF CROSS PLANE CLUSTERS

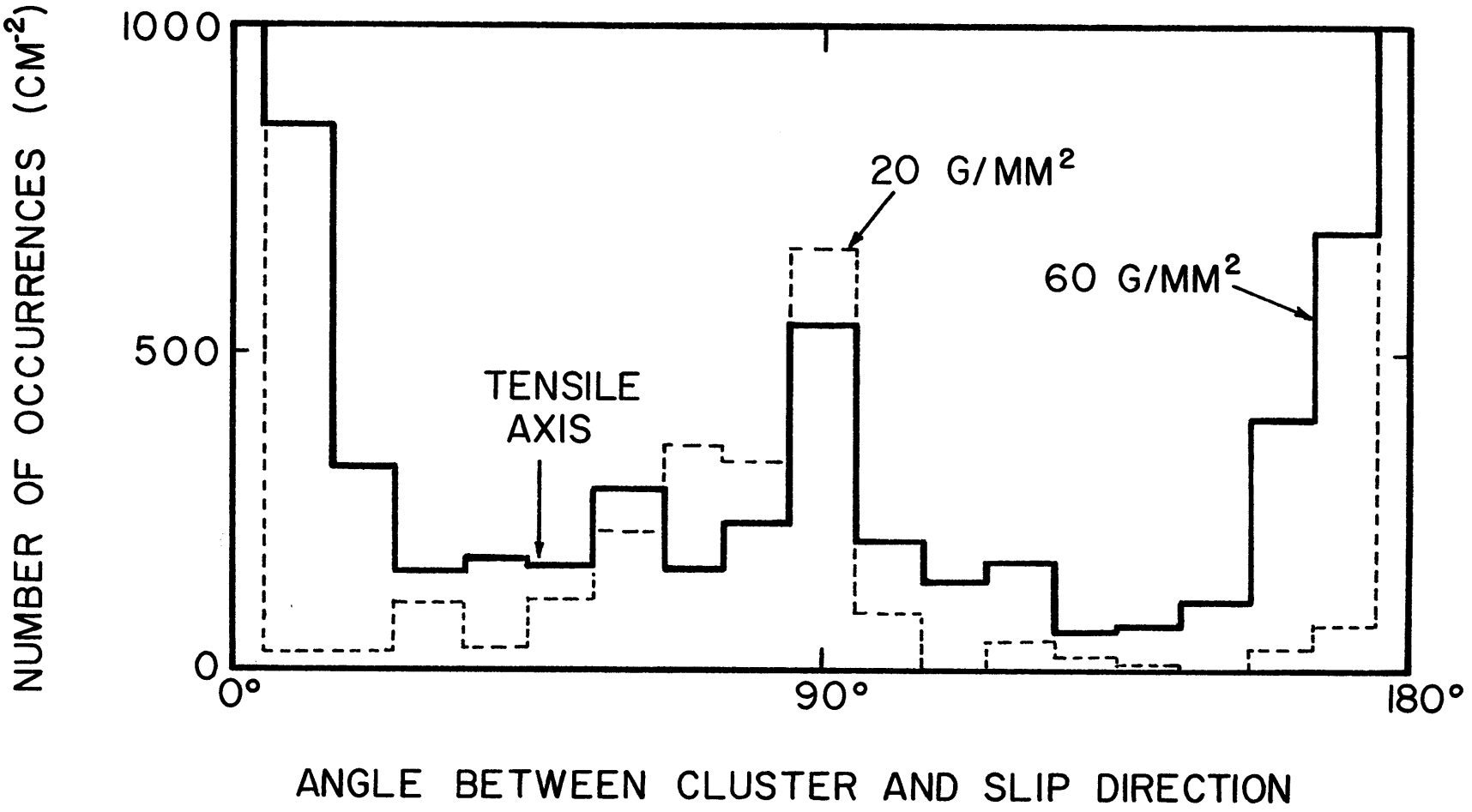

FIGURE 3.1-4 THE STRESS DEPENDENCE OF CLUSTER ORIENTATION

into stage II. The larger array of clusters at angles other than 0^0 or 90^0 results from a smearing of dipole streamers over angles around 0^0, from a larger percentage of elongated clusters, and from the union of minor kink bands to form extended groups not at 90^0. Position angles above 90^0 do not normally result from the free growth of a cluster but from the coalescence of clusters along the shortest path.

Since a fundamental difficulty in studying cluster lengths arises through the omission of very short clusters, only the distribution of lengths is truly meaningful, although absolute lengths in a given data set are sometimes useful. Clusters longer than 0.03 mm were cataloged at 20 and 60 g/mm^2 and the results normalized to eliminate differences in cluster density between these stresses (Fig. 3.1-5). The longest cluster was a streamer of dislocation dipoles 0.88 mm long existing at the lower stress. Excluding well developed kink bands which form near the end of stage I, such long clusters can be disregarded due to their rarity. Attention should be devoted instead to clusters less than 0.2 mm long. It is obvious from the figure that cluster lengths are slightly affected by stress, tending to decrease as the stress rises. This behavior is surprising at first, but indicates that longer clusters formed early in the deformation process do not tend to lengthen, although they do become more densely packed, while short new clusters forming between the first generation clusters shift the normalized curve. Table 3 indicates a 30% decrease in average length over this stress interval.

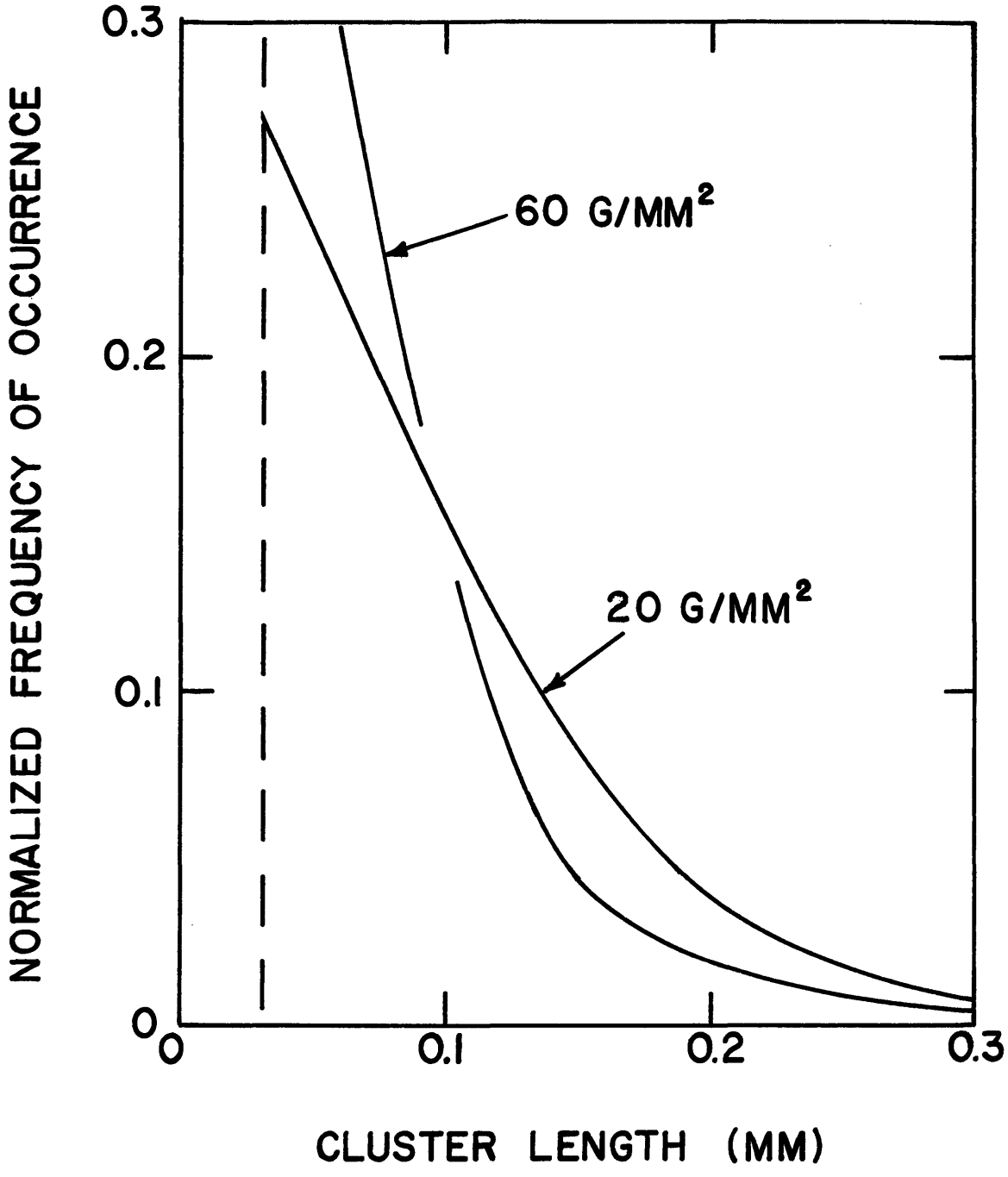

FIGURE 3.1-5 THE DISTRIBUTION OF CLUSTER LENGTHS AT 20 AND 60 G/MM^2

20 g/mm^2 PRESTRESS

CLUSTER TYPE	AVERAGE LENGTH (mm)	AVERAGE DISLOCATION DENSITY (dislocations/mm^2)	DISLOCATIONS PER CLUSTER	FREQUENCY	TOTAL
dipole	0.101	816	82.4	0.525	43.2
elongated	0.136	1128	153.4	0.251	38.5
compact	0.102	1512	154.2	0.224	34.5
			Dislocations/cluster.....		116.2
			Clusters/cm^2.....		x 4990
			Cluster dislocations/cm^2.....		5.79×10^5
			Background dislocations/cm^2...		+ 1.16×10^5
			TOTAL.....		6.95×10^5
			By actual count.....		7.74×10^5

60 g/mm^2 PRESTRESS

CLUSTER TYPE	AVERAGE LENGTH	AVERAGE DISLOCATION DENSITY (dislocations/mm^2)	DISLOCATIONS PER CLUSTER	FREQUENCY	TOTAL
dipole	0.064	1108	71.9	0.329	23.6
elongated	0.097	1758	170.5	0.377	64.3
compact	0.073	2536	185.1	0.294	54.4
			Dislocations/cluster.....		142.3
			Clusters/cm^2.....		x 9150
			Cluster dislocations/cm^2.....		1.30×10^6
			Background dislocations/cm^2...		+ 1.23×10^6
			TOTAL.....		2.53×10^6
			By actual count.....		2.51×10^6

TABLE 3 PROPERTIES OF CROSS PLANE CLUSTERS

The influence of the stress on the clusters is given in Table 3 which indicates that the dipole streamers predominate shortly after yielding then become less common as some are absorbed into more complex clusters. Although the internal dislocation density increased by 36% between the two stresses, the decreased average length offset this, resulting in fewer dislocations per streamer. These dipole chains account for 27% of the dislocation etch pits appearing on the cross plane at 20 g/mm^2 but only 8.5% at 60 g/mm^2. Lying in the slip plane, these streamers are unable to intercept many moving dislocations as is done by the other clusters which lie across the slip direction. Sometimes they do develop, but are immediately cataloged as elongated or compact. More frequently a streamer disappears with increasing stress, apparently moving along the slip direction until meeting an obstacle. This implies that the streamers are not entirely composed of dipoles but have a slight excess population of one sign.

The elongated and compact clusters are of roughly equal importance, the longer extent of one being offset by the higher density of the latter. The dislocation content of the elongated clusters remains about 15% higher than in compact clusters throughout easy glide while both almost double going from 20 to 60 g/mm^2. This growth and the increased frequency of occurrence of these clusters make them become the dominant features on the cross plane at higher stresses, accounting for 83% of the clustered dislocations.

The large number of clusters and their complex inner

structures necessitated the estimation of internal density based on comparing each cluster's appearance with ones which had been accurately counted. As a check on the accuracy of this method the density per unit length, cluster length per square centimeter, and background density can be combined to independently calculate a total cross plane dislocation density which agrees with direct counts (Table 3).

Those dislocations not associated with clusters, the background density, become quite numerous by the end of easy glide. Initially the annealed crystal shows no clustering, except for sub-boundaries, but even the slightest strain causes much grouping. A crystal yielding at 15.6 g/mm^2 had 82% of the cross plane etch pits in clusters at 20 g/mm^2. However, at 60 g/mm^2, the background dislocations were as numerous as those in the clusters.

The background density was counted over small patches of 125μ square ignoring those dislocations associated with clusters. An estimate of the surface covered by the clusters was made in each sample to determine the actual areas involved in each count. This estimate provides an independent indication of cluster growth (Fig. 3.1-6).

Not all clusters are permanently bound to the lattice. As mentioned, streamers of dislocation dipoles are not rigidly fixed but frequently move. Other more complex clusters are quite immobile, normally accumulating dislocations and slowly lengthening. However, there are examples of substantial clusters breaking down. The rarity of these events should result

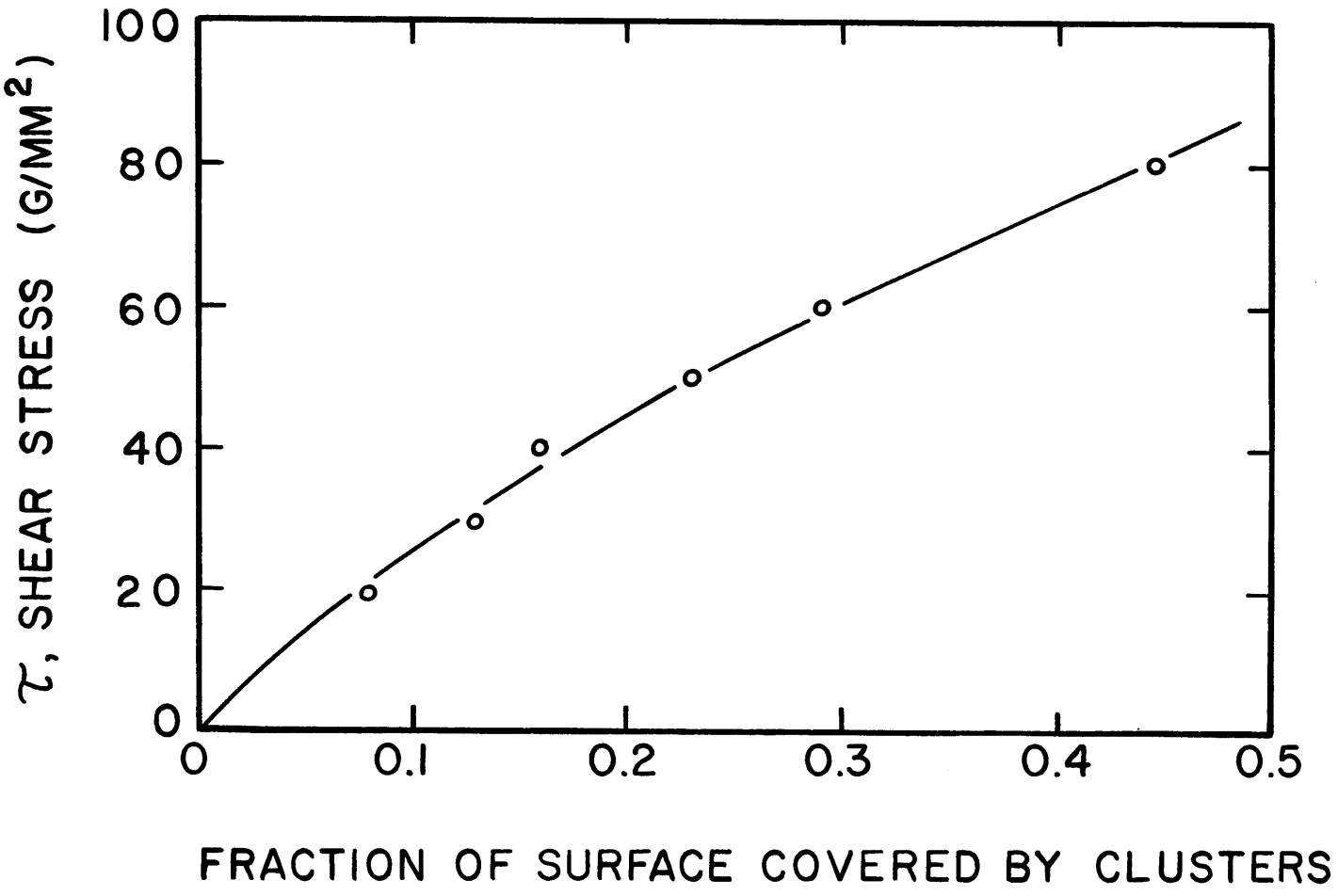

FIGURE 3.1-6 THE EXTENT OF CLUSTER FORMATION ON THE CROSS PLANE

in no observable effect on the macroscopic behavior of the crystals and thus may be ignored.

Kink bands become a dominant feature especially at the end of stage I. Not only do they become very long and densely populated with dislocations, but become more numerous. Experiments by Nigam (1967) on ionic crystals showed a relation between the flow stress and the mean spacing of birefingent bands of the form

$$\tau \propto 1/\ell^2$$

Similarly the equation

$$\tau = 39 + 1.55\times10^{14}\left\{\frac{b}{\ell}\right\}^2 \quad g/mm^2$$

was found to hold for the spacing of kink bands in copper single crystals (Fig. 3.1-7).

Previous investigations have provided contradictory results concerning surface effects. Fourie (1968) has measured lower flow stresses near the surface while the work of Kramer (1965) indicates the opposite. These possibilities were checked. Despite generally being able to observe within 0.1 mm of the true edge, a slight rounding preventing etching at closer distances, no differences are noticeable. It was shown (Fig. 3.1-3) that orientation is not affected by surface proximity, a similar result holding for cluster lengths. Likewise no differences in density or cluster appearance is seen. This uniformity may result from the observation of a plane which itself was a free surface during loading.

Having quantitatively described the properties of

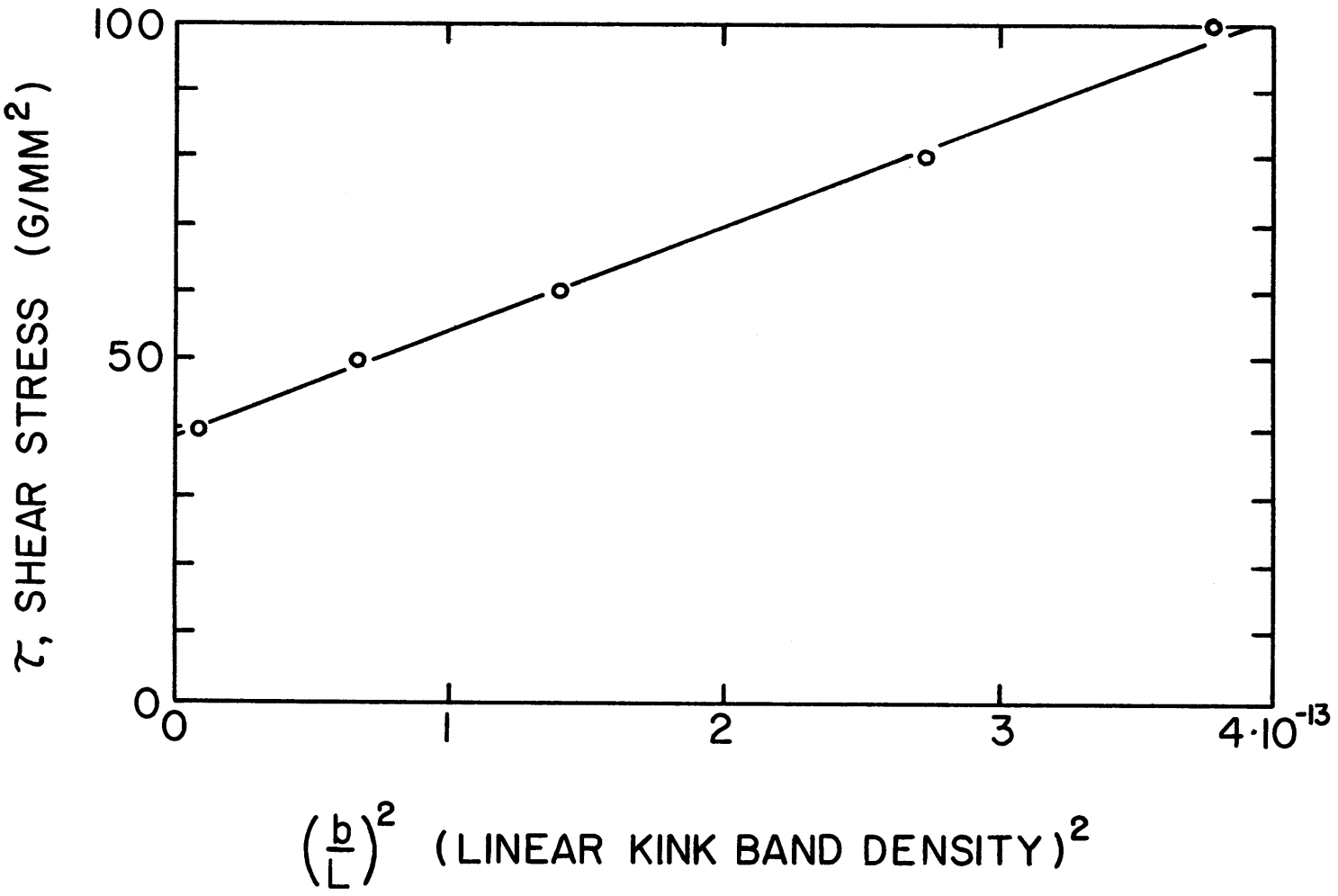

FIGURE 3.1-7 THE DEPENDENCE OF MEAN KINK BAND SPACING ON STRESS

dislocation clustering on the cross plane at two stresses selected to describe the initiation and termination of easy glide, a qualitative description of cluster origin and growth throughout the laminar slip region follows. The series of photographs showing two regions of the same crystal at intervals of 10 g/mm^2 indicates that quite dissimilar configurations are capable of supporting the same flow stress (Fig. 3.1-2). Each region initially begins with its own characteristic cluster population which does not necessarily appear to strengthen in unison with the other region. One strange effect is the early formation of kink bands in one area with none in the other, slowly transforming so that at high stresses the bands are much more prominent in the region which originally had none. The kink bands in the first area are short, not densely populated, and change relatively little throughout the history while in the other region very long, substantial bands grow very rapidly beyond 40 g/mm^2 to become the dominant feature by transition to stage II. This diversity may result from slightly different starting conditions remaining from crystal growth. Two obvious possibilities are the orientation change due to the cumulative effect of sub-boundaries and the increased crystal perfection away from the seed as indicated by larger subgrains. A separate account of both regions demonstrates the great diversity in one specimen.

At 20 g/mm^2 and 0.34% strain the first region shows mostly kink bands and dipole streamers, with a few elongated clusters and, in one region, some compact clusters. Some kink bands

are already connected to others by irregular arrays. The distribution of clusters is reasonably even, showing very few unoccupied regions as large as 5×10^{-4} cm^2. Almost nothing more occurs through 50 g/mm^2, only minor rearrangements of clusters and the appearance of very few new ones. The rearrangements may be artifacts resulting from electropolishing, but the small amount (7μ) removed at every 10 g/mm^2 increment makes this doubtful. At 60 g/mm^2 most dipole streamers are short and no longer appear important. The spaces between earlier clusters are filled by small irregular groups and a much higher background density, while the original clusters have developed links to their neighbors. The surface distribution is not uniform since regions have developed where only one cluster type dominates. Changes of a similar nature continue through 100 g/mm^2, in stage II, with no indication that the transition has occurred.

The other end of the specimen, nearer the seed, has a dramatically different history. As mentioned there are no kink bands at 20 g/mm^2. Instead the specimen exhibits a uniform distribution of compact and elongated clusters but very few dipole streamers. From this beginning a rapidly changing pattern evolves. By 30 g/mm^2 clusters have linked and new ones, especially dipole streamers, have appeared. As the stress continues to rise these clusters become more densely packed with dislocations but more of similar appearance are not generated. Instead strong kink bands begin to develop at 40 g/mm^2 and gradually come into dominance.

3.2 DISLOCATION CLUSTERING

OBSERVATIONS OF FOREST DISLOCATIONS

Although the resolved shear stress on the most favored non-coplanar slip system is 82% of that on the primary system, the forest grows relatively slowly as detailed in the section on the orientation dependence of the forest density. During the ten-fold density change during easy glide, the forest dislocations move as evidenced by pile-ups seen on the primary plane (Fig. 3.2-1), yet there is little clustering. The groups which do form are loosely knit, frequently not being significantly denser than the random background of dislocations, especially at low stresses.

At 30 g/mm^2 enough dislocation concentration has occurred to differentiate the clusters from the background (Fig. 3.2-2b). In regions where no apparent damage was introduced in the sectioning process, the spacing between distinct clusters is about 0.2 mm. The etch pits either form irregular groups or rows of overlapping pits, neither containing more than fifteen dislocations. If a systematic approach to cataloging these clusters was undertaken, the results would hinge greatly on whether such small groups were considered as clusters or merely as random fluctuations of the normal background density. Thus such a program would probably be meaningless.

However, it is possible to show that the distribution of etch pits is not random. By placing a regular grid over a photograph of the primary plane, etch pits were selected using a random number table to provide the grid coordinates. The

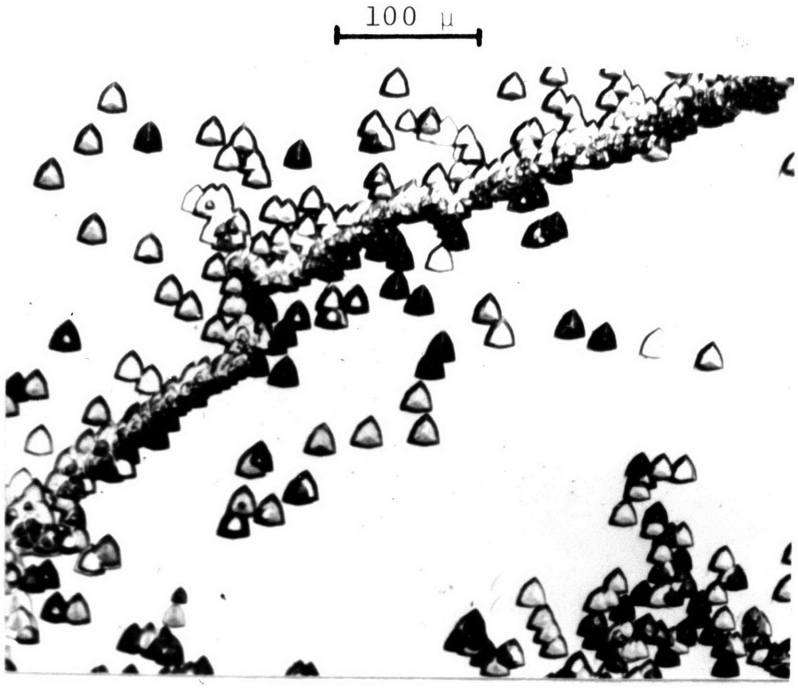

FIGURE 3.2-1 PILE-UP OF DISLOCATIONS OF OPPOSITE SIGN AT A BOUNDARY (200X)

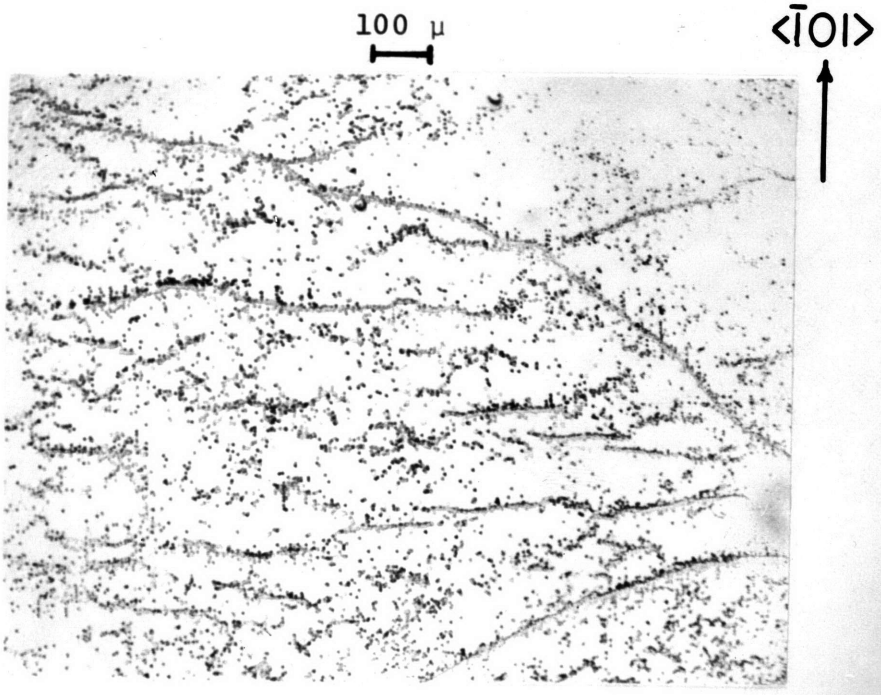

FIGURE 3.2-4 CHAINS OF DISLOCATIONS OBSERVED ON THE PRIMARY PLANE AT A PRESTRESS OF 80 G/MM^2 (80X)

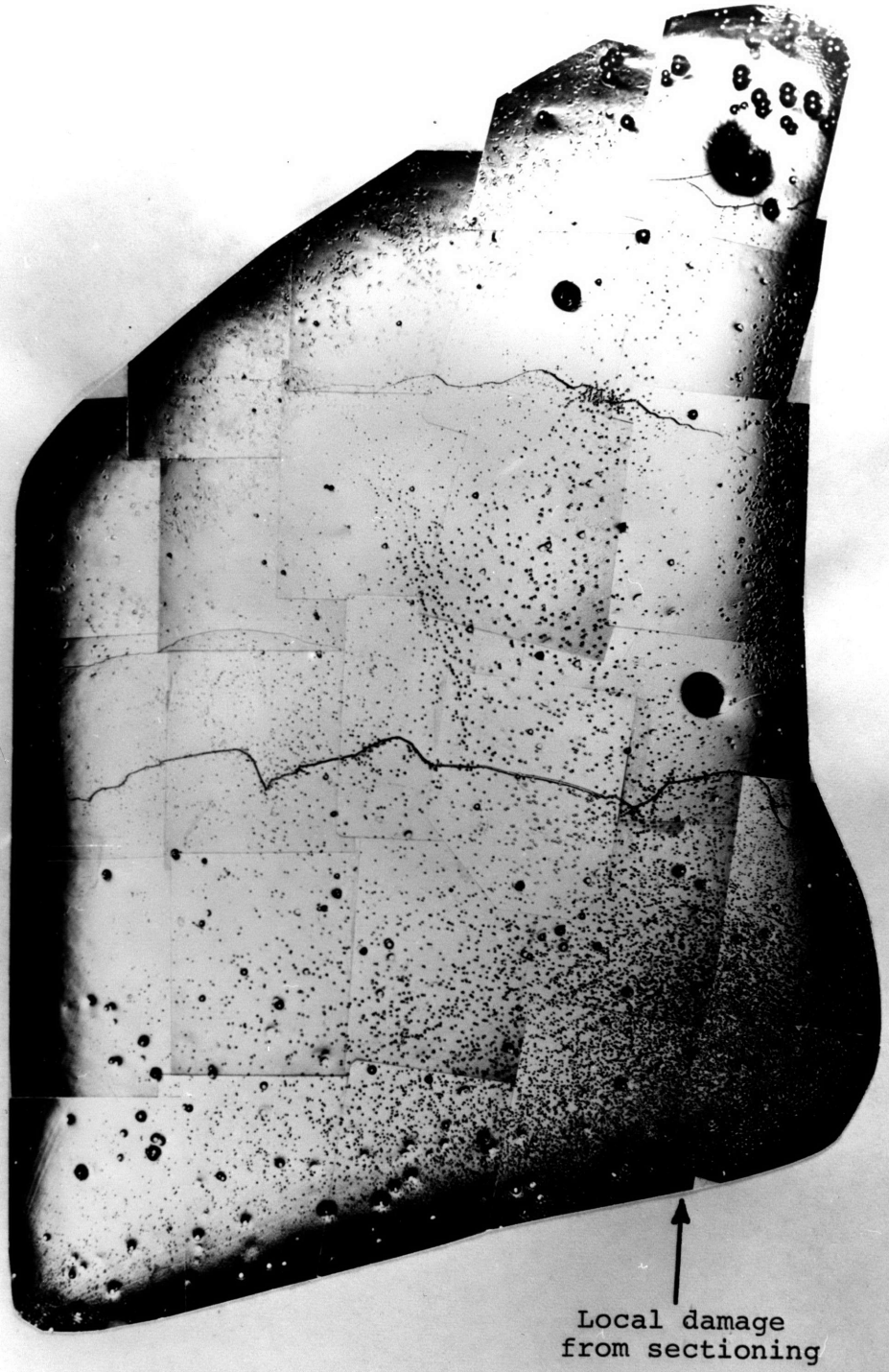

FIGURE 3.2-2a THE PRIMARY PLANE, ANNEALED (25X)

FIGURE 3.2-2b THE PRIMARY PLANE, 30 G/MM^2 PRESTRESS (25X)

FIGURE 3.2-2c THE PRIMARY PLANE, 60 G/MM^2 PRESTRESS (25X)

distance to the nearest neighbor was measured for 100 pits. The resulting histogram (Fig. 3.2-3) indicates conclusively that the forest dislocations are not randomly arranged since the nearest neighbor distances do not follow the predicted Poisson distribution, but show an excess of close dislocations.

As the stress is raised a definite change occurs between 50 and 60 g/mm^2 indicating a transition to stage II. At 50 g/mm^2 there is still a low density with loosely packed clusters. The appearance is similar to 30 g/mm^2 if the magnification of photographs taken at the two stresses is adjusted to give the same apparent density. At 60 g/mm^2 the clusters are more numerous and closely packed with a strong tendency to form elongated chains. While these chains are profuse in some regions, they do not exist in others (Fig. 3.2-4). No correlation was found between the existence of chains and bending in the crystal.

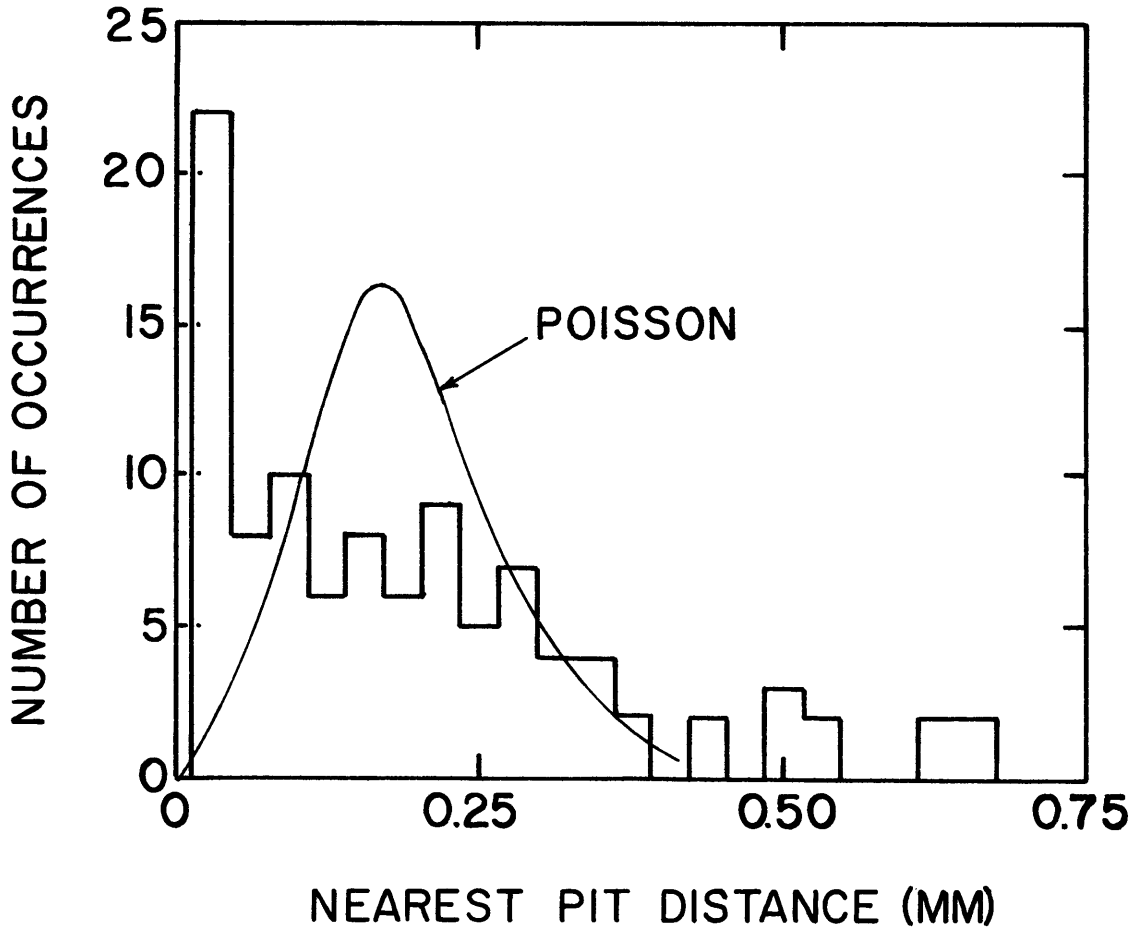

FIGURE 3.2-3 THE DISTRIBUTION OF NEAREST NEIGHBOR DISTANCES FOR ETCH PITS ON THE PRIMARY PLANE

3.3 ORIENTATION SENSITIVITY OF THE DISLOCATION DENSITY OBSERVATIONS OF PRIMARY DISLOCATIONS

Observations of the cross plane throughout easy glide indicate no significant differences due to a small change in orientation (Fig. 3.3-1). At all stresses sufficiently above yield the mean etch pit densities are almost exactly the same for both orientations specified in Figure 2-1. The only noticeable difference between the two is the extent of the error bars which indicates that a real variation in the spread of the local etch pit densities exists between these orientations. The range is greatest in the specimen most favorably oriented for laminar slip. The discrepancies between the two curves at very low stresses is probably not a real effect but more likely only a reflection of differences in the annealed structure of the individual crystals. The crystal having the higher etch pit density yielded at a lower stress and was more highly strained at 20 g/mm^2, the stress at sectioning.

The observations indicate that the rate of primary dislocation accumulation decreases throughout easy glide. An uncertainty in this effect results from the inability to resolve etch pits in the dense clusters which become very numerous as the stress increases. Although estimates of the dislocation density in the nuclei of these clusters were included in the etch pit counts, they are probably conservative. However, these estimates indicate that the unresolved nuclei contain about 15% of the primary dislocations and thus only a gross misestimate would cause significant errors in the

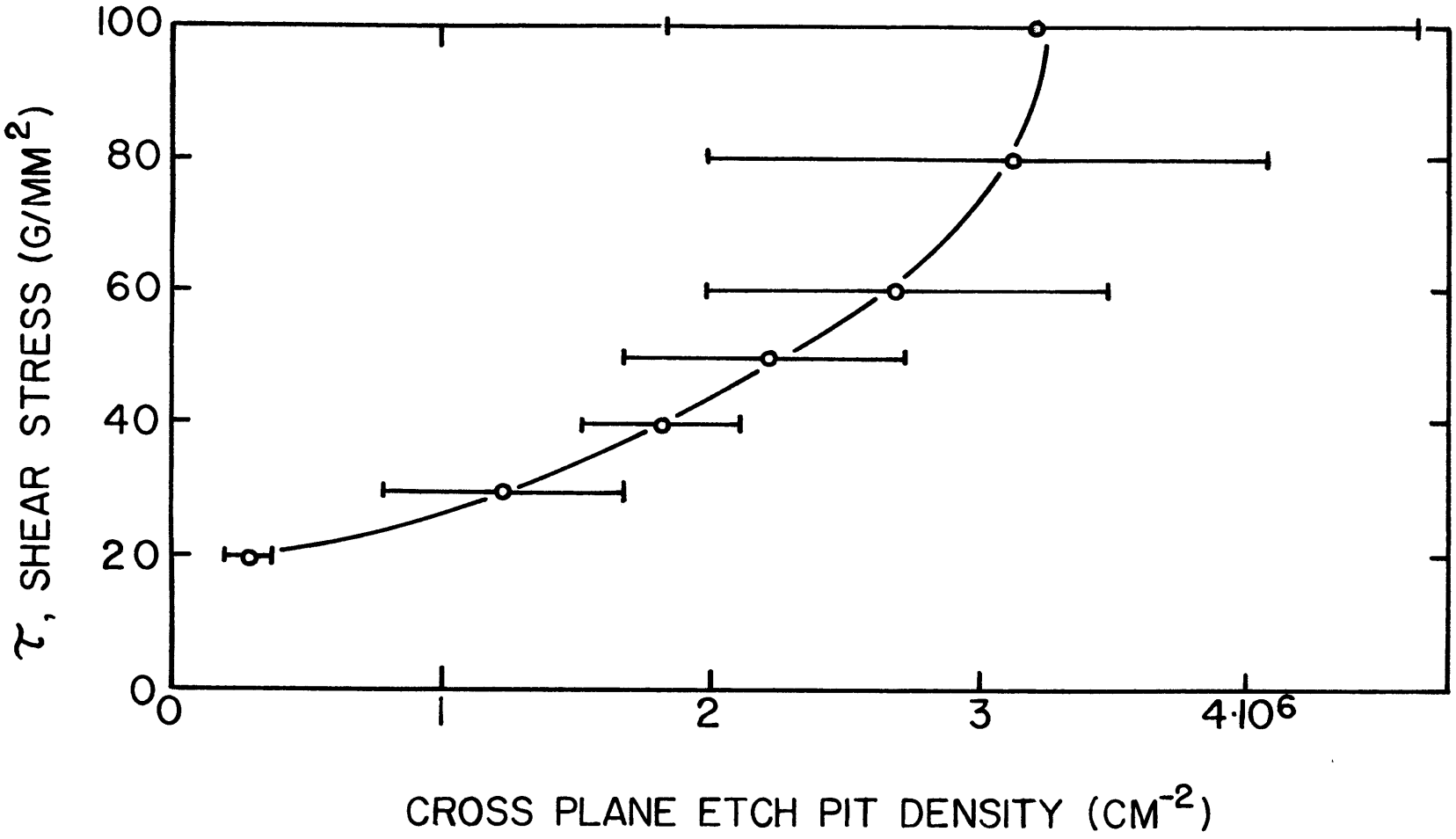

FIGURE 3.3-1 THE CROSS PLANE ETCH PIT DENSITY OF A CRYSTAL OPTIMALLY ORIENTED FOR EASY GLIDE

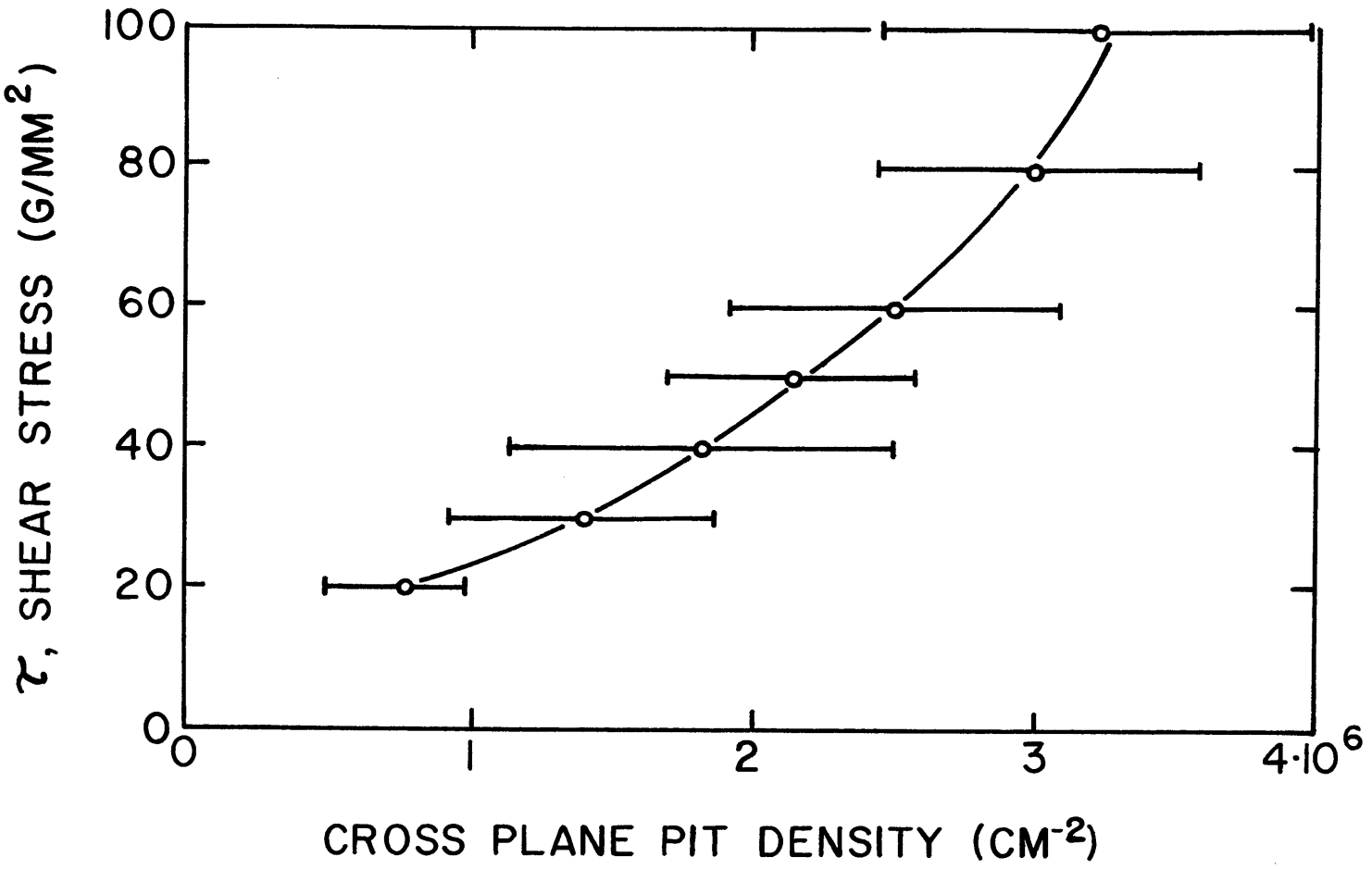

FIGURE 3.3-2 THE CROSS PLANE ETCH PIT DENSITY OF A CRYSTAL 5^0 FROM THE OPTIMUM ORIENTATION

total. The decreasing rate of accumulation must be a real effect which becomes especially pronounced in transition to stage II.

OBSERVATIONS OF FOREST DISLOCATIONS

The study of etch pit densities on the primary plane as functions of stress and orientation indicate several important phenomena. First, the accumulation of forest dislocations follows a simple power law of the form

$$N_f = c \cdot \tau^n$$

where τ is the shear stress on the primary slip system. Small changes in orientation produce no variation in the exponent but do result in a marked difference in the constant "c". For the most favored orientation the relation is

$$N_f = 3.25 \cdot (\tau)^{2.76 \pm 0.30}$$

and for the other orientation

$$N_f = 6.44 \cdot (\tau)^{2.76 \pm 0.30}$$

These relations not only hold throughout easy glide but also into tranistion to stage II, the limit of this investigation.

The exponent, 2.76, which differs from the value 2 found by Brydges (1966) for a crystal with forest dislocations produced by torsion, has significant implications. Many phenomena can be shown to produce hardening inversely proportional to the mean spacing of the obstacles and result in an exponent of 2. Lower exponents indicate that long range stresses exist while the observed value indicates some form of

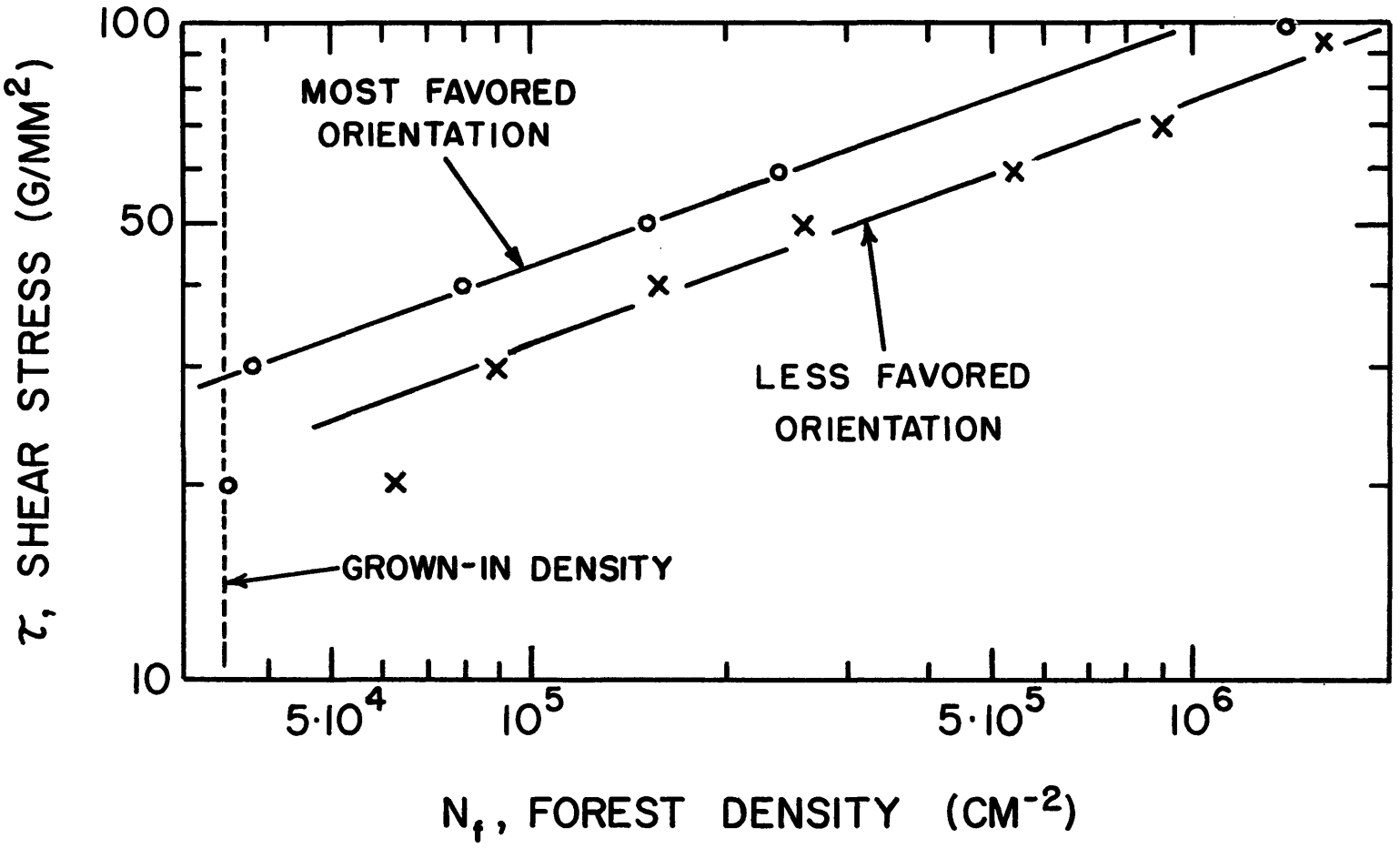

FIGURE 3.3-3 THE STRESS AND ORIENTATION DEPENDENCE OF THE FOREST ETCH PIT DENSITY

shielding or clustering.

The orientation sensitivity of the forest density is very strong. For comparison assume that for small orientation changes the same forest density will be produced with the same stress (τ_s) on the most highly favored slip system non-coplanar with the primary system. From Table 2 the ratios of this stress on the secondary system to the stress (τ) on the primary system for the two orientations are

$$\tau_s/\tau = 0.767 \qquad \text{(favored orientation)}$$

$$\tau_s/\tau = 0.822 \qquad \text{(other orientation)}$$

Since

$$N_f = c \cdot \tau^{2.76}$$

the assumed nonvariance of the forest density with constant shear stress on the secondary slip system leads to

$$c(\text{favored}) \cdot \{\tau(\text{favored})\}^{2.76} = c(\text{other}) \cdot \{\tau(\text{other})\}^{2.76}$$

$$\frac{c(\text{favored})}{c(\text{other})} = \left(\frac{\tau_s/0.822}{\tau_s/0.767}\right)^{2.76} = 0.933^{2.76} = 0.826 \ .$$

However, the measured ratio is

$$\frac{c(\text{favored})}{c(\text{other})} = \frac{3.25}{6.44} = 0.505 \ .$$

This indicates that small variations from the ideal easy glide orientation cause the observed forest density to increase much more rapidly than the difference due to the change in resolved shear stress on the secondary systems.

3.4 DETERMINATION OF THE ACTIVATION PARAMETERS

To devise a method for determining the activation parameters, a thought experiment was performed to predict the shape of the free energy - stress curve so that a suitable test might be conceived. In a crystal with only a single dislocation reversibly forced against one obstacle, Argon, Ashby, and Kocks (1971) considered the fundamental interaction of the dislocation with the obstacle using the Helmholtz free energy (F) of the crystal which changes with the area (A) the dislocation sweeps out in a manner shown by the schematic curve of Figure 3.4-1. The net effect of cutting through the obstacle where a certain amount of free energy production (such as jog formation) is possible is a small rise in free energy ΔF. Subsequently cutting another obstacle raises the free energy again.

Argon, Ashby, and Kocks have called the rate of change of the free energy of interaction (F) with the area (A) of a dislocation with a collection of identical obstacles equally spaced on a line the "glide resistance",

$$\sigma = \frac{1}{b} \cdot \left(\frac{\Delta F}{\Delta A}\right).$$

In reality the obstacles are not distributed uniformly in a plane so that a dislocation which is straight on the average will touch obstacles at spacings obeying different frequency distributions. The case of the motion of a single dislocation through random obstacles has been discussed by Labusch (1962), Foreman and Makin (1966), Kocks (1966), Dorn, Guyot, and

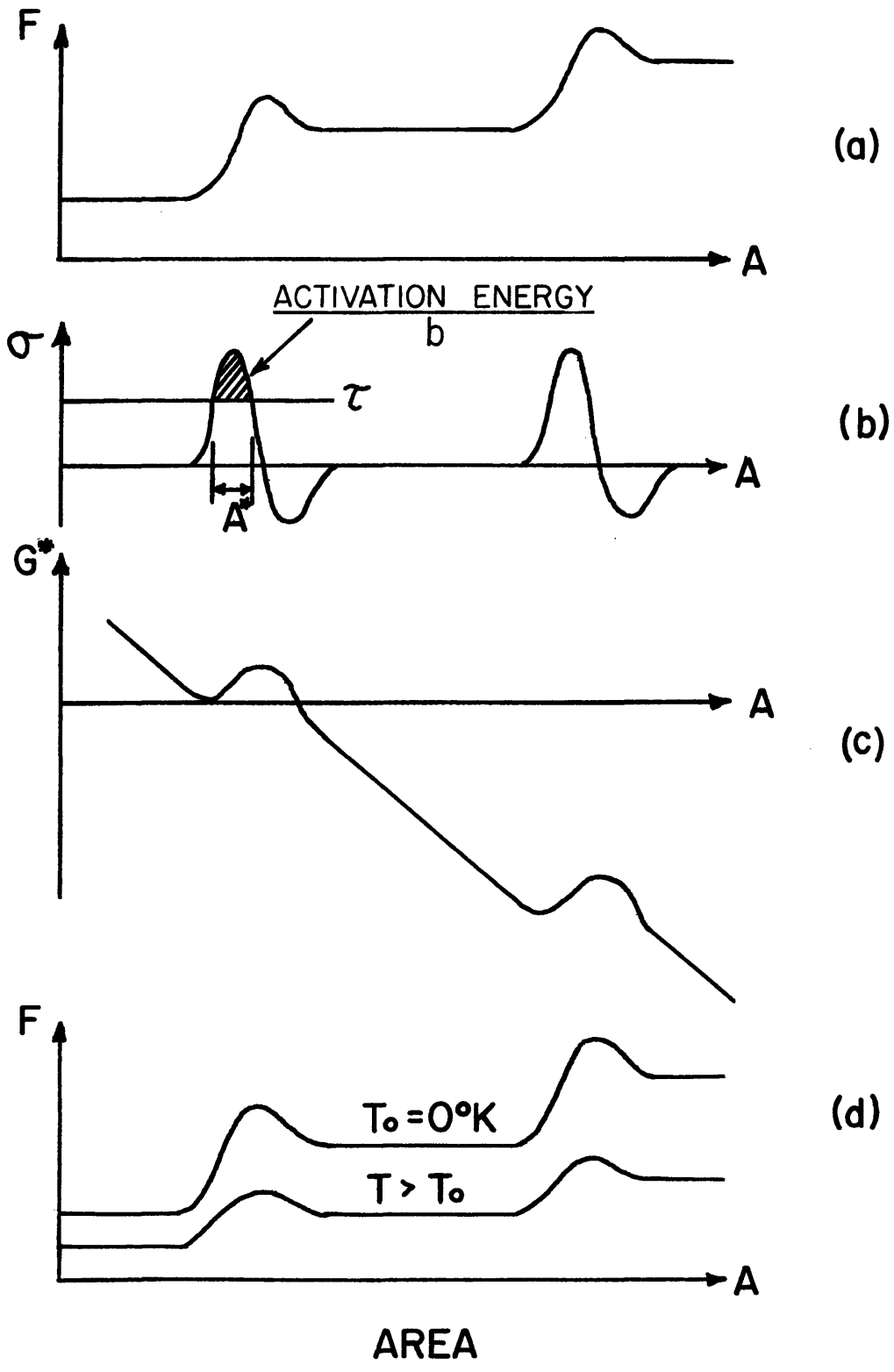

FIGURE 3.4-1 THE THERMODYNAMIC EFFECTS OF A DISLOCATION CUTTING AN OBSTACLE

Stefansky (1969), and others. The variability of the effective obstacle spacing along a dislocation reduces the stress for obstacle penetration by about 15%; this new stress has been called the "line-glide resistance" by Argon et al. In addition to the variability of obstacles along the line of the dislocation, there can be a variability of the line-glide resistance in the direction of motion of the dislocation, the long wave length forms of which can be smoothed by cooperative motion of more than one dislocation. This effective resistance of the plane to steady slip by cooperative motion of groups of dislocations, termed by Argon et al. as the "slip-plane resistance", does not differ from the line glide resistance for random point obstacles of nearly uniform strength. At macroscopic plastic flow an additional complexity arises from the interaction of active slip planes, which according to Argon (1970) almost always produces destructive interference resulting in a "flow resistance" larger than the "slip-plane resistance". The main effect of the active slip plane interaction is a rise in the exponent of the stress dependence of the strain rate resulting from a stress dependence of the mobile dislocation density. According to Argon (1970) the change in the exponent cannot be greater than 2 and is fully accounted for in the statistical theory of easy glide (Argon and East (1968), and Argon (1969)). In summary, then, the flow resistance measured by the applied stress is only indirectly related to the characteristics of the internal obstacles and a strain rate change experiment of the type to be described

below can only measure the smoothed-out contour of an average equivalent obstacle.

Within the limitations discussed above it is possible to construct the relation between the Gibbs free energy (ΔG^*) and stress (τ) from the Helmholtz free energy - area curve. First, from the glide resistance

$$\sigma = \frac{1}{b} \cdot \left(\frac{\Delta F}{\Delta A^*}\right) \tag{1}$$

we get Figure 3.4-1b. By definition the difference between the Gibbs and Helmholtz free energies is

$$\Delta G^* \equiv \Delta F - \tau b \Delta A^*. \tag{2}$$

The applied stress (τ) is averaged over the obstacles and must supply at least enough energy to provide the net rise in free energy produced by cutting the obstacles. Subtracting $\tau b \Delta A^*$ from ΔF we get Figure 3.4-1c. Cross plotting ΔG^* and τ, the shape of the Gibbs free energy - stress curve is obtained (Fig. 3.4-2). It is necessary to select an origin for the stress axis that allows for two possible types of background stress which must be overcome for the process to procede at a measurable rate. There may be either a possible elastic background stress that is essentially constant over the volume of the local process or another set of thermally impenetrable obstacles holding the dislocation back along its length, in addition to the stress associated, on the average, with the local obstacles characterized by the free energy diagrams.

Referring again to the Helmholtz free energy - area

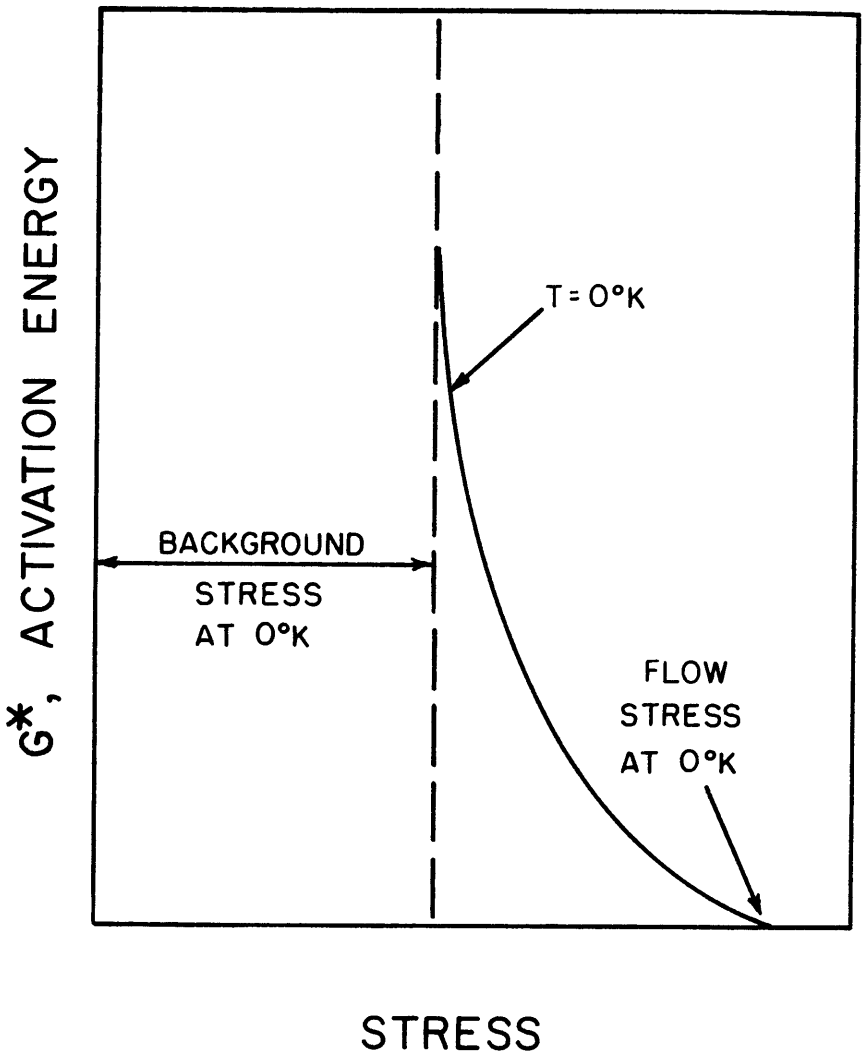

FIGURE 3.4-2 THE THEORETICALLY DERIVED STRESS DEPENDENCE OF THE ACTIVATION ENERGY

diagram, the effect of raising the temperature can be seen in Figure 3.4-1d. With increasing temperature the change in the entropy component reduces the free energy. We assume also that both of the background stresses are proportional to the shear modulus μ and that these likewise decrease as the temperature increases. Using these temperature dependences it is possible to demonstrate that the ΔG^*-τ curve will move left with increasing temperature (Fig. 3.4-3).

An experimental determination of the ΔG^*-τ curve for absolute zero is desired. The only measurable point on the curve is the flow stress at 0^0K since without thermal activation there is no flow at stresses $\tau<\tau_0$. To gain information about the remainder of the curve it is necessary to experiment at higher temperatures to provide differing amounts of thermal activation, at the expense of shifting the curve. At a higher temperature the decreased entropy term affecting the modulus causes the ΔG^*-τ curve to move left (Fig. 3.4-3). Simultaneously the effect of higher temperature introduces thermal energy so the measurements are also made at non-zero values of ΔG^*. Specifically, if the structure is assumed to remain constant (including the assumption of no mobile dislocation density change or an equivalence between the flow resistance and the slip plane resistance), the pre-exponential term of the rate equation

$$\dot{\varepsilon} = c \cdot \{e\}^{(-G^*/\{kT\})} \qquad (3)$$

is fixed and experiments performed at the same strain rate will give activation free energies proportional to kT, say

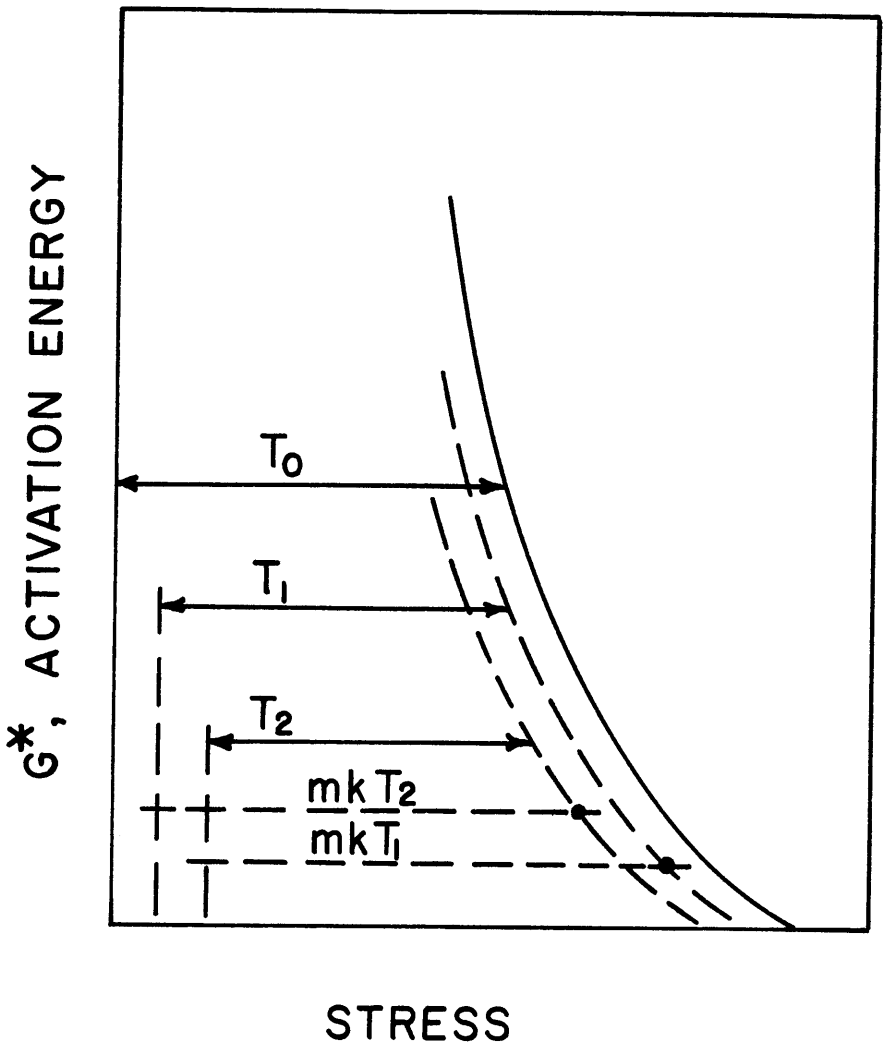

FIGURE 3.4-3 THE INTERDEPENDENCE OF TEMPERATURE AND ACTIVATION ENERGY

mkT (Fig. 3.4-3). By using these relations it is possible to construct the free energy curve at 0^0K from experiments executed at several temperatures.

After performing several creep experiments which gave non-repeatable results, a method to decrease the errors was sought. Since most errors arose from not being exactly at the flow condition when the creep test commenced, the obvious solution was to force this condition on the specimen by having some creep at constant stress, suddenly adding a stress increment $\Delta\tau$, and observing the change in the creep rate. This technique measures the activation area as demonstrated by the following analysis.

Using equation (3) we see that a sudden change in strain rate causes a change in the free energy

$$\frac{\dot{\varepsilon}_2}{\dot{\varepsilon}_1} = \{e\}^{\{-G^*_2/kT_2 + G^*_1/kT_1\}}$$

or

$$\Delta G^* = -kT\cdot\{\ln(\dot{\varepsilon}_2/\dot{\varepsilon}_1)\}_T \ . \qquad (4)$$

Combining the Maxwell relation

$$\left(\frac{\Delta G^*}{\Delta\tau}\right)_T = bA^*$$

with equation (4) we get

$$A^* = \frac{kT}{b}\left(\frac{\ln(\dot{\varepsilon}_2/\dot{\varepsilon}_1)}{\Delta\tau}\right)_T \ . \qquad (5)$$

Thus the activation area will be determined by this experiment.

The temperature dependence of the flow stress, necessary to scale data taken at other temperatures to absolute zero,

was determined in one set of experiments. Specimens with various initial properties resulting from nonuniformities in crystal growth and annealing may be made more similar by straining them to the same flow stress. Therefore, two groups of specimens, each containing samples of mechanically equivalent dislocation structure, were produced by prestressing at 25^0C to either 30 or 60 g/mm^2 at a rate of 1.0×10^{-4} sec^{-1}. Upon restressing at the same rate in constant temperature baths ranging from 77^0K to 460^0K, yield stresses were measured in this temperature interval (Fig. 3.4-4a and b). In a reverse experiment specimens were initially loaded at other temperatures to the prestress indicated by this graph for the particular test temperature and found to yield at 30 or 60 g/mm^2 when restressed at room temperature. This reversibility coupled with the proportionality between the curves at the two stresses agrees with the earlier assumption that the nature of the process does not change over the range of stress and temperature employed in these experiments.

The flow stress data must be corrected for the temperature variation of the anisotropic line energy of the dislocation. Lacking this information, the temperature variation of the modulus for the proper orientation will be substituted. The degree of anisotropy is indicated by the data of Overton and Gaffney (1955), which extends to 300^0K and shows a 66% difference between the temperature sensitivities of the C_{44} and C_{12} elastic constants. Making use of direction cosines to transform their measured elastic constants to the coordinate

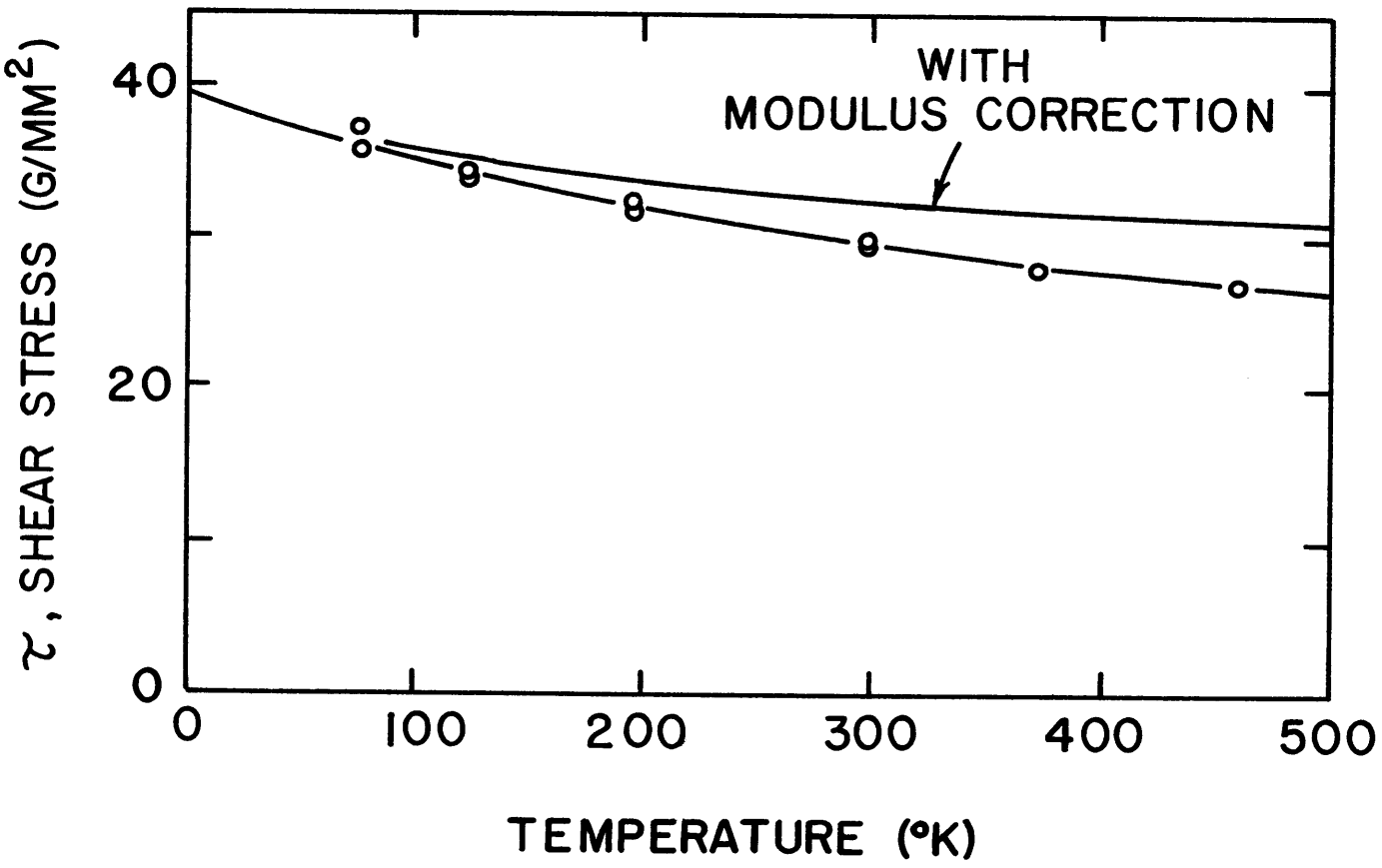

FIGURE 3.4-4a THE TEMPERATURE DEPENDENCE OF THE FLOW STRESS
(30 G/MM^2 PRESTRESS AT 273^{0}K)

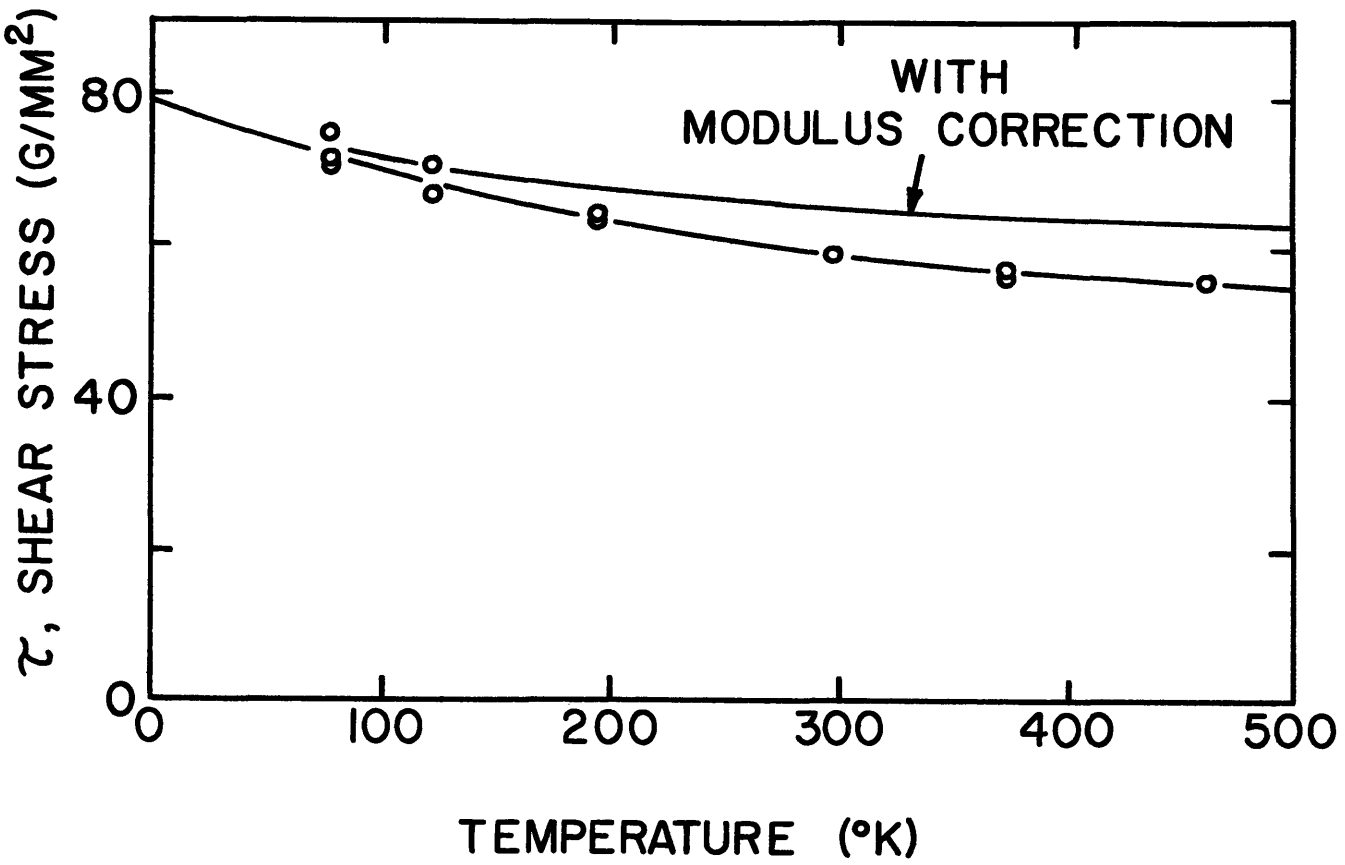

FIGURE 3.4-4b THE TEMPERATURE DEPENDENCE OF THE FLOW STRESS (60 G/MM^2 PRESTRESS AT 273^{0}K)

system corresponding to the (111)<110> slip system, we find that

$$C = \frac{1}{3}\cdot\left(C_{11}-C_{12}+C_{44}\right).$$

The variation of this term with temperature is slightly greater than that of any of the original elastic constants. Since data is available only below 300°K, it has been necessary to extrapolate to 460°K to plot all the flow stress-temperature measurements (Fig. 3.4-4). This will introduce some error but the total effect of this correction amounts to 8% and thus an inaccuracy in this term introduces much smaller errors in the final result.

The flow stress is highest at absolute zero where the obstacles to dislocation motion must be overcome entirely by the applied stress. However, as the temperature increases the stress is assisted by thermal activation in overcoming penetrable obstacles causing the observed reduction in the flow stress. Tests at high temperatures show that the flow stress levels off with temperature indicating that the thermally penetrable obstacles are no longer offering resistance. Although experiments were conducted to temperatures high enough to observe this, the exact stress at which the slope of the curve becomes zero is difficult to ascertain due to the extrapolation of the modulus correction. The factor applied to the data is reasonably accurate, causing at worst an uncertainty of 2% when relating the flow stress of impenetrable obstacles to absolute zero. The other extreme, the actual flow stress at absolute zero is likewise uncertain

due to the extrapolation from 77^0K and the increased experimental scatter in the low temperature tests. However, since the data is sufficiently accurate to introduce no significant errors when used in later calculations, the trouble of performing tests in liquid helium was deemed unnecessary.

The activation area, calculated by means of equation (5) using creep test data taken at a constant base stress and involving an almost constant stress increment $\Delta\tau$, is shown in Figures 3.4-5a and b. The increased scatter at higher temperatures is the result of irregular thermal drift in the extensometer resulting from rising warm air currents from the hot water bath. This effect was less troublesome at lower temperatures but is difficult to avoid when using the highly sensitive instrumentation necessary to measure small strains. Table 4 shows the actual values of the strain rates before and after adding the load increment, indicating that the initial strain rates are not repetitive. Due to the difficulty of regulating the strain rate exactly during the 0.1 second preceding the test and the secondary nature of such differences after their effect is included in the calculation, no attempt was made to automatically govern this rate.

The shape of the activation area - temperature curves results both from the T in the numerator of the equation for A* and from a variation in the instantaneous creep rate change with temperature. The nearly identical nature of the results at 30 and 60 g/mm^2 is further justification for the assumption that no change occurs in the nature of the deformation process.

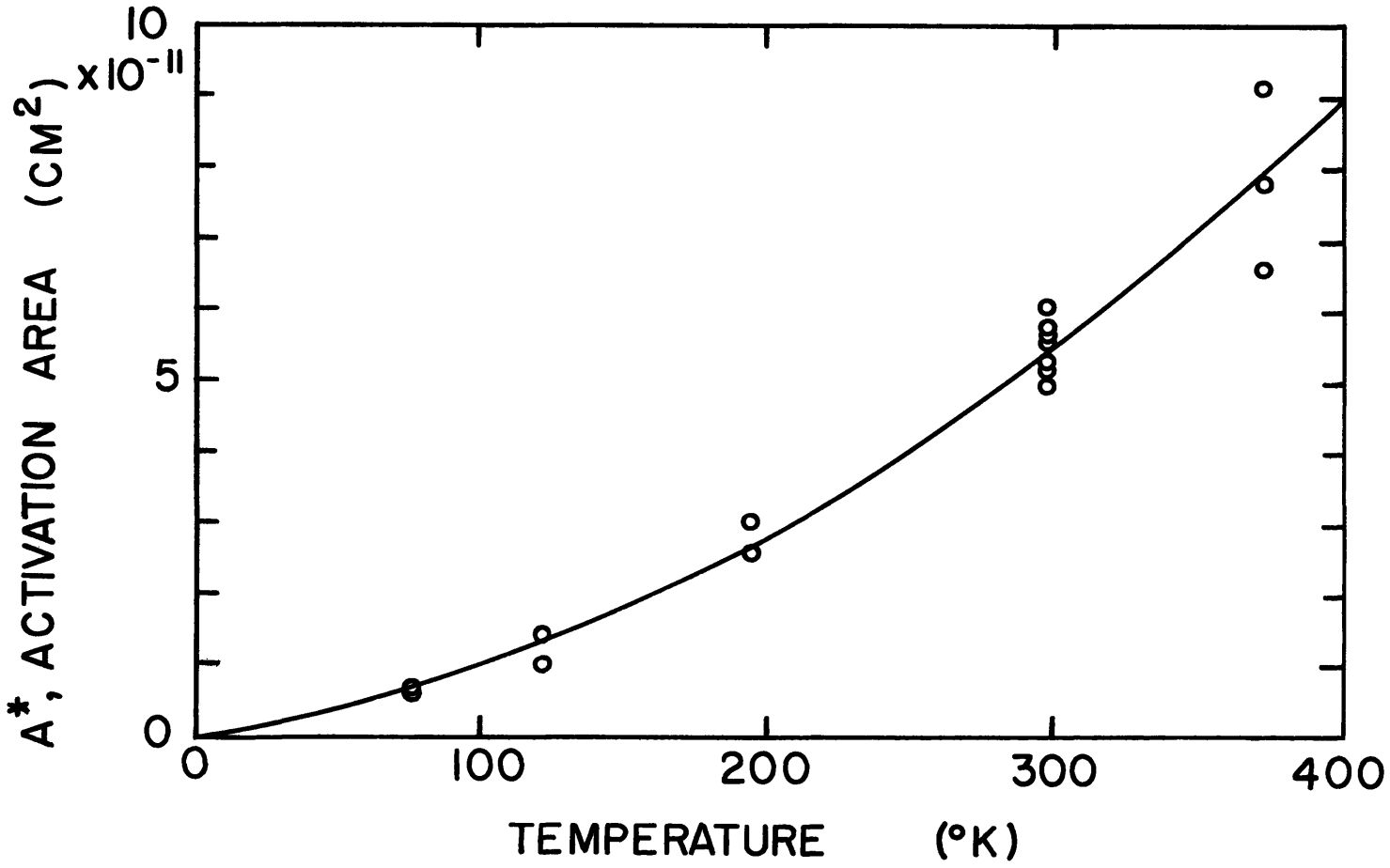

FIGURE 3.4-5a THE ACTIVATION AREA MEASURED AT SEVERAL TEMPERATURES (30 G/MM^2 PRESTRESS AT 273^{0}K)

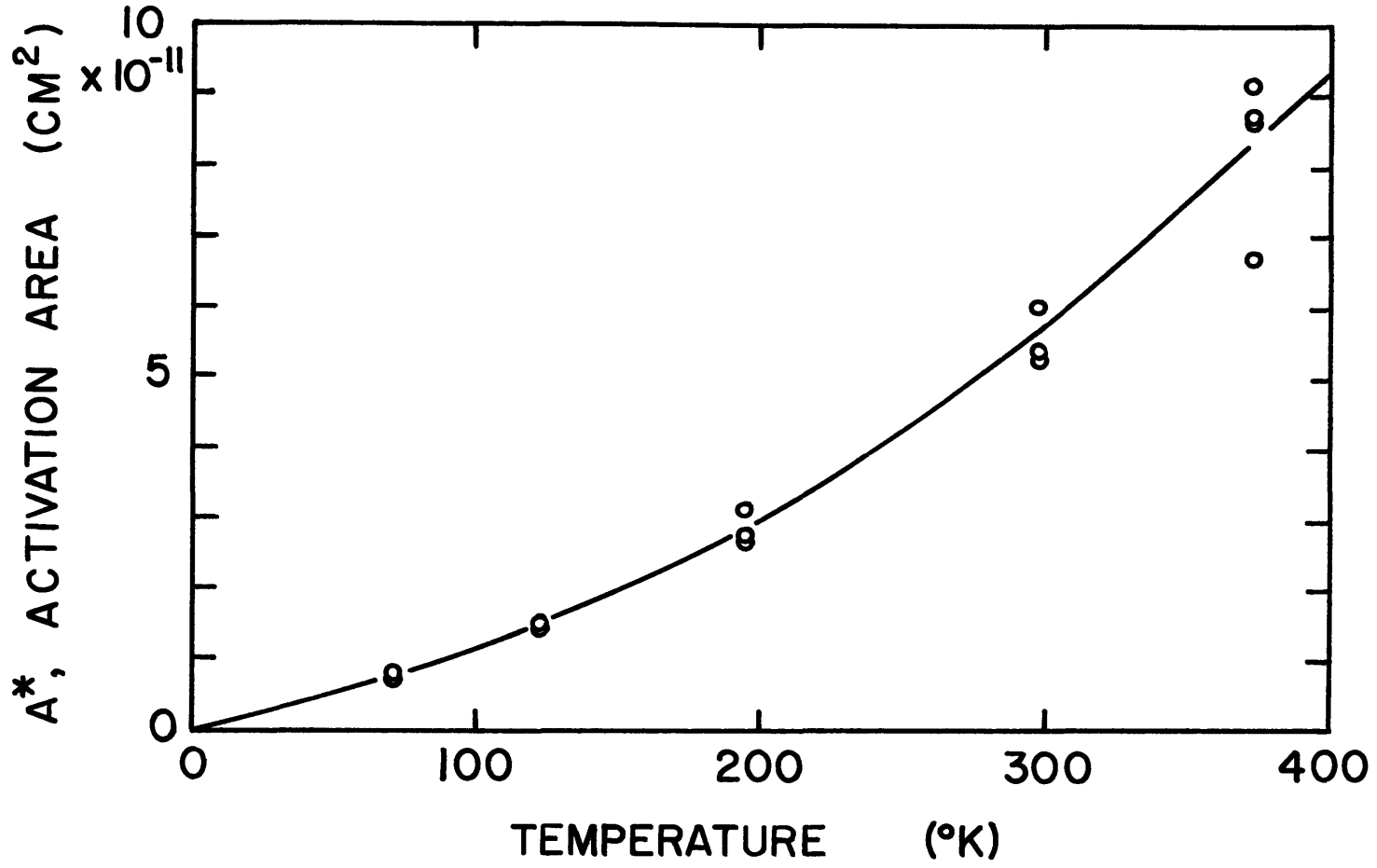

FIGURE 3.4-5b THE ACTIVATION AREA MEASURED AT SEVERAL TEMPERATURES (60 G/MM^2 PRESTRESS AT 273^{0}K)

TABLE 4 CREEP TEST DATA

SPECIMEN NUMBER	$\dot{\varepsilon}_1$ (sec^{-1})	$\dot{\varepsilon}_2$ (sec^{-1})	$\Delta\sigma_p$ (g/mm^2)	$\frac{Ln(\dot{\varepsilon}_2/\dot{\varepsilon}_1)}{\Delta\sigma_p}$ (mm^2/g)	A* (cm^2)
30 g/mm^2 PRESTRESS					
T = 77°K					
22/4	6.90×10^{-5}	8.11×10^{-4}	1.56	1.58	6.67×10^{-12}
22/8	2.00	1.40	1.39	1.40	5.93
T = 123°K					
22/9	1.26×10^{-5}	7.43×10^{-4}	1.85	2.20	1.49×10^{-11}
22/10	4.40	4.88	1.60	1.50	1.02
T = 195°K					
21/19	1.62×10^{-5}	1.46×10^{-3}	1.56	2.89	3.09×10^{-11}
22/1	3.66	8.10	1.26	2.46	2.64
T = 298°K					
21/12	5.06×10^{-5}	2.53×10^{-3}	1.20	3.35	5.33×10^{-11}
21/13	10.8	5.10	1.03	3.75	6.13
21/16	5.29	3.68	1.39	3.06	5.00
21/17	5.10	3.67	1.20	3.57	5.82
21/17	4.70	3.24	1.33	3.17	5.20
21/17	10.1	3.34	1.02	3.43	5.62
21/17	6.73	2.73	1.07	3.45	5.66
T = 373°K					
22/17	2.41×10^{-6}	1.66×10^{-4}	0.94	4.50	9.19×10^{-11}
22/19	4.83	7.25	1.31	3.82	7.83
23/1	9.80	4.64	1.19	3.24	6.64
60 g/mm^2 PRESTRESS					
T = 77°K					
22/4	2.50×10^{-5}	1.94×10^{-4}	1.17	1.75	7.41×10^{-11}
22/8	5.55	3.12	0.99	1.88	7.94
T = 123°K					
21/10	2.65×10^{-5}	3.06×10^{-4}	1.11	2.21	1.49×10^{-11}
22/9	0.64	1.76	1.53	2.17	1.46
T = 195°K					
21/7	1.84×10^{-5}	5.76×10^{-4}	1.17	2.94	3.14×10^{-11}
22/1	1.68	4.33	1.27	2.56	2.74
22/3	1.07	2.74	1.27	2.55	2.72
T = 298°K					
21/12	1.68×10^{-5}	2.99×10^{-3}	1.57	3.30	5.39×10^{-11}
21/13	0.94	1.36	1.36	3.66	6.00
21/16	2.36	1.64	1.33	3.18	5.22
T = 373°K					
21/8	4.14×10^{-5}	2.24×10^{-3}	1.23	3.24	6.68×10^{-11}
22/13	1.21	0.65	0.94	4.15	8.67
22/19	0.68	0.73	1.11	4.22	8.62
23/1	0.69	0.82	1.07	4.46	9.13

By cross plotting the results for activation area and flow stress as functions of temperature the A^*-τ curve at absolute zero is obtained (Figs. 3.4-6a and b). This will be discussed shortly in conjunction with a theoretical development to determine the nature of the penetrable obstacles but is presently considered only in relation to the determination of the Gibbs free energy through integration:

$$\Delta G^* = b\int_{\tau}^{\tau_0} A^* \cdot d\tau \ .$$

The result, shown in Figures 3.4-7a and b, agrees with the expected behavior. It is readily seen that the thermally penetrable obstacles account for a maximum of 25% of the resistance to dislocation motion. The remainder could be due to either impenetrable obstacles or long range stresses. Since this graph provides no direct information on the strength of the obstacles or their density, no conclusions may be drawn immediately about the properties of the obstacles.

If this data is to be properly understood, it should be checked against a reasonable model for the dislocation behavior. As dislocations move through the lattice, they become pinned to obstacles which in this case are forest dislocations threading through the primary plane. Two types of interaction are possible between a primary dislocation and a forest dislocation in an F.C.C. crystal: repulsive and attractive. If two dislocations form an attractive junction during cutting they become so tightly bound that the forest dislocation acts as an impenetrable obstacle. On the other hand a repulsive

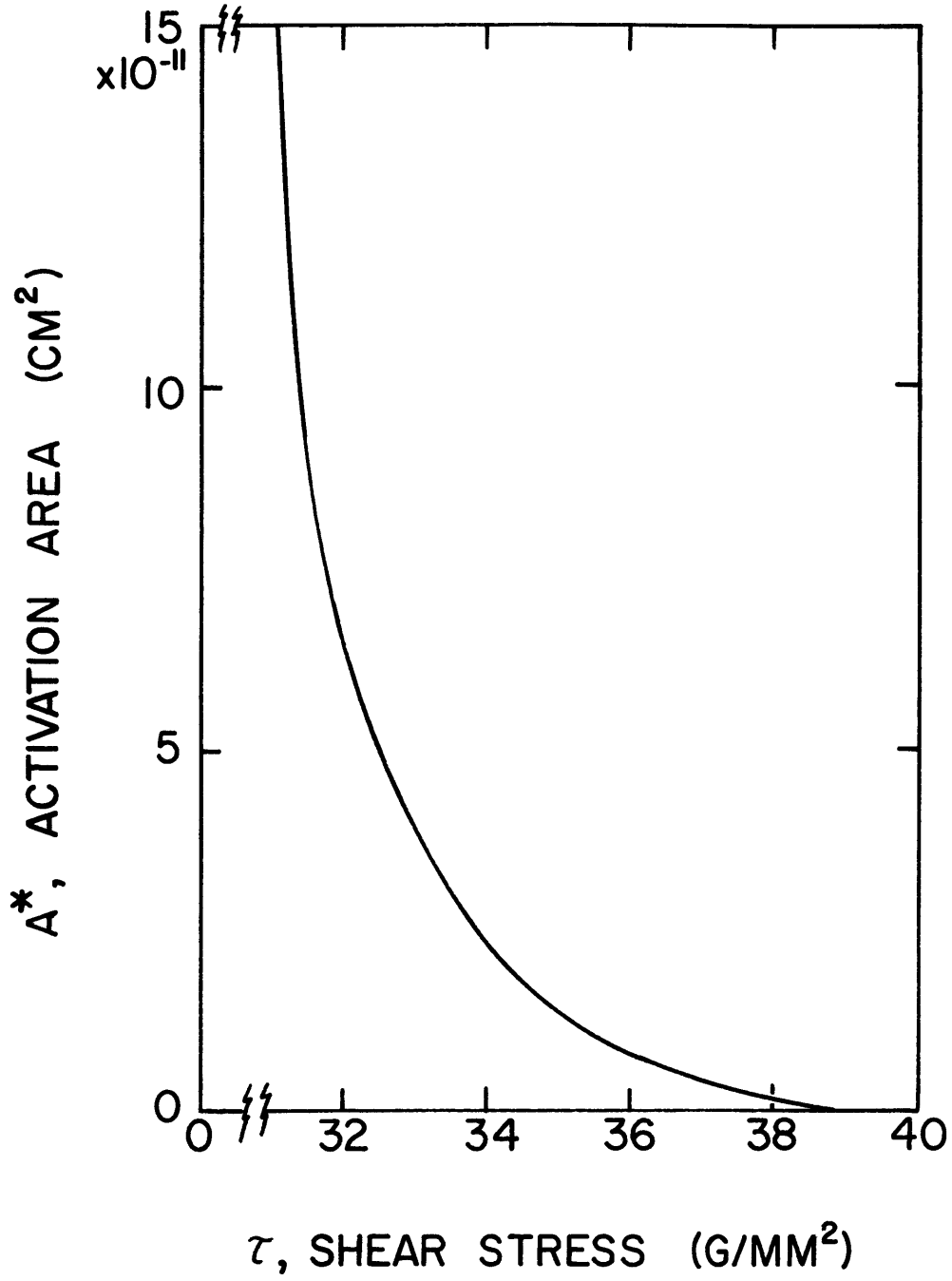

FIGURE 3.4-6a THE STRESS DEPENDENCE OF THE ACTIVATION AREA (30 G/MM^2 PRESTRESS AT 273^{0}K)

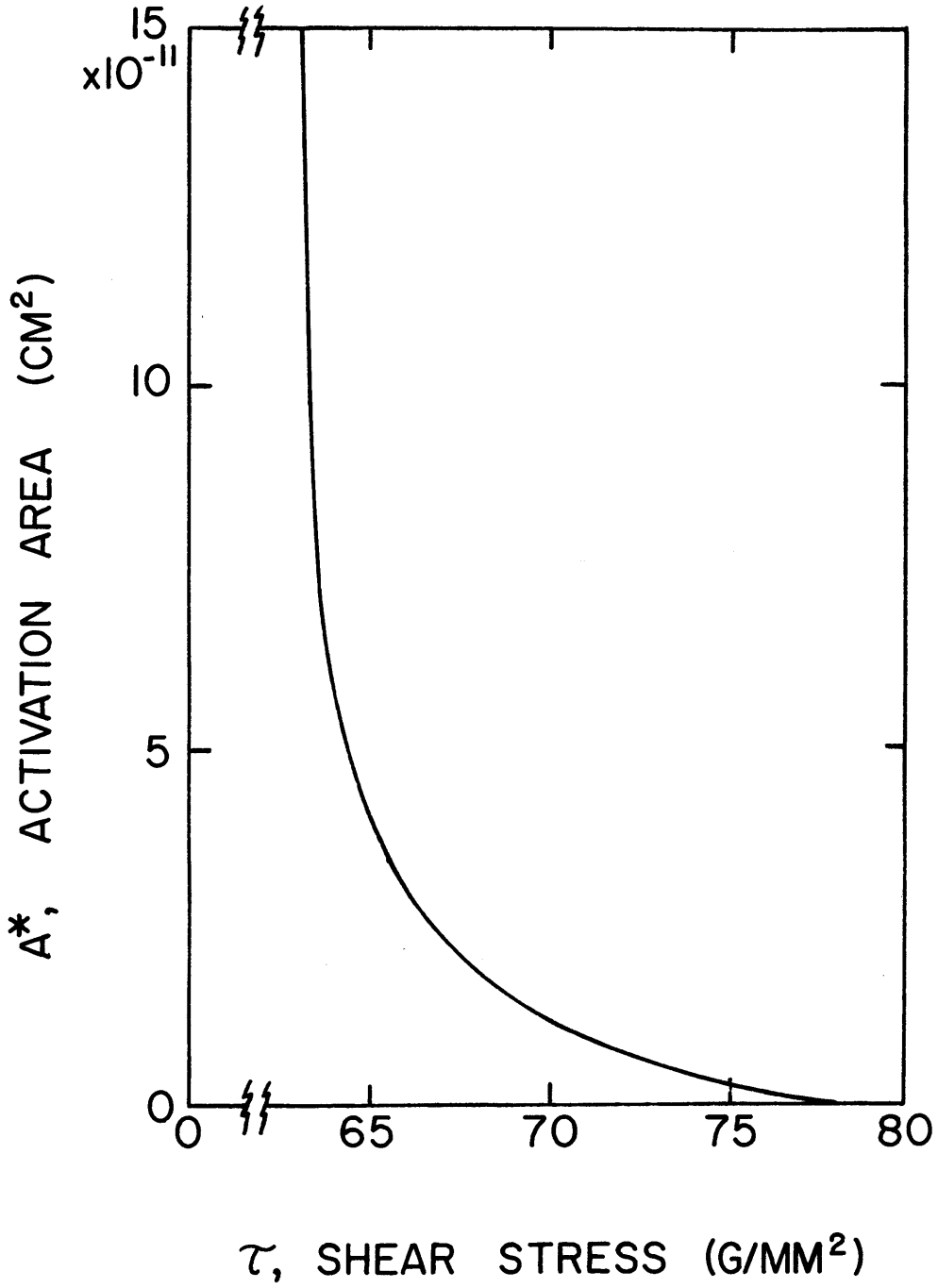

FIGURE 3.4-6b THE STRESS DEPENDENCE OF THE ACTIVATION AREA (60 G/MM^2 PRESTRESS AT 273^{0}K)

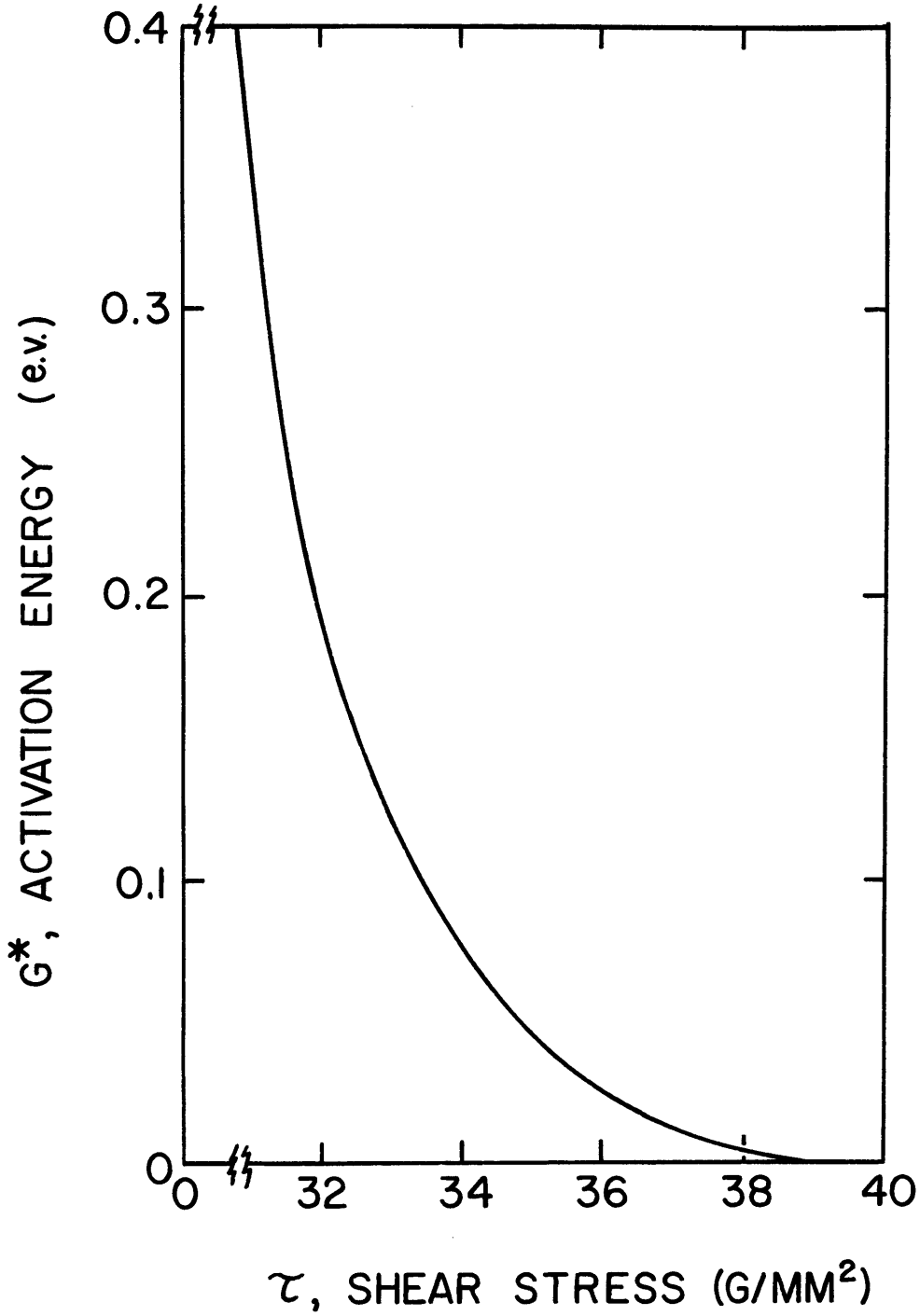

FIGURE 3.4-7a THE STRESS DEPENDENCE OF THE ACTIVATION ENERGY (30 G/MM^2 PRESTRESS AT 273^{0}K)

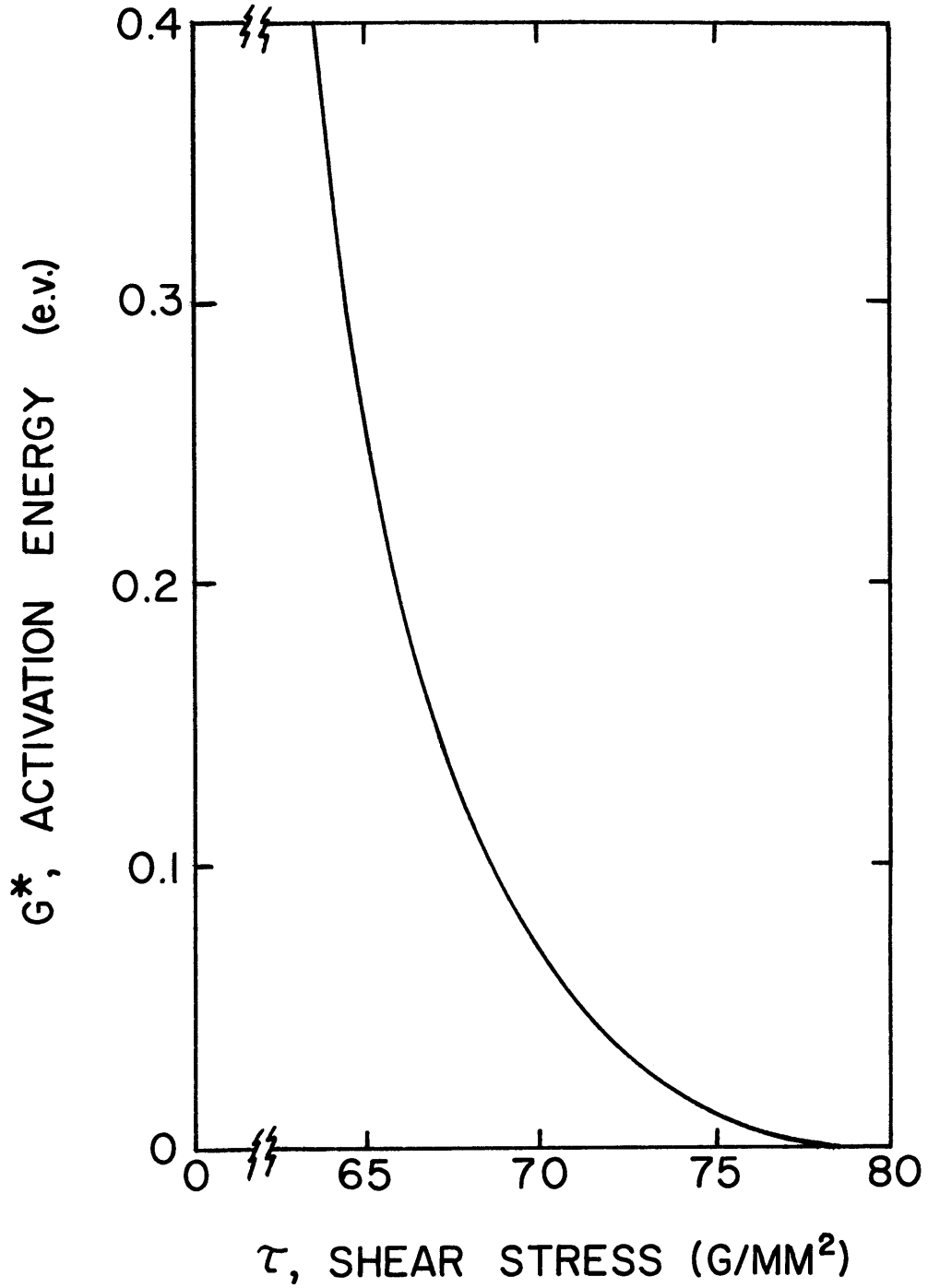

FIGURE 3.4-7b THE STRESS DEPENDENCE OF THE ACTIVATION ENERGY (60 G/MM^2 PRESTRESS AT 273^{0}K)

junction is much weaker and may be thermally penetrated. A theoretical investigation of all possible combinations was conducted by Baird and Gale (1965). Their results indicate that for F.C.C. crystals six out of thirteen interactions are attractive. The exact forest dislocation structure produced in easy glide is unknown. However, since no better information is available and since changing the strength of the penetrable obstacles is similar in its effect to making small changes in the relative density of the two obstacles, this ratio of attractive to repulsive junctions will be assumed to be the theoretical fraction of Baird and Gale, and the strength of the obstacles will be determined from the experimental data.

Developing a solution for a dislocation forest with roughly equal densities of penetrable and impenetrable obstacles, as suggested by the above, is somewhat more difficult than when one population dominates. Appendix C provides a detailed solution of this problem based on a model where the stress is gradually raised and penetrable obstacles are succesively cut until the entire array of obstacles is at the flow condition. If m is the number of times the dislocation has cut through penetrable obstacles as the stress is raised to the flow condition, then with equal densities of both obstacles,

$$\sqrt{\frac{6A_0}{\alpha}}\left(\frac{\sigma \cdot b}{2\alpha E}\right) = \frac{1}{2^{m+1}}\sqrt{\frac{(2^{m+1}-1)^3(6/5)^m}{\left(\frac{5}{3}\right)\left(\frac{12}{5}\right)^{m+1}-1-2^{m+1}}}\left[\frac{\left(\frac{5}{6}\right)\cdot\left(\frac{12}{5}\right)^{m+1}}{\left(\frac{5}{6}\right)\cdot\left(\frac{12}{5}\right)^{m+1}-1}\right]$$

where α is the cutting angle at the impenetrable obstacles

and A_0 is the mean area on the slip plane alloted to each obstacle. At higher temperatures where the penetrable junctions are weaker m becomes larger and τ decreases. The force on the penetrable obstacle is proportional to the cutting angle ϕ which is calculated from

$$\frac{\phi}{\alpha} = \frac{(5/6)^m}{\frac{n_2}{n_1}\left(1 - (5/6)^m\right) + 1}$$

The distance of penetration is computed from the mean spacing of obstacles along the dislocation, λ, divided into the measured activation area. In the case where there are equal numbers of penetrable and impenetrable obstacles

$$\lambda = \sqrt{\frac{6A_0}{\alpha}\left(\frac{5}{6}\right)^m\left(\frac{2 - \phi/\alpha}{\phi/\alpha}\right)}$$

Using the density of etch pits on the primary plane to determine A_0 and the creep test data for A*, we can obtain the force - distance curve shown in Figure 3.4-8.

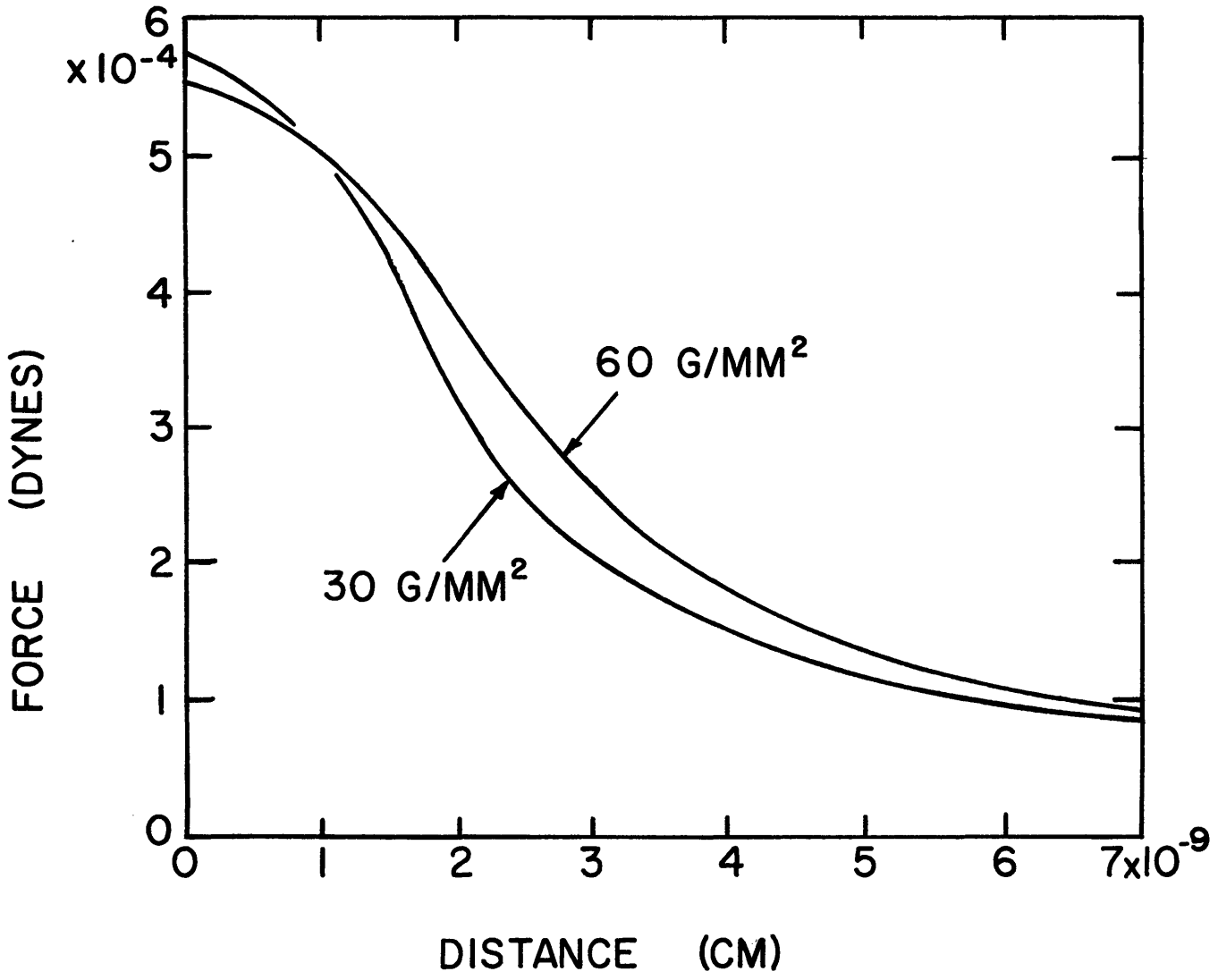

FIGURE 3.4-8 AVERAGE FORCE-DISTANCE CHARACTERISTIC OF THE PENETRABLE OBSTACLES

IV. DISCUSSION

The details of primary dislocation clustering show some agreement with the statistical theory of easy glide (Argon and East (1968), Argon (1969)) but there are discrepancies which result in part from simplifications in the theory or from the inadequacy of the etch pit technique when determining absolute dislocation densities.

First, the theory assumes that the number of clusters is constant. This is true only to a first approximation. A very large number of clusters indeed do exist after very little strain but this number roughly triples before transition to stage II. Newly developed clusters are much smaller than the original ones so their net effect on the crystal behavior is not fully in proportion to their number. Making allowances for this in the statistical theory would introduce considerable and perhaps unjustified complication.

The observed size of clusters may be compared to predictions by the theory. The width of the distribution $Q_{\mu n}$, the probability of dislocation capture, will be considered as the theoretical multipole size. This width is reasonably constant after μ (the number of dislocations in a multipole) exceeds 100. Assume $\mu = 500$. According to the theory, the capture distance (θ) at 60 g/mm^2 is 1.28×10^{-4} cm. With the value for the critical cross slip distance (δ) used in the theory (3×10^{-4} cm), the ratio θ/δ equals 0.43. From Figure 16.7 (Argon (1969)) the multipole width (2ξ) is seen to be 25δ or 7.5×10^{-3} cm. Values from Table 3 in Section

3.1 show the experimental result at 60 g/mm^2 to be 8 x 10^{-3} cm which is in excellent agreement.

However, the agreement is not so good when the absolute values of dislocation density are compared. For example, the theory expects a rate of dislocation accumulation with unit strain of

$$\frac{\partial N_p}{\partial \gamma} \simeq 10^9$$

whereas the result from etch pit counts is

$$\frac{\partial N_p}{\partial \gamma} \simeq 1.3 \times 10^8.$$

Likewise the theory expects up to 2000 dislocations per multipole at one to two percent strain. Observed values can reach several thousand dislocations per multipole but average only about 150 due to the continuous introduction of small new clusters. These discrepancies follow to some extent from the inability of etch pits to reveal all dislocations (Section II).

Another difference between the statistical theory and experiment is the observation of strong kink bands which are not included in the theory. These develop only in some regions and, near their ends, have a local influence on crystal behavior during transition to stage II. However, since they are observed only late in stage I and occur only in some regions, they do not affect most of easy glide and only have a limited effect at transition.

The array of forest dislocations is not random as proved by the distribution of nearest neighbor distances observed on

the primary plane. Instead there is an excess of very close pairs compared to the predicted Poisson distribution for a perfectly random sample having the same average etch pit density.

This result is not unexpected for two reasons. First the secondary dislocations multiply and the effect of their motion is indicated at the higher stresses by pile-ups occasionally seen on the primary plane. This motion should introduce some degree of clustering. However, there is also a more fundamental reason why a perfectly random distribution is not expected. Recent calculations by Kocks and Scattergood (1969) and Wilkens (1969) are in substantial agreement concerning the elastic interactions between randomly distributed dislocations in a finite body. Long range stress fields of the size of the body will exist if the array of dislocations is random. There is no shielding of stress fields. Despite the fact that the net interaction energy over the whole body is zero, local conditions cause the pairing of dislocations.

Observations of the cross plane etch pits provided data on primary dislocation densities. The orientation dependence of this density agrees with the statistical theory but the stress dependence is different. Since the resolved shear stress on the primary slip system is used as the measure of stress in these experiments, the recorded stresses for the two orientations are directly comparable when considering primary dislocations. The results show no significant

difference in the etch pit densities observed on the cross plane despite important differences in the forest density. Apparently the rate of primary dislocation multiplication is governed only by the stress on the primary slip system without regard to the forest density. Since the statistical theory of easy glide expected dislocation sources in multipoles and does not require a knowledge of the forest density to obtain the stress-strain curve, it agrees with these observations.

However, the observed stress dependence of the primary dislocation density does not agree with the theory. The statistical theory predicts that the strain increment associated with the addition of a single dislocation to a multipole is slightly less at higher stresses. Thus, for the same mean free path there should be a very small increase in the rate of dislocation accumulation with strain. This effect is enhanced, however, since the mean free path decreases. On the other hand the observations show the rate of dislocation accumulation decreasing with stress. Since some dislocations are not counted by the etch pit technique if clusters become very densely packed, the observations at high stresses are underestimates. Although it is difficult to ascertain whether this accounts for the entire discrepancy, it likely does not.

Realizing that the density of forest dislocations could not respond in proportion to the resolved shear stress on the most highly stressed non-coplanar slip system and lacking information on the exact behavior, the statistical theory

could only assume a behavior partially consistent with observations. The measurements reported here eliminated uncertainty in the relative changes in forest density with stress and small orientation variations. However, a theoretical explanation for the observations has not been found. The forest density is of the form

$$N_f = c \cdot \tau^{2.76}$$

where the constant "c" is much more orientation dependent than the stress on the secondary systems. The exponent has little or no dependence on orientation and is higher than the value of 2 which follows from many arguments for hardening, indicating some shielding of stress fields or clustering. Other observers (Brydges (1967b), Basinski and Basinski (1964)) have reported an exponent of 2 but their work was done at higher stresses and an examination of the Basinski paper shows a slightly higher exponent if only the lower stresses are considered.

The flow stress of mechanically equivalent specimens is temperature dependent near absolute zero but becomes nearly temperature independent above 400^0K. The thermally sensitive component supports 26% of the applied stress at absolute zero while the remainder constitutes a "background stress". Although this thermally independent portion may be the combined effect of long range stresses and thermally impenetrable obstacles, reasonable assumptions lead to the conclusion that the expected obstacles can account for the entire effect.

Since junctions between primary and forest dislocations may be either attractive or repulsive, the junctions will form impenetrable and penetrable obstacles. The exact ratio of the two types is unknown for the specific case of easy glide but the assumption of roughly equal densities has been made based on the 6:7 ratio reported by Baird and Gale (1965) for a random dislocation population. An error in this assumption changes the cutting angles at the two types of obstacles. The theoretical analysis of a dislocation passing through an array containing equal densities of both obstacles indicates that, when the thermally sensitive component of the flow stress is 26% of the total at absolute zero, the maximum cutting angle at the penetrable obstacles must be about 90% that at the impenetrable obstacles.

Although the available data should be sufficient to determine whether the activation process at the penetrable obstacles is a local process, there are several reasons why no definite conclusion may be reached. Using all available data leads to Figure 3.4-8 in which the force was calculated from the cutting angle at the penetrable obstacles while the displacement was derived by dividing the measured activation area by the spacing of obstacles on the dislocation line. Since, after correcting for the obstacle spacing, similar force-distance curves are computed for the penetrable obstacles, the activation does not appear to be a local process. However, this result cannot be relied upon for several reasons. First, the displacement axis is exceedingly sensitive to the

thermally independent component of the flow stress. For example, a 3% error in the data will shift the relative position of the two measured force-distance curves enough to make the activation independent of the obstacle spacing, thus implying local activation. This occurs if the flow stress measured at any temperature is proportional to the reference stress. Experimentally, two reference stresses in the ratio of 2:1 resulted in flow stresses in the ratio 2:1 (within 0.05%) when averaged over all temperatures but at 460^{0}K a 3% difference from the exact ratio is noted. This small quantity changes the conclusion from local to non-local activation.

Other problems are encountered. The computed cutting angle of almost 90^{0} is too large in light of recent, unpublished calculations by Scattergood and Kocks on the effect on the cutting angle of the interaction of the two arms of a dislocation on opposite sides of an obstacle of small width. However, this discrepancy is partially explained since the etch pit density is less than the actual dislocation density and, with flexible dislocations for obstacles, the dislocation can move and touch more obstacles than indicated by the simple analysis used here. The analysis, itself, is also deficient. It uses small angle approximations which may not be applicable and, since the observed forest density does not change as the square of the stress, gives different cutting forces for the two reference stresses. Therefore, a decisive solution concerning activation is not possible.

CONCLUSIONS

1) Several observations support the statistical theory of easy glide. According to the theory, clusters of primary dislocations govern the stress-strain relation without being significantly influenced by forest dislocations. Similarly, observations indicate that the density of primary dislocations is directly related to the stress without being influenced by a doubling of the forest density produced by a 5° orientation change. The observed average cluster size, 8×10^{-3} cm, and the small changes in this value throughout easy glide also agree with the theory. The number of clusters is not truly constant, as assumed by the theory, but this is not a bad approximation.

2) Although the statistical theory does not agree with all observations, some discrepancies may not be serious since the etch pit technique will neither determine absolute dislocation densities nor provide adequate resolution at the centers of dense clusters. The accumulation of cross plane etch pits with unit strain, 1.3×10^{-8} cm^{-2}, is 7 times less than the theoretical rate of primary dislocation accretion. This rate was found to decrease throughout easy glide, especially near transition to stage II, despite the nearly constant behavior expected by theory. One observation not predicted by the statistical theory is the formation of kink bands with spacings (in cm) related to the stress by

$$\tau = 39 + 1.55 \times 10^{14} (b/\ell)^2 \text{ g/mm}^2$$

3) Some observations more completely describe the deformation process and will permit an extension of the theory particularly where interactions with forest dislocations are concerned. The density of etch pits corresponding to forest dislocations varies as

$$N_f = C\tau^{2.76} \text{ cm}^{-2}$$

where "C" is strongly orientation dependent and equals 3.25 for a crystal most favorably oriented for laminar slip. This information will permit computation of temperature and strain rate sensitivities of the flow stress and hardening rate.

The process of cutting forest dislocations, which form both repulsive and attractive junctions with the primary dislocations, is also better understood. The junctions act as penetrable and impenetrable obstacles, the former supporting 26% of the applied stress at absolute zero and the remainder supported by the impenetrable junctions without the necessity of an additional long range stress. The activation area was found to have no dependence on the reference stress but to depend only on temperature. Using the analysis of Appendix C, the data is unable to differentiate between local activation of the penetrable obstacles or activation along the length of the dislocation up to the nearest obstacle.

Primary dislocations observed on the cross plane aggragate in several distinct cluster types. Since clusters of one type frequently predominate in one area, although other regions show several types coexisting, the same flow stress may be supported in many ways.

4) In addition to providing a more complete description of easy glide, the data gathered in the transition region sheds some light on hardening in stage II. No observable change occurred in the law governing forest dislocation multiplication while a rapid drop in the rate of primary dislocation accumulation was noted. With the exception of increased clustering of the forest dislocations, no other effect was seen. This implies that the forest eventually becomes dense enough to strongly effect the multiplication of primary dislocations and this change in the governing mechanism is responsible for the transition.

REFERENCES

Andrade, E.N. Da C., and Henderson, C., 1951, Phil. Trans., 244, 177.

Argon, A.S., 1969, "Physics of Strength and Plasticity", (M.I.T. Press), 217; 1970, Scripta Met., 4, 1001.

Argon, A.S., Ashby, M.F., and Kocks, U.F., 1971 (to be published).

Argon, A.S., and Brydges, W.T., 1968, Phil. Mag., 18, 817.

Argon, A.S., and East, G., 1968, Trans Jap Inst. Met., 9 (suppl.), 756.

Baird, J.D., and Gale , B., 1965, Phil. Trans. Royal Soc., 257, 553.

Basinski, Z.S., and Basinski, S.J., 1964, Phil. Mag., 9, 51.

Brydges, W.T., 1963, "Growth and Deformation of Magnesium Single Crystals", S.M. Thesis, M.I.T.; 1966, "The Early Stages of Plastic Flow in Copper", Ph.D. Thesis, M.I.T.; 1967a, J. Inst. Metals, 95, 223; 1967b, Phil. Mag., 15, 1079; 1968, J. Phys. Chem. Solids, 30, 1294.

Cottrell, A.H., 1953, "Dislocations and Plastic Flow in Crystals", (Oxford Press), 174.

Dorn, J.E., Guyot, P., and Stefansky, T., 1969, "Pysics of Strength and Plasticity", (M.I.T. Press) 133.

Foreman, A.J.E., and Makin, M.J., 1966, Phil. Mag., 14, 911.

Fourie, J.T., 1968, Phil. Mag., 17, 735

Frank, F.C., and Read, W.T., 1950, Phys. Rev., 79, 772.

Friedel, J., 1956, "Les Dislocations", (Gauthier-Villars), 140.

Johnston, W.G., and Gilman, J.J., 1959, J. Appl. Phys., 30, 129.

Kitajima, S., Ohta, M., and Kaieda, H., 1968, J. Japan Inst. Metals, 32,]64.

Kocks, U.F., 1966, Phil. Mag., 13, 541.

Kocks, U.F., and Scattergood, R.O., 1969, Acta Met., 17, 1161.

Kramer, I.R., 1965, Trans. AIME, 233, 1462.

Labusch, R., 1962, Z. Phys., 167, 452.

Livingston, J.D., 1960, J. Appl. Phys., 31, 1071; 1962, Acta Met., 10, 229.

Mader, S., 1957, Z. Phys., 149, 73.

Mott, N.F., 1953, Phil. Mag., 44, 742.

Nigam, A.K., 1967, "Strain Hardening in Ionic Crystals", S.M. Thesis, M.I.T.

Overton, W.C., and Gaffney, J., 1955, Phys. Rev., 98, 969.

Ruff, A.W., 1962, J. Appl. Phys., 33, 3392.

Seeger, A., 1957, "Dislocations and Mechanical Properties", (Wiley), 243.

Seeger, A., Kronmuller, H., Mader, S., and Trauble, H., 1961, Phil. Mag., 6, 639.

Taylor, G.I., 1934, Proc. Roy. Soc., A145, 362.

Wilkens, M., 1969, Acta Met., 17, 1155.

Young, F.W., 1966, "Proc. Int. Conf. on Crystal Growth", Boston, Ll.

Young, F.W., and Wilson, T.R., 1961, Rev. Sci. Instr., 32, 559.

APPENDIX A

CYCLIC ANNEALING

The grown-in dislocation density of 0.6-2 x 10^6 cm^{-2} could be reduced to 0.7-4 x 10^5 cm^{-2} by isothermal annealing at 1000^{0}C for five days (Figs. A-1 and A-2). With these densities Brydges (1966) reported yield stresses upwards of 31 g/mm^2. The scatter in some of his work is possibly due to the large variation in initial dislocation density since his highest forest densities after annealing correspond to flow stresses five times the yield of the best crystals used in this work. Realizing this, the decision was made to explore the method of cyclic annealing.

On the basis of an investigation of cyclic annealing on aluminum, Livingston (1962) tried to anneal copper single crystals by periodically switching off the furnace current so that the temperature ranged between 750^{0}C and 1050^{0}C each hour. After 100 cycles the dislocation density was 4 x 10^4 cm^{-2}. More recently Kitajima (1968) subjected a stationary specimen in an evacuated tube to a periodic temperature variation resulting from the repeated passage of a furnace with a strong thermal gradient. The temperature at a measured point off-center ranged smoothly from 800^{0}C to 1050^{0}C and dropped back to 880^{0}C before completing a cycle by the reverse sequence. A period with two maxima lasted one hour. Although the influence of changes in period or temperature range on annealing

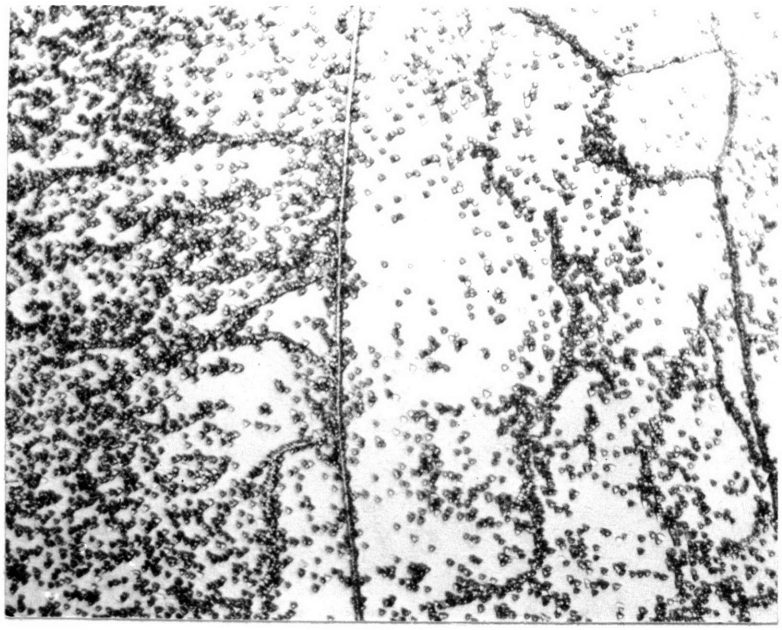

FIGURE A-1 CRYSTAL BEFORE ANNEALING ($N = 2.6 \times 10^{6} cm^{-2}$, 200X)

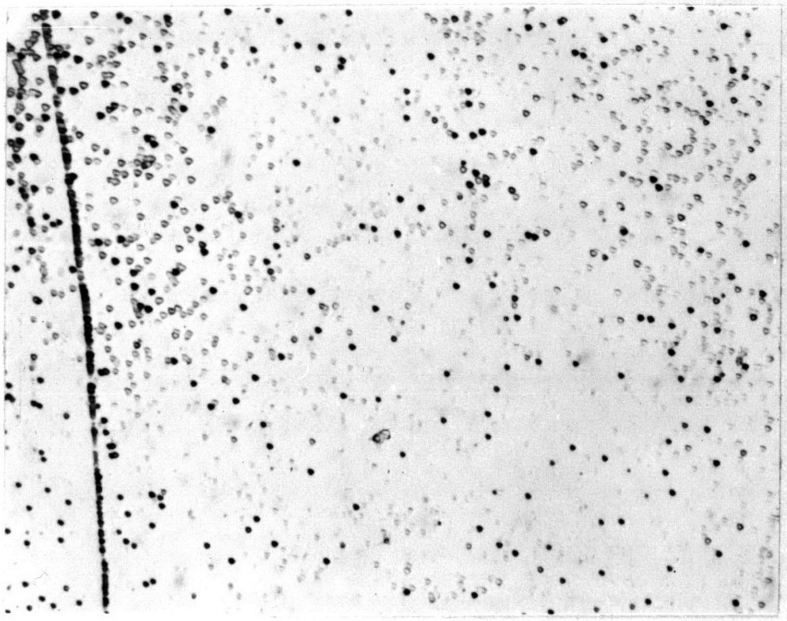

FIGURE A-2 CRYSTAL AFTER ISOTHERMAL ANNEALING AT $1000^{0}C$ FOR 119 HOURS ($N = 3 \times 10^{5} cm^{-2}$, 200X)

was not reported, it was shown that dislocation densities of 10^4 cm^{-2} could be achieved in 24 hours with further improvement to 10^3 cm^{-2} within 216 hours.

An experimental furnace with an unknown temperature distribution was constructed and first tried with a travel of 6 inches and a round trip period of 82 minutes for a full week with a peak temperature of 1000^0C. This produced a density of 1.2×10^5 cm^{-2} (Fig. A-3) which could have been obtained more readily by isothermal annealing. Feeling that a 6 inch travel did not move the specimen out of a fairly constant temperature region in the center of the furnace, the stroke was increased to 8 inches at the expense of lengthening the period. This small change caused the density to drop to 3×10^4 cm^{-2} in 117 hours of annealing (Fig. A-4). Since more experiments of a similar nature proved that this method is superior to isothermal annealing, a larger furnace capable of annealing five specimens simultaneously was constructed. A thermocouple in a graphite boat supporting the crystals within the furnace was used to obtain a steady state temperature profile (Fig. A-5) which indicated the stroke length necessary to match the conditions specified by Kitajima. The drive rate of the furnace was then set to give a one hour period with two maxima. However, in operation the steady state temperature profile is never realized. The actual temperature variation at one point along the length of a crystal is shown in Figure A-6.

Unfortunately the low density reported in the Japanese

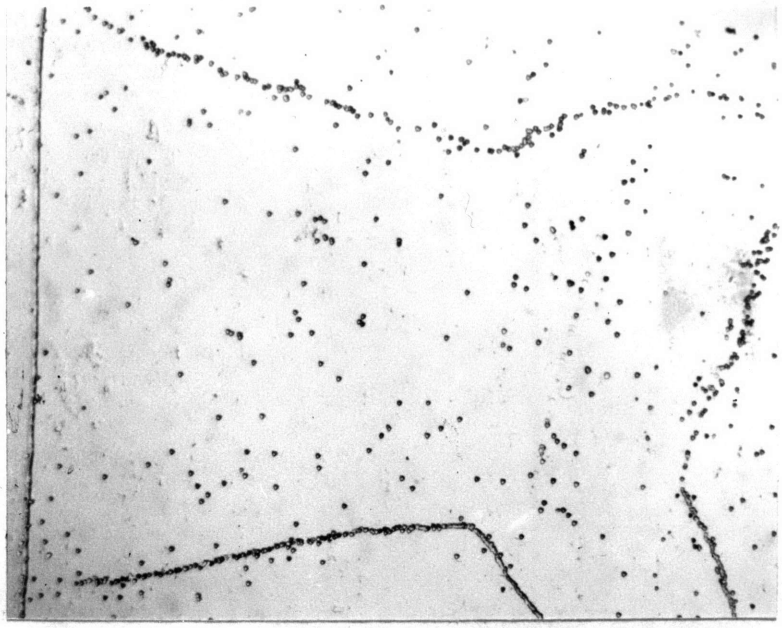

FIGURE A-3 CRYSTAL AFTER CYCLIC ANNEALING AT 1000°C FOR 159 HOURS (15cm Stroke in Prototype Furnace, N = 1.2 x $10^5 cm^{-2}$, 200X)

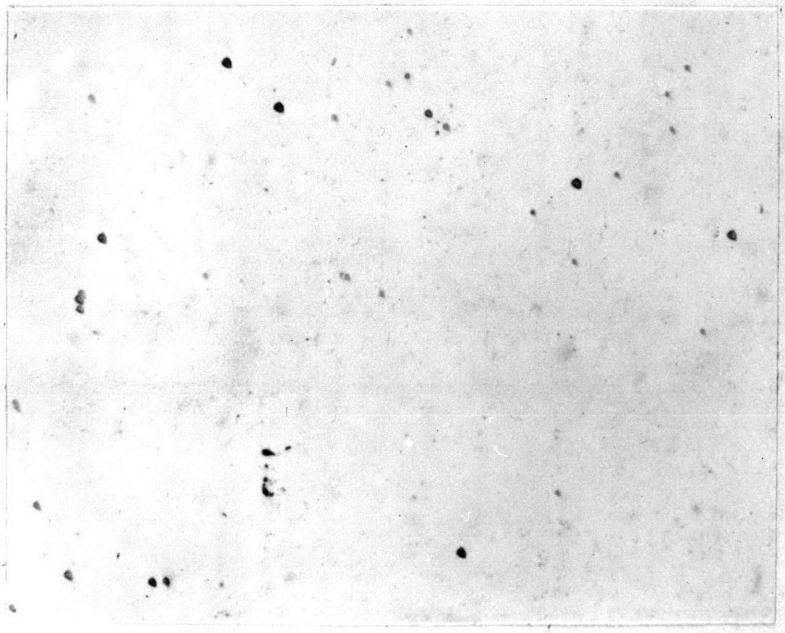

FIGURE A-4 CRYSTAL AFTER CYCLIC ANNEALING AT 1000°C FOR 117 HOURS (20.3cm Stroke in Prototype Furnace, N = 1.6 x $10^4 cm^{-2}$, 200X)

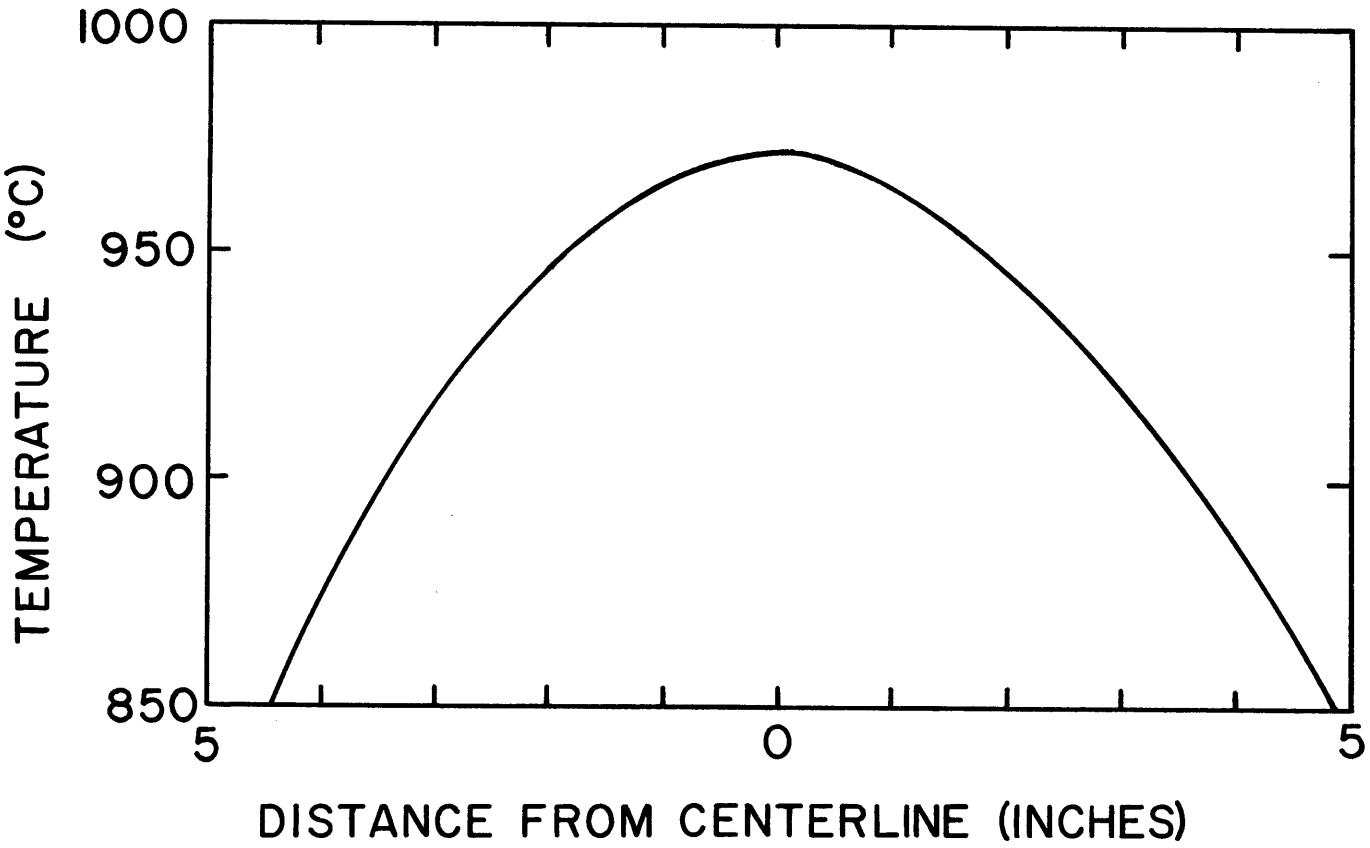

FIGURE A-5 TEMPERATURE PROFILE OF THE ANNEALING FURNACE

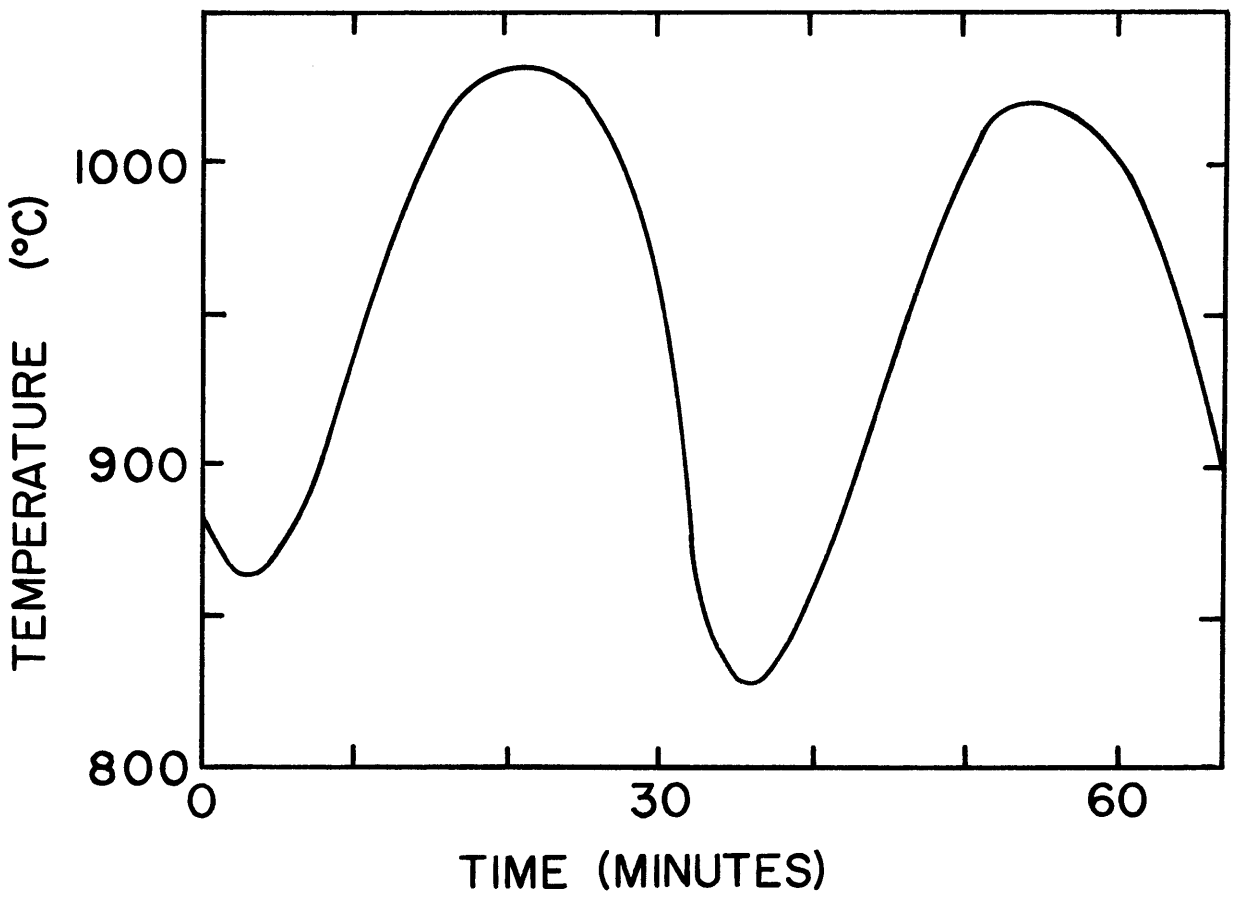

FIGURE A-6 ONE TEMPERATURE CYCLE IN THE ANNEALING FURNACE
(42 CM TRAVEL)

paper could not be reproduced but nevertheless the crystals were greatly improved with densities of 1-3 x 10^4 cm^{-2} and yield points of 9-25 g/mm^2. Occasionally large areas are observed with very low densities (3 x 10^3 cm^{-2}) and others, usually associated with a small subgrain, with locally high densities.

APPENDIX B

SECTIONING

Studies of the primary plane dislocation density and distribution as functions of stress and orientation require the sectioning of many crystals in a damage-free manner. Certainly any conventional machining process cannot be used and resort must be made to either spark-cutting or acid machining. The spark sectioning technique had been investigated by Brydges (1966) and shown to produce locally higher dislocation densities near the cut. Although it was shown that electropolishing removed this damaged surface layer, the possibility exists that problems might arise particularly when annealed or lightly prestressed crystals are sectioned. More reliance can be placed on the results if this damage was not introduced or at least was not so severe. Acid machining appeared to offer this possibility but techniques and equipment had to be developed to allow cuts to be made exactly along a (111) plane without requiring exorbitant amounts of labor or introducing significant damage. Using the findings of Young (1961) as a guide the following procedures have evolved.

A simple acid saw constructed of Plexiglass proved to be highly unsatisfactory. The main complaint, its inability to cut a straight line, resulted from a poorly designed device to apply tension to the thread and inadequate guides on either side of the specimen. The breaking of the cotton thread which

was attacked by the acid, the short lengths of thread on a spool which required frequent rethreading, and the deterioration of the plastic parts in the presence of acid all caused problems.

An improved acid saw (Fig. B-1) eliminated these difficulties while operating almost without attention. The two guides (a,b) in conjunction with the tensioning device (c) position the string sufficiently well to produce a straight cut. The cotton thread has been replaced with multi-filament Dacron which, although not absorbent, holds sufficient acid between the filaments especially in the presence of the droplet perpetually suspended beneath the upper guide. The advantages of Dacron are strength in an acid environment and a long, knot-free strand which runs for extended periods without attention. The parts of the saw are made from acid-resistant stainless steel alloys and Teflon which have shown no signs of deterioration. The crystal is held in a slotted soft-plastic fixture by elastic bands oriented so the cut will be made at the angle of the primary plane.

While being cut, the bulk of the specimen is protected from excess acid trickling over its surface by a coating of lacquer which covers the whole surface except for a narrow band where the cut is to be made. If this is not done, erosion of the surface near the cut prevents one from observing the primary plane near the original surface of the crystal. The jig holding the crystal is positioned such that the thread is bowed out of a straight line by its contact with the specimen

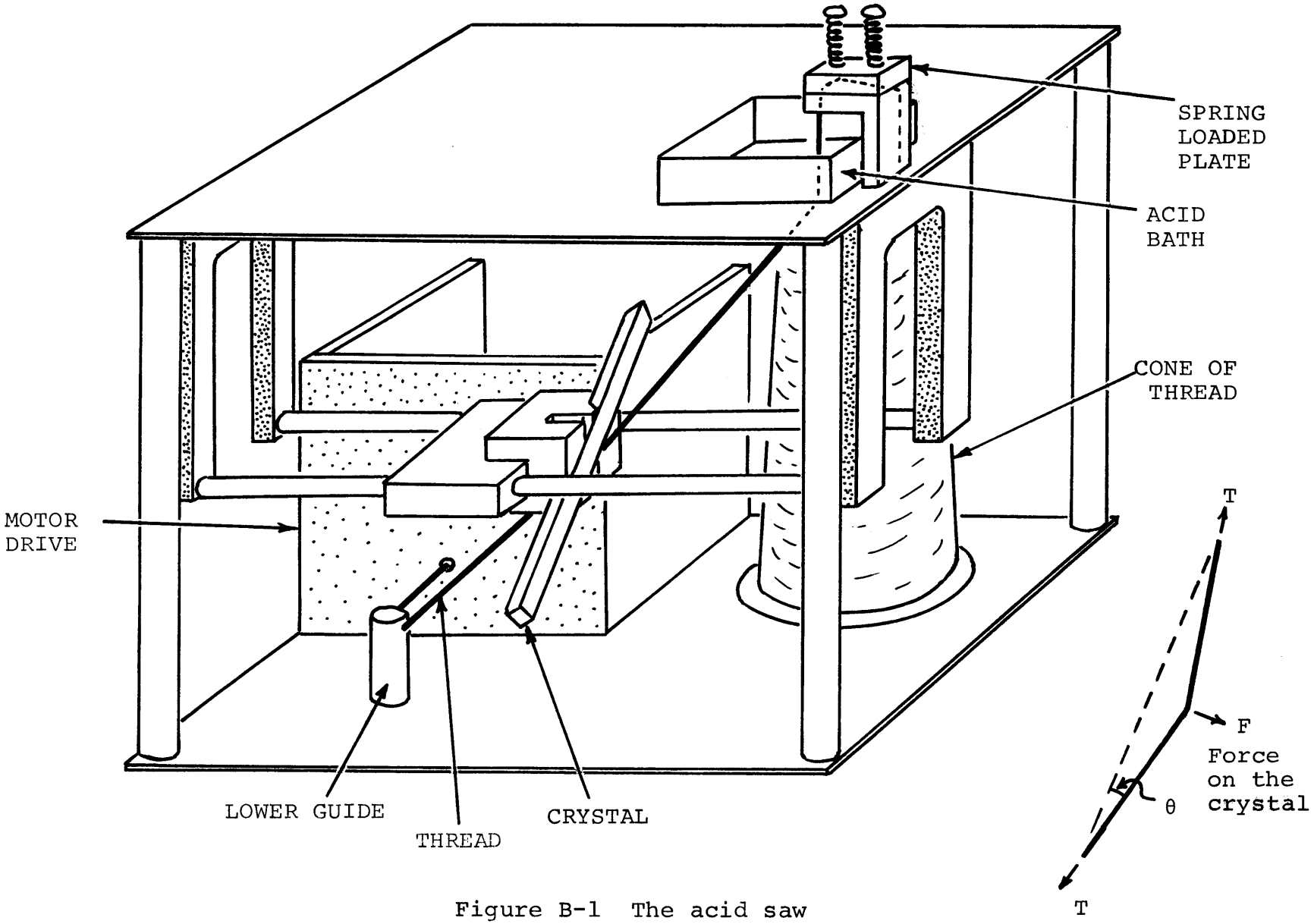

Figure B-1 The acid saw

providing a form of automatic feed as the cut progresses but at the same time offering the likelihood of damaging the crystal. It is obvious from Figure B-1 that the force on the crystal is

$$F = 2T \tan(\theta) \simeq T/5$$

which indicates that the 100 g tension in the thread produces a 20 g force on the crystal. The area of contact, being the thread diameter times the crystal thickness, is 0.9 mm so the stress is about 20 g/mm . This is considered to be an adequately low stress since it is not significantly higher than the yield stress of an annealed crystal and exists only in a region which will be dissolved by acid milling before the surface is observed. Indeed the milling process itself will introduce damage of equal or greater degree.

The operation of the acid miller is self evident from Figure B-2. The rotating cloth coated wheel serves merely as a plane surface freshly coated with acid while the specimen rotation guarantees that the cut will be perpendicular to the axis of rotation. Since it is necessary to expose a (111) plane for Livingston's dislocation etch to be effective, the specimen mounting jig is slotted at roughly the proper angle and has a ball joint base to permit bringing the normal to the (111) plane into coincidence with the axis of rotation after X-raying. Less adjustable jigs prove difficult to use. Nitric acid cut well in the acid saw but was found unsatisfactory for milling since it left a poor surface finish and preferentially attacked the edges of the crystal. A solution

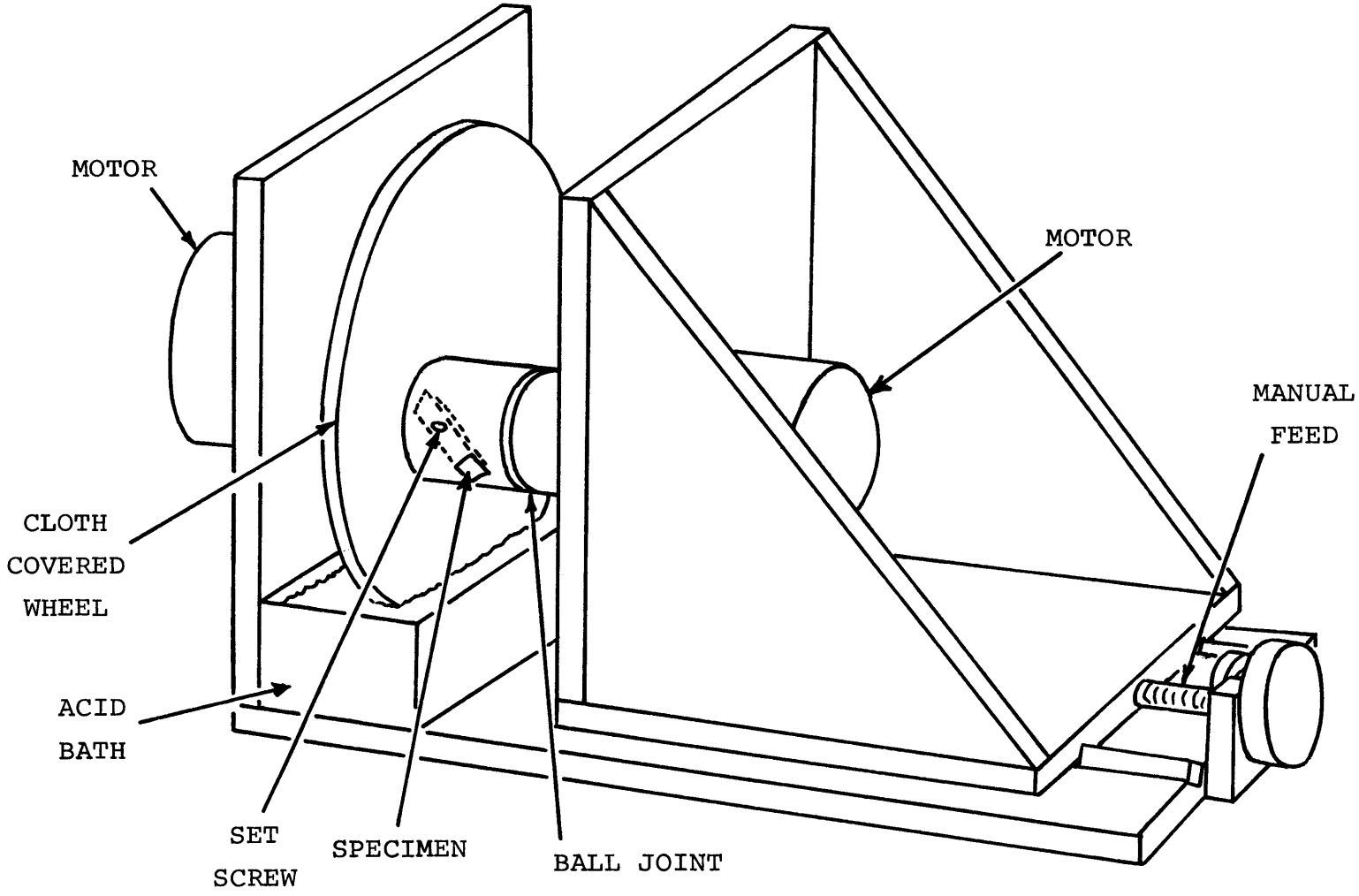

Figure B-2 The acid milling machine

of hydrochloric acid saturated with cupric chloride was suggested by Young (1961) and found to be quite satisfactory. It should be noted that the lacquer protecting the crystal during sawing should be removed from regions near the face being milled since it does not dissolve and soon extends from the side, occasionally folding over the (111) face causing uneven cutting rates.

The optimal mode of operation is to only wet the crystal without touching the cloth and thereby introducing dislocations. In practice it is quickly seen that unless the crystal remains close to the cloth a rounded surface results and the dislocation etch is effective over only a small portion of the surface. Therefore the crystal is advanced towards the polishing wheel once a minute until there is a barely audible indication of contact. Although such techniques are frowned upon, Young also found them necessary and an examination of the surface produced on an annealed crystal indicates that the damage is slight and readily removed by electropolishing (Fig. B-3). It is seen that the initial surface has a higher dislocation density than interior layers revealed by damage-free electropolishing. As material is removed a density unchanging with depth and equal to or less than the density on the cross plane is quickly reached. In circumstances where the damage persisted to about 0.3 mm due to coming into uncommonly close contact with the polishing wheel, removal of about 1 mm by electropolishing, remilling the rounded face carefully, and re-electropolishing with constant monitoring of the dislocation density proved effective.

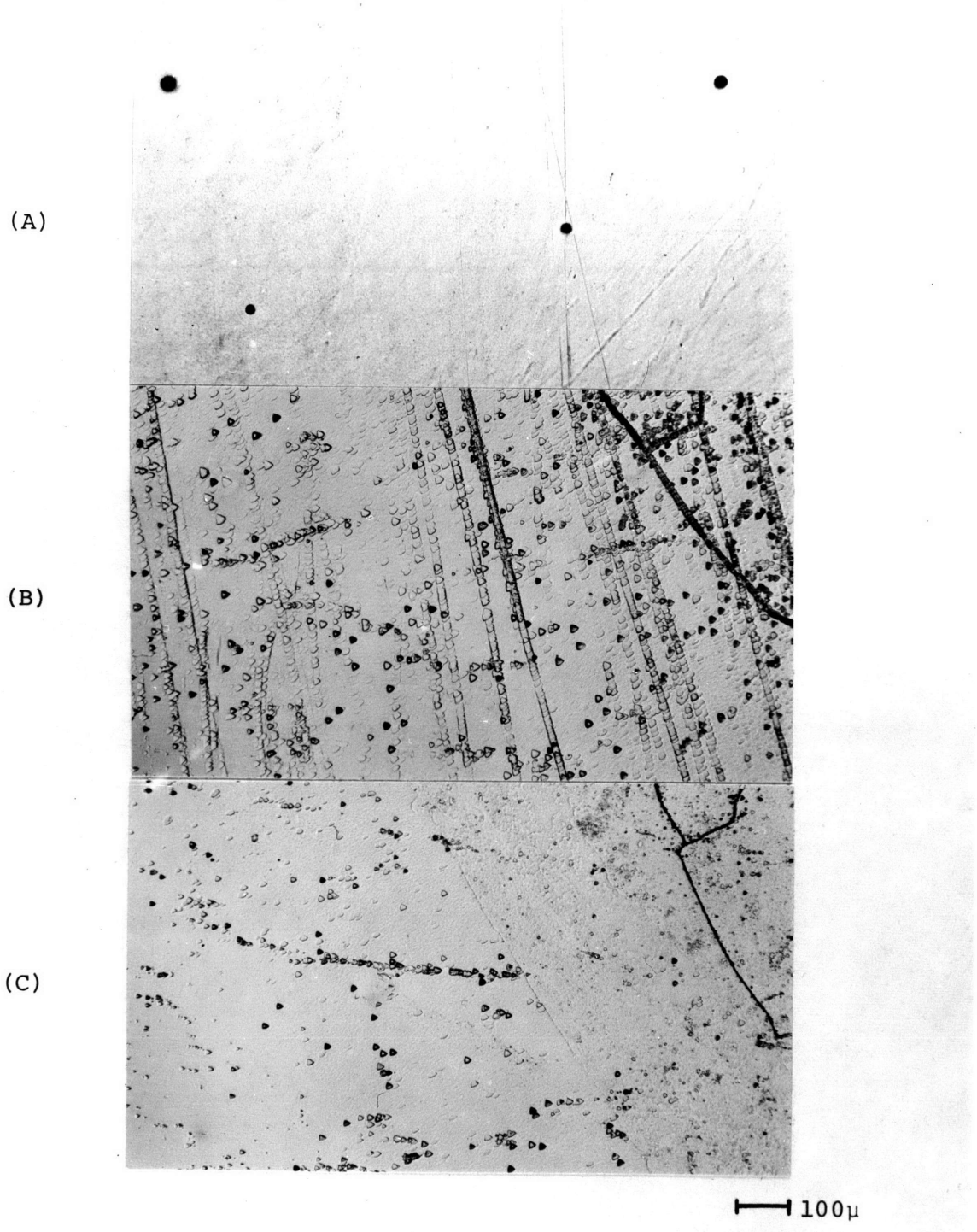

FIGURE B-3 SURFACE DAMAGE PRODUCED BY ACID MILLING (A- AS MILLED, NOT ETCHED; B- 15μ REMOVED BY ELECTROPOLISHING, ETCHED; C- 50μ REMOVED BY ELECTROPOLISHING, ETCHED)

APPENDIX C

THE FLOW CONDITION FOR THE PASSAGE OF A DISLOCATION THROUGH A FOREST WITH TWO OBSTACLE POPULATIONS

Consider the problem of a dislocation in a forest consisting of impenetrable and penetrable obstacles. If the stress (τ) applied to the dislocation is very small it will cut through neither obstacle population and thus the pinning points will depend on the total forest density

$$N_f = N_1 + N_2,$$

where

N_1 = impenetrable forest density

N_2 = penetrable forest density.

From the statistics of a dislocation touching random obstacles, the area between the bowed out dislocation and a straight line connecting the pinning points is

$$A_0 = 1/N_f = 1/(N_1+N_2).$$

We see from Figure C-1 that

$$A_0 = \frac{(\lambda_0)^3}{12 r_0}$$

and

$$2\phi r_0 = \lambda_0$$

where ϕ is the cutting angle at the penetrable obstacles. Thus when the dislocation is about to break through a penetrable obstacle

$$\lambda_0 = \sqrt{\frac{6A_0}{\phi}}$$

If β is the ratio of penetrable to impenetrable obstacles,

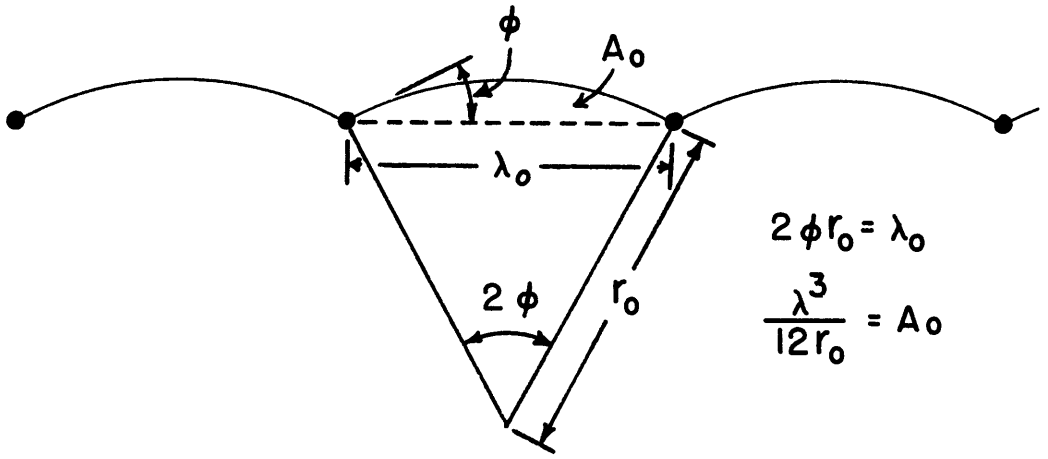

FIGURE C-1 PARAMETERS ASSOCIATED WITH A DISLOCATION AMONG OBSTACLES

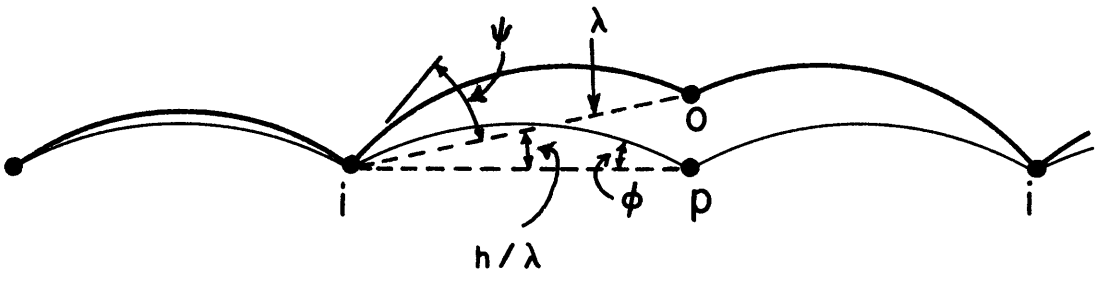

FIGURE C-2 DEFINITION OF SOME OBSTACLE BREAK-THROUGH PARAMETERS

then the linear densities of the two obstacle types along the dislocation are

$$n_1 = \frac{1}{1+\beta}\,\frac{1}{\lambda_0} \qquad \text{(impenetrable)}$$

$$n_2 = \frac{\beta}{1+\beta}\,\frac{1}{\lambda_0} \qquad \text{(penetrable)}.$$

Consider the case where the stress has increased to the point where a penetrable obstacle is overcome. The dislocation moves from point "p" (Fig. C-2) to "o". The probability that "o" is an impenetrable obstacle is

$$\frac{N_1}{N_1+N_2}$$

and that it is penetrable

$$\frac{N_2}{N_1+N_2}\ .$$

If the obstacle is impenetrable it will be added to the existing linear density of impenetrable obstacles but if penetrable it too may be overcome by increasing the stress so the new bowing angle is

$$\psi = \frac{6A}{\lambda^2}\ .$$

Using the geometrical relations

$$\frac{h}{\lambda} = \frac{A}{\lambda^2} = \frac{\psi}{6}$$

$$\psi = \phi + \frac{A}{\lambda^2} = \phi + \frac{\psi}{6}\ ,$$

we see that

$$\psi = \frac{6}{5}\,\phi.$$

The force on the impenetrable obstacle on either side has increased due to the displacement of the pinning point

$$\frac{f_i}{E} = 2\psi + \frac{\psi}{6} = 2\psi + \frac{\phi}{5}$$

but remains

$$\frac{f_p}{E} = 2\cdot\phi$$

for the cutting condition at the penetrable obstacle.

The linear density of both obstacle types along the dislocation becomes

$$n_2 = \frac{\beta}{1+\beta}\,\frac{1}{\lambda}\,\frac{N_2}{N_1+N_2} = \left(\frac{\beta}{1+\beta}\right)^2\frac{1}{\lambda}$$

$$n_1 = \left(\frac{1}{1+\beta} + \frac{\beta}{1+\beta}\cdot\frac{1}{1+\beta}\right)\frac{1}{\lambda}\ .$$

If this cutting process is considered one more time it is readily seen that the following generalizations may be made.

$$\psi = \left(\frac{6}{5}\right)^m\cdot\phi$$

$$\frac{f_i}{E} = 2\psi + \frac{\phi}{6}\left[\frac{6}{5} + \left(\frac{6}{5}\right)^2 + \cdots\cdots + \left(\frac{6}{5}\right)^m\right]$$

$$\frac{f_p}{E} = 2\phi$$

$$n_2 = \left(\frac{\beta}{1+\beta}\right)^{m+1}\frac{1}{\lambda}$$

$$n_1 = \frac{1}{1+\beta}\left[1 + \frac{\beta}{1+\beta} + \cdots\cdots + \left(\frac{\beta}{1+\beta}\right)^m\right]\frac{1}{\lambda}$$

$$\lambda = \sqrt{\frac{6A}{\psi}} = \sqrt{\frac{6A}{\phi\,(6/5)^m}}$$

where m is the number of times the cutting process has occurred at the penetrable obstacle. These equations take the form of a geometric series and may be rewritten in closed form.

$$\psi = \left(\frac{6}{5}\right)^m \phi$$

$$\frac{f_i}{E} = \phi\left[3\left(\frac{6}{5}\right)^m - 1\right]$$

$$\frac{f_p}{E} = 2\phi$$

$$n_2 = \left(\frac{\beta}{1+\beta}\right)^{m+1} \cdot \frac{1}{\lambda} \qquad \text{C-1}$$

$$n_1 = \left[1 - \left(\frac{\beta}{1+\beta}\right)^{m+1} \cdot\right] \frac{1}{\lambda} \qquad \text{C-2}$$

A flow condition must be introduced which includes the cutting of impenetrable obstacles. Although it is possible to set the condition for breakthrough at the highly stressed impenetrable obstacles on either side of the penetrable obstacle, hoping the other obstacles will unzip after the adjacent obstacle is cut, a safer assumption will be made. The average angle at the impenetrable obstacles will be made the cutting angle α despite the result that the pinning point adjacent to the penetrable obstacle will be overstressed. Then the flow condition is

$$\alpha = \frac{2n_2}{n_1} \frac{\phi}{2} \left[3\left(\frac{6}{5}\right)^m - 1\right] + \frac{n_1 - 2n_2}{n_1} \phi \left(\frac{6}{5}\right)^m$$

which simplifies to

$$\frac{\phi}{\alpha} = \frac{(5/6)^m}{\frac{n_2}{n_1}\left[1 - \left(\frac{5}{6}\right)^m\right] + 1} \quad . \qquad \text{C-3}$$

At the flow condition the external stress must overcome the resistance to dislocation motion. Therefore

$$\frac{\tau b}{2E} = n_2 \cdot \frac{f_p}{2E} + n_1 \cdot \frac{f_i}{2E}$$

where

$$\frac{f_i}{2E} = \alpha$$

$$\frac{f_p}{2E} = \phi$$

So

$$\frac{\tau b}{2E} = n_2 \phi + n_1 \alpha \qquad \text{C-4}$$

Looking at the limiting behavior of the mean spacing we see that the wrong value is reached as $\phi \to 0$ since no account of the softening of penetrable obstacles was included. A heuristic correction to maintain a bow angle $\psi > \phi$ at the new obstacles will be developed. The requirements are

ϕ	0	$\to$	α
$\frac{A}{A_0}$	$1+\beta$	$\to$	1
$\frac{n_2}{n_1}$	0	$\to$	β
$\frac{\phi}{\alpha}$	0	$\to$	1
m	∞	$\to$	0

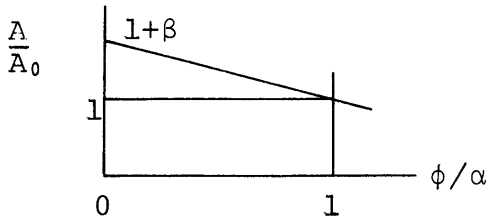

FIGURE C-3 SCHEMATIC REPRESENTATION OF CORRECTION FACTOR

From Figure C-3 we see that the correction term is

$$A = A_0(1 + \beta\{1 - \phi/\alpha\}).$$

So

$$\lambda = \sqrt{\frac{6A_0}{\alpha}\left(\frac{5}{6}\right)^m\{\frac{1 + \beta(1 - \phi/\alpha)}{\phi/\alpha}\}} \quad . \qquad \text{C-5}$$

Substitution of all the numbered equations into one another allows the solution for m. If β=1, then

$$\sqrt{\frac{6A_0}{\alpha}}\left(\frac{\tau b}{2\alpha E}\right) = \frac{1}{2^{m+1}}\sqrt{\frac{(2^{m+1} - 1)^3(\frac{6}{5})^m}{(\frac{5}{3})\left(\frac{12}{5}\right)^{m+1} - 1 - 2^{m+1}}}\left[\frac{(\frac{5}{6})\left(\frac{12}{5}\right)^{m+1}}{(\frac{5}{6})\left(\frac{12}{5}\right)^{m+1} - 1}\right].$$

APPENDIX D

COMPUTER PROGRAM FOR THE STATISTICAL THEORY FOR EASY GLIDE

The ultimate test of the statistical theory for easy glide (Argon and East (1968)) is the agreement of its predictions with experimental data. This requires the solution of the equations after introducing reasonable values for a few necessary input parameters. Since the complexity and repetitiveness of the equations suggests the use of a digital computer, a program was written in Fortran IV, Level G. It consists of a main program, seven special subroutines and one machine supplied subprogram for numercial integration.

The main program begins by reading the input data. These are:

H: The average spacing of multipole nuclei,

DELTA: The limiting distance for the cross-slip of screw dislocations,

MUOUT(I): The values of μ at which data printout will occur,

MNP(I,J): The frequency distribution of segment groupings, ${}_{mn}p(J)$,

N: The number of segments in the jogged dislocation,

MUMAX: The value of μ at which calculations should cease, and

THETA: The capture distance for edge dislocations.

Most variable names in the program are equally self explanatory. For example, PMUN means P-MU-N or $p_{\mu n}$, CAPMUN means CAPITAL P-MU-N or $P_{\mu n}$, and INTGQP means the INTEGRAL of the product

Q*P. The main program also initializes certain arrays to zero, calculates preliminary parameters, including limits, calls all special subroutines, six of which are in a "Do Loop" which indexes over μ, and provides a means of exit when the program is complete.

The first subroutine, P1NYXI, computes the integral of $p_{1n}(\eta-\xi)$ giving an array as a result. First it forms the symmetric probable width distribution of a single segmented dislocation by rearranging an asymmetric array from the main program. This is stored as PMUN1(I). From this it computes the fraction of a dislocation passing at $y=\xi$ which will be captured by a dislocation at y=0,

$$\int_{y-\theta}^{y+\theta} p_{1n}(\eta-\xi)\,d\eta,$$

and stores the result in an array P1N(I) before returning to the calling program.

The main program then indexes several subroutines over the variable μ, beginning with the subprogram QSMUN which calculates $q_{\mu n}(\xi)$, the probability of capturing a segment of a passing dislocation with its center of gravity at ξ. The procedure is a direct numercial solution of equation (6) of the statistical theory (Argon and East (1968)) complicated by the limits of integration. Next the main program calculates the function $Q_{\mu n}(\xi)$, the probability of capturing a glide dislocation with n segments, saves the result as QMUN(I), determines an integration limit, and calls subroutine INTEGQ.

The purpose of INTEGQ is to evaluate $p_{\mu n}(y)$, the segment distribution of a multipole with μ dislocations. It first integrates the product of $Q_{\mu n}(\xi)$ times $p_{1n}(y-\xi)$ over ξ forming an array dependent on y called INTGQP. This is then integrated over y to form a normalizing function NORM, normalized, and added to $P_{(\mu-1)n}(y)$ to give $p_{\mu n}(y)$.

The subroutine PMUNK calculates $P_{\mu n}^{(k)}(\xi)$ in a straightforward manner using a factorial table supplied by the main program and a frequency distribution of segmented groupings supplied as a table during the initial reading of the input parameters. The result is stored as a two dimensional array CAPMUN(K,I), the probability of producing k sources in a space interval governed by I.

Subroutine RATE is simple in appearance but actually involves considerable calculation since it calls the integration subroutine QSF three times. The rates of dislocation capture R_g, of source production R_p, and of source inactivation R_i are all determined at this point and designated RG, RP, and RIK respectively. As first calculated the RG is incomplete until RP is added later.

The mean free path of a dislocation Λ and the total accumulated strain γ are determined by subroutine STRAIN. Although there are many lines of instructions, the actual computer time is probably not long since this part does not have the long nested "Do Loops" of some other subroutines. Midway through the instructions the transmitted dislocation density N_t is calculated by reiteration until an accuracy of

one part in 10^6 is reached. The strain GAMMA is computed several ways depending on the value of μ. At high μ changes occur so slowly that the entire program jumps in steps of 2μ and the correction to the strain increment is made accordingly at this point.

The final subroutine, ANSWER, is activated by the main program only when μ = MUOUT. Only one minor calculation is performed at this stage. The bulk of this program is devoted to printing the output including suitable headings.

```
C       THE SOLUTION OF FORMULAS RELATING TO EASY GLIDE IN
C       FCC AND HCP METALS.
        DIMENSION PMUN(250), PMUN1(100), PMUN2(500), MUOUT(10),
       1 P1N(100), QMUN(250), QMUN2(500), QS(250), CAPMUN(11,250),
       2 GAMMA(2000), QSN(250), QS2N(250), FACT(21), ARG(250),
       3 SMUN(250)
        INTEGER A, B, C, D
        REAL N0, NT, K, INTGQP(250), MNP(20,20)
        READ (5,1) H, DELTA, (MUOUT(I), I = 1, 10)
1       FORMAT 2F10.5/10I5)
        READ (5,20) ((MNP(I,J), I = 1, 20), J = 1, 20)
20      FORMAT (10F7.5)
2       READ (5, 3, END=14) N, MUMAX, THETA
3       FORMAT (2I5, F10.5)
        DO 4 I = 1, 250
        DO 16 J = 1, 11
16      CAPMUN(J,I) = 0.0
        ARG(I) = 0.0
        QS(I) = 0.0
        QMUN(I) = 0.0
4       PMUN(I) = 0.0
        FACT(1) = 1
        DO 17 I = 2, 21
17      FACT(I) = FACT(I-1)*I-1)
        DEL = 0.5
        A =(N-1)/DEL
        M = A + 1
        MX2 = 2*A + 9
        MU = 1
        LIM1 = M
        INI = 1
        E = 0.80774/(N**0.55349)
        F = 1.0/(3.1415926*E**2)
        DO 5 I = 1, M
5       PMUN(I) = E/2.7182818**(((I-1)*DEL)**2/F)
        CALL P1NYXI (M, MX2, THETA,PMUN, P1N, PMUN1, DEL)
        WRITE (6,6) (PMUN(I), I = 1, M)
6       FORMAT (1P5E20.7)
7       MU = MU + 1
        IF (MU.GT.MUMAX) GO TO 2
        IF (MU.GT.100) MU = MU + 1
        B = LIM1
        C = 2*B - 1
        LIM2 = (MU-1)*2*A+1
        CALL QSMUN (B, C, LIM2, P1N, PMUN, PMUN2, QS, DEL, INI,
       1 N, THETA, DELTA, MX2)
        IF (MU.GT.2) GO TO 10
        QS1 = QS(1)
        DO 9 I = 1, LIM2
9       QSN(I) = QS(I)**N
        CALL QSF (DEL, QSN, QS2N, LIM2)
        Q2N = 2*QS2N(LIM2)*DELTA
```

```
10      DO 8 I = INI, LIM2
8       QMUN(I) = QS(I)**N
        IF (QMUN(INI).GT.0.99999) INI = INI + 1
        IF (INI.EQ.1) GO TO 18
        QMUN(INI-1) = 1.0
        QS(INI-1) = 1.0
18      D = 2*LIM2 - 1
        LIM1 = LIM2 + A
        CALL INTEGQ (D, LIM1, LIM2, INTGQP, PMUN, PMUN1, QMUN,
       1 QMUN2, DEL, INI, MU, MX2)
        CALL PMUNK (QS, CAPMUN, N, THETA, DELTA, LIM2, QS1,
       1 FACT, MNP)
        CALL RATE (DEL, QMUN, CAPMUN, LIM2, RG, RP, RIK, N,
       1 THETA, DELTA, ARG, QS)
        CALL STRAIN (N, LAMBDA, H, CAPMUN, DEL, LIM2, RP, RIK,
       1 K, Q2N, NT, GAMMA, QMUN, DELTA, MU)
        N0 = 1/H**2
        DO 11 I = 1, 10
        IF (MU.EQ.MUOUT(I)) GO TO 12
11      CONTINUE
        GO TO 7
12      WRITE (6, 13)
13      FORMAT (1H1, 50X, 'STATISTICAL THEORY FOR EASY GLIDE'
       1 ///)
        DO 19 I = 1, LIM1
19      SMUN(I) = ARG(I)*K/RP
        CALL ANSWER(QS, QMUN, PMUN, N, MU, LIM1, H, THETA,
       1 DELTA, DEL, CAPMUN, N0, INI, GAMMA, K, RG, RP, LAMBDA,
       2 SMUN, NT)
        GO TO 7
14      WRITE (6, 15) N, MUMAX, THETA
15      FORMAT (1H1, 2I5, F10.5)
        CALL EXIT
        STOP
        END
```

```
      SUBROUTINE PlNYXI (M, MX2, THETA, PMUN, PlN, PMUN1,
     1 DEL)
C     A SUBROUTINE TO COMPUTE THE INTEGRAL OF P SUB lN OF
C     (ETA-XI) GIVING AN ARRAY P(Y-XI) AS A RESULT
      DIMENSION PlN(100), PMUN(250), PMUN1(100)
      DO 4 J = 1, MX2
      IF (J.LT.5.OR.J.GT.(MX2-4)) GO TO 3
      IF (J.GE.(M+4)) GO TO 1
      I = M - J + 5
      GO TO 2
1     I = J - M - 3
2     PMUN1(J) = PMUN(I)
      GO TO 4
3     PMUN1(J) = 0.0
4     CONTINUE
      NA = THETA/DEL
      NB = 2*NA + 1
      NC = -NA - 1
      A = NB
      DO 6 I = 1, MX2
      PlN(I) = 0.0
      DO 5 J = 1, NB
      ND = NC + J + I
      IF (ND.LE.0.OR.ND.GT.MX2) GO TO 5
      PlN(I) = PMUN1(ND) + PlN(I)
5     CONTINUE
6     PlN(I) = 2*THETA*PlN(I)/A
      RETURN
      END
```

```
      SUBROUTINE QSMUN (B, C, LIM2, PlN, PMUN, PMUN2, QS,
     1 DEL, INI, N, THETA, DELTA, MX2)
      INTEGER B, C
C     A SUBROUTINE TO COMPUTE THE EXPONENTIATED FORM OF Q
C     SUB (MU,N) OF XI
      DIMENSION TERM(500), ARRAY(500), QS(250), PMUN(250),
     1 PMUN2(500), PlN(100)
      X = 1.0E-77**(1.0/N)*THETA*DELTA/5.0E-6
C     GENERATE PMUN2 FROM PMUN
      DO 2 J = 1, C
      IF (J.GE.B) GO TO 1
      I = B-J+1
      GO TO 2
1     I = J-B+1
2     PMUN2(J) = PMUN(I)
C     PERFORM THE INTEGRATION AND EXPONENTIATION TO GET
C     SMALL Q SUB (MU,N) OF XI
      LIM5 = LIM2-2
      K = (C-MX2)/2 - 1
      DO 4 I = 1, MX2
4     TERM(I) = 0.0
      DO 10 I = INI, LIM5
      LIMIT = C-I-K
      IF (LIMIT.GT.MX2) LIMIT = MX2
      J1 = 1
      IF ((1+I+K).LE.0) J1 = 1-(I+K)
      DO 3 J = J1, LIMIT
3     TERM(J) = PMUN2(I+J+K)*PlN(J)
      CALL QSF (DEL, TERM, ARRAY, LIMIT)
      Q = ARRAY(LIMIT)
      IF (Q.LT.1.0E-4) GO TO 30
      QS(I) = 1.0-1.0/EXP(Q)
      GO TO 31
30    QS(I) = Q
31    IF (QS(I).LT.X) GO TO 9
10    CONTINUE
      RETURN
9     E = I
      IF ((E/2-I/2).GT.0.2) I = I-1
      LIM2 = I + 1
      QS(LIM2-1) = 0.0
      QS(LIM2) = 0.0
      RETURN
      END
```

```
      SUBROUTINE INTEGQ (E, LIM1, LIM2, INTGQP, PMUN, PMUN1,
     1 QMUN, QMUN2, DEL, INI, MU, MX2)
      REAL NORM, INTGQP(250)
      INTEGER E
      DIMENSION PMUN1(100), QMUN(250), QMUN2(500), PMUN(250),
     1 TERM(250), ARRAY(250)
      DO 3 K = 1, E
      IF (K.GE.LIM2) GO TO 2
      I = LIM2 - K + 1
      GO TO 3
2     I = K - LIM2 + 1
3     QMUN2(K) = QMUN(I)
      LIM4 = LIM1 - 2
      K = (E-MX2)/2 - 1
      DO 5 I = INI, LIM4
      LIMIT = E - I - K
      IF (LIMIT.GT.MX2) LIMIT = MX2
      DO 4 J = 1, LIMIT
4     TERM(J) = QMUN2(I+J+K)*PMUN1(J)
      CALL QSF (DEL, TERM, ARRAY, LIMIT)
5     INTGQP(I) = ARRAY(LIMIT)
      CALL QSF (DEL, INTGQP, ARRAY, LIM4)
      NORM = 2*ARRAY(LIM4)
      IF (MU.GT.100) NORM = NORM/2
      DO 9 JD = 1, LIM4
9     PMUN(JD) = PMUN(JD) + INTGQP(JD)/NORM
      PMUN(LIM1-1) = 0.0
      PMUN(LIM1) = 0.0
      RETURN
      END
```

```
      SUBROUTINE PMUNK (QS, CAPMUN, N, THETA, DELTA, LIM2,
     1 QS1, FACT, MNP)
      DIMENSION QS(250), CAPMUN(11,250), FACT(21), E(250),
     1 F(250,20), G(250,20), H(250)
      REAL KFACT, MFACT, M1FACT, M1KFAC, NFACT, NMFACT,
     1 MNP(20,20)
      C = 5.0E-6/(THETA*DELTA)
      DO 1 I = 1, 11
      DO 1 J = 1, LIM2
1     CAPMUN(I,J) = 0.0
      LIM = 1
      DO 5 I = 1, LIM2
      IF (QS(I).GT.9.99) LIM = I
5     CONTINUE
      NFACT = FACT(N+1)
      DO 4 I = LIM, LIM2
      P = (1-QS(I))**N*(1-QS1)**(N-1)
      H(I) = 2*P - P**2
      E(I) = C*QS(I)
      DO 4 J = 1, N
      F(I,J) = (E(I)**J)*(1-E(I))**(N-J)
4     G(I,J) = (1-QS(I)**J)*H(I)
      KMAX = N/2 + 1
      DO 3 K = 1, KMAX
      KFACT = FACT(K+1)
      M1 = K - 1
      IF (K.EQ.1) M1 = 1
      DO 2 M = M1, N
      IF (F(1,M).LT.(1.0E-7*F(1,M1))) GO TO 3
      MFACT = FACT(M+1)
      M1KFAC = FACT(M+2-K)
      M1FACT = FACT(M+2)
      L = N - M
      NMFACT = FACT(L+1)
      A = M1FACT/(M1KFAC*KFACT)
      B = NFACT/(MFACT*NMFACT)
      DO 2 J = 1, L
      IF (MNP(M,J).EQ.0) GO TO 2
      D = A*B*MNP(M,J)
      DO 6 I = LIM, LIM2
6     CAPMUN(K,I) = D*F(I,M)*G(I,J) + CAPMUN(K,I)
2     CONTINUE
3     CONTINUE
      RETURN
      END
```

```
      SUBROUTINE RATE (DEL, QMUN, CAPMUN, LIM2, RG, RP, RIK,
     1 N, THETA, DELTA, ARG, QS)
      DIMENSION QMUN(250), CAPMUN(11,250), SUM(250), RG1(250),
     1 ARG(250), QS(250)
      CALL QSF (DEL, QMUN, RG1, LIM2)
      RG = 2*DELTA*RG1(LIM2)
      DO 1 I = 1, LIM2
      SUM(I) = CAPMUN(1,I)
      KMAX = N/2 + 1
      DO 1 K = 2, KMAX
1     SUM(I) = K*CAPMUN(K,I) + SUM(I)
      CALL QSF (DEL, SUM, RG1, LIM2)
      RP = 2*DELTA*RG1(LIM2)
      RG = RG + RP
      DO 2 I = 1, LIM2
2     ARG(I) = 1.0E-5*QS(I)*SUM(I)
      CALL QSF (DEL, ARG, RG1, LIM2)
      RIK = 2*DELTA*RG1(LIM2)/RP
      RETURN
      END
```

```
      SUBROUTINE STRAIN (N, LAMBDA, H, CAPMUN, DEL, LIM2,
     1 RP, RIK, K, Q2N, NT, GAMMA, QMUN, DELTA, MU)
      DIMENSION CAPMUN(11,250), GAMMA(2000), SUMP(250),
     1 TOTAL(250), TERM(250), QMUN(250)
      REAL LAMBDA, K, NT
      N2 = N/2 + 1
      H1 = 2.56E-8*H
      DO 2 I = 1, LIM2
      SUMP(I) = 0.0
      DO 1 J = 1, N2
1     SUMP(I) = SUMP(I) + CAPMUN(J,I)
2     TOTAL(I) = QMUN(I) + SUMP(I)
      CALL QSF (DEL, TOTAL, TERM, LIM2)
      K = RP/RIK
      A = 2*DELTA*TERM(LIM2)/H1
      B = 2*Q2N*H1
      C = 2*K/H1
      NT = (C/(EXP(A)-1))**2
      I = 0
      X = 10
      VALUE = 1.0E70
      IF ((A+B*NT).GT.170) NT = (170-A)/B
3     PART1 = EXP(A+B*NT)
      PART2 = 1 + C/SQRT(NT)
      IF (ABS(VALUE-NT).LT.(NT*1.0E-6)) GO TO 6
      VALUE = NT
      IF (PART2-PART1) 4, 6, 5
4     IF (I.EQ.2) X = 1 + (X-1)/10
      NT = NT/X
      I = 1
      GO TO 3
5     IF (I.EQ.1) X = 1 + (X-1)/10
      NT = NT*X
      I = 2
      GO TO 3
6     X = A + B*NT
      LAMBDA = H1/X
      IF (MU.GT.100) GO TO 9
      IF (MU.GT.2) GO TO 8
      GAMMA(2) = 5.12E-8/(H1*X)
      RETURN
8     GAMMA(MU) = 2.56E-8/(H1*X) + GAMMA(MU-1)
      RETURN
9     GAMMA(MU) = 5.12E-8/(H1*X) + GAMMA(MU-2)
      RETURN
      END
```

```
      SUBROUTINE ANSWER (QS, QMUN, PMUN, N, MU, LIM1, H,
     1 THETA, DELTA, DEL, CAPMUN, N0, INI, GAMMA, K, RG,
     2 RP, LAMBDA, SMUN, NT)
      DIMENSION QS(250), QMUN(250), CAPMUN(11,250),
     1 SMUN(250), XI(250), PMUN(250), GAMMA(2000)
      REAL N0, K, LAMBDA, NT
      WRITE (6,1) GAMMA(MU), LAMBDA
1     FORMAT (' STRAIN =', 1PE14.7, T65, 'LAMBDA =',
     1 1PE14.7)
      DO 2 I = 1, LIM1
2     XI(I) = DEL*(I-1)
      WRITE (6,3) N, MU, THETA, DEL
3     FORMAT (1H0, 'NUMBER OF SEGMENTS (N) =', I3, T65,
     1 'MULTIPOLE POPULATION (MU) =', I4// ' CAPTURE DISTANCE
     2(THETA) =', 1PE14.7, '*DELTA', T65, 'INTEGRATION
     3 INTERVAL (DEL) =', 1PE14.7, '*DELTA'/)
      WRITE (6,4) NT, H, DELTA, K
4     FORMAT (' TRANSMITTED DENSITY (NT) =', 1PE14.7, T65,
     1 'MULTIPOLE SPACING (H) =', 1PE14.7//' CROSS SLIP
     2 DISTANCE (DELTA) =', 1PE14.7, T65, 'K =', 1PE14.7/)
      WRITE (6,5) RG, RP
5     FORMAT (' GROWTH RATE (RG) =', 1PE14.7, T65, 'RATE OF
     1 PRODUCTION (RP) =', 1PE14.7/)
      WRITE (6,6)
6     FORMAT (' THE PROBABILITY OF', 5X, 'THE PROBABILITY
     1 OF', 4X, 'DISTANCE FROM CENTER', 4X, 'THE PROBABILITY
     2 OF', 5X, 'THE PROBABILITY OF', 11X, 'WIDTH')
      WRITE(6,7)
7     FORMAT (' SOURCE PRODUCTION', 5X, 'SOURCE INACTIVATION',
     1 5X, 'IN TERMS OF DELTA', 6X, 'DISLOCATION CAPTURE',
     2 7X, 'FULL CAPTURE', 10X, 'DISTRIBUTION')
      WRITE (6,8) (CAPMUN(1,I), SMUN(I), XI(I), QS(I), QMUN(I),
     1 PMUN(I), I = 1, INI, 5)
8     FORMAT (' P SUB (MU,N) OF XI', 5X, 'S SUB (MU,N) OF XI',
     1 13X, 'XI', 19X, 'SMALL Q', 14X, 'CAPITAL Q', 14X,
     2 'SMALL P'//(1PE16.7, 10X, 1PE14.7, 9X, 1PE14.7, 9X,
     3 1PE14.7, 9X, 1PE14.7, 9X, 1PE14.7))
      INIT = I + 2
      WRITE(6,9) (CAPMUN(1,I), SMUN(I), XI(I), QS(I), QMUN(I),
     1 PMUN(I), I = INIT, LIM1, 2)
9     FORMAT (1PE16.7, 10X, 1PE14.7, 9X, 1PE14.7, 9X, 1PE14.7,
     1 9X, 1PE14.7, 9X, 1PE14.7)
      RETURN
      END
```

ACKNOWLEDGEMENTS

The author is indebted to all those who gave him encouragement and advice. Particular thanks are due to Professor A. S. Argon, the thesis supervisor, for his timely guidance and to members of the thesis committee, Professors M. F. Ashby, F. A. McClintock, and I. V. Yannas.

The author also wishes to acknowledge the technical assistance of Mr. W. Henry and Mr. R. Leonard.